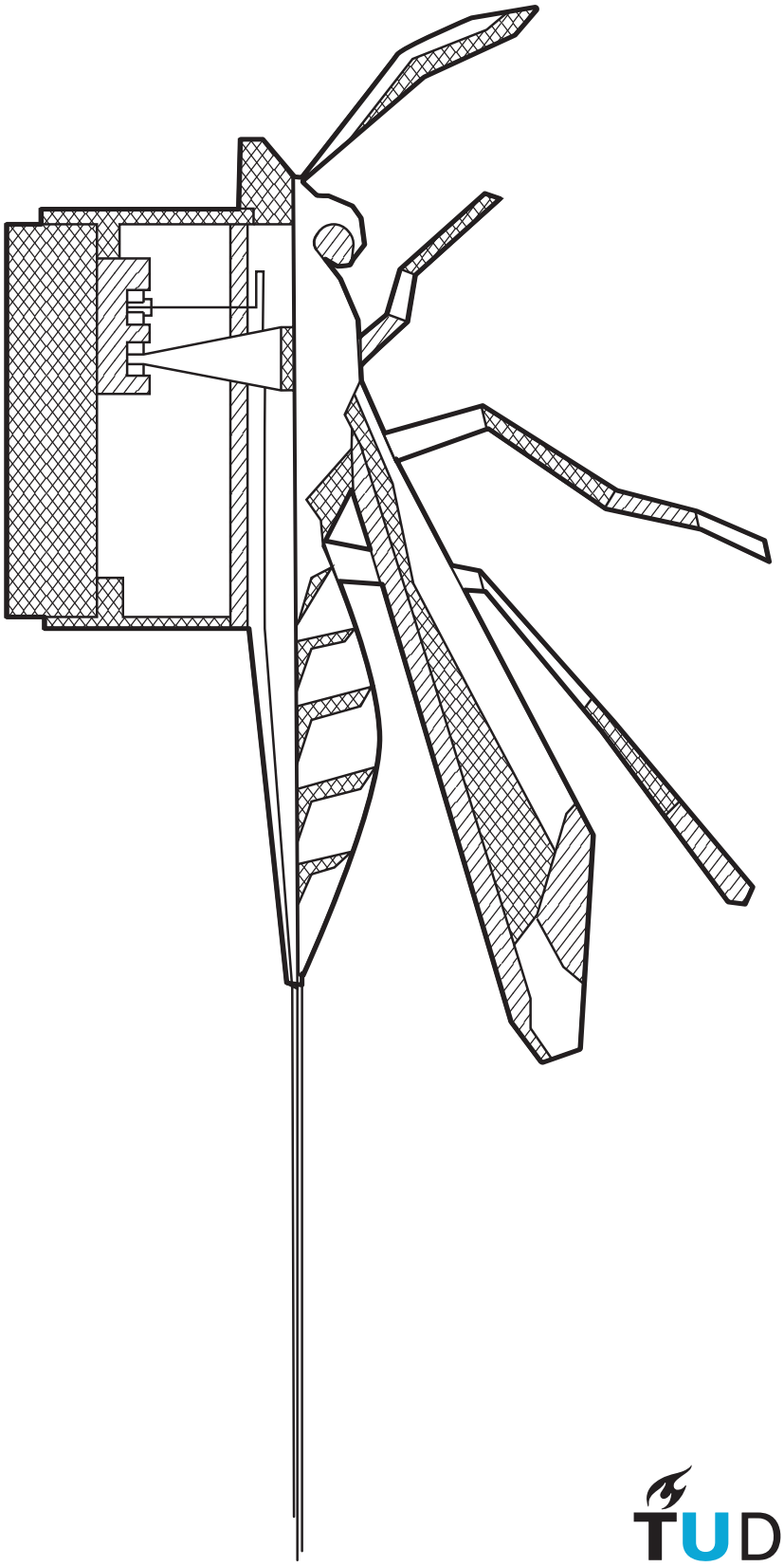
MR-Conditional Wasp-Inspired Needle with Integrated Laser Functionality for Transperineal Laser Ablation

A Design-Driven Experimental Approach

David Vainer



TU Delft

MR-Conditional Wasp-Inspired Needle with Integrated Laser Functionality for Transperineal Laser Ablation

A Design-Driven Experimental Approach

by

David Vainer

in partial fulfilment of the requirements of

Master of Science
in BioMedical Engineering
following the Medical Devices track

at the Delft University of Technology,
to be defended publicly on Tuesday October 22, 2024 at 15:45 PM.

Student number:	4847830	
Project duration:	February 1, 2024 – October 22, 2024	
Supervisors:	Dr. ir. A. Sakes	TU Delft
	Ir. J. Bloemberg	TU Delft
Thesis committee:	Dr. ir. A. Sakes	TU Delft, Chair
	Ir. J. Bloemberg	TU Delft
	Prof. dr. ir. P. Breedveld	TU Delft
	Dr. ir. T. Horeman	TU Delft
	Dr. ir. G. Radaelli	TU Delft

This thesis is confidential and cannot be made public until October 22, 2026.

All illustrations (including the cover design) are made by: David Vainer

An electronic version of this thesis is available at http://repository.tudelft.nl/.

TU Delft

PREFACE

I would like to thank Jette Bloemberg for the time she has spent providing me with thorough, detailed, and solution-oriented feedback. I cannot understate the extent to which this feedback has helped me improve my writing, design, and process. Not only that but also how this feedback was communicated to me was praiseworthy. I could always ask questions and explain my problems, and she would always help me find a solution. This has made my thesis, which in general is quite stressful and tough, an enjoyable project. Next to Jette Bloemberg, I would like to thank Aimée Sakes for her insightful feedback that enabled me to steer my project in the right direction from an early stage. The meetings always contained interesting and fruitful discussions that helped me progress. Of course, I have to thank my family for the additional feedback and support throughout this project. Together with my roommates, Brian Holtkamp and Jos van der Velden, and my girlfriend Laure Slot they have made this time a very enjoyable one and helped me never feel isolated or lonely. So to all of you, thank you!

David Vainer
Rotterdam, September 2024

CONTENTS

I Introduction 7
- I-A **Transperineal laser ablation** 7
- I-B **Wasp-inspired needles** 8
- I-C **Problem statement and research goal** 9
- I-D **Structure** 9

II Requirements 9
- II-A **Requirements** 9
  - II-A1 **Overall requirements** 9
  - II-A2 **Needle system requirements** 10
  - II-A3 **Actuation system requirements** 10
  - II-A4 **Laser system requirements** 10
- II-B **Nice-to-haves** 10

III Design direction 11
- III-A **Evolution method** 11
- III-B **Ideation** 12
- III-C **Concept design** 13
- III-D **Design iteration** 14
  - III-D1 **Needle system iteration** 14
  - III-D2 **Actuation system iteration** 14
  - III-D3 **Laser system iteration** 14
  - III-D4 **Buckling prevention system iteration** 15

IV Design 15
- IV-A **Overall design** 15
  - IV-A1 **Needle system** 15
  - IV-A2 **Actuation system** 16
  - IV-A3 **Laser system** 16
  - IV-A4 **Buckling prevention system** 18
- IV-B **Prototype** 18
  - IV-B1 **Material** 20
  - IV-B2 **Needle system** 20
  - IV-B3 **Actuation system** 20
  - IV-B4 **Laser system** 21
  - IV-B5 **Buckling prevention system** 21

V Evaluation 22
- V-A **Slip ratio experiment** 22
  - V-A1 **Goal** 22
  - V-A2 **Variables** 22
  - V-A3 **Setup** 22
  - V-A4 **Procedure** 22
  - V-A5 **Test results** 23
- V-B **Push force experiment** 23
  - V-B1 **Goal** 23
  - V-B2 **Variables** 25
  - V-B3 **Setup** 25
  - V-B4 **Procedure** 25
  - V-B5 **Test results** 26
- V-C **Friction force experiment** 26
  - V-C1 **Goal** 26
  - V-C2 **Variables** 26
  - V-C3 **Setup** 26
  - V-C4 **Procedure** 26
  - V-C5 **Test results** 27

V-D **Laser damage experiment** . . . 28
V-D1 **Goal** . . . 28
V-D2 **Variables** . . . 28
V-D3 **Setup** . . . 28
V-D4 **Procedure** . . . 28
V-D5 **Test results** . . . 28

VI Discussion 28
VI-A **Main findings** . . . 28
VI-A1 **Slip ratio** . . . 28
VI-A2 **Push force** . . . 29
VI-A3 **Friction force** . . . 30
VI-A4 **Laser damage** . . . 30
VI-B **Limitations** . . . 30
VI-B1 **Design** . . . 30
VI-B2 **Prototype** . . . 30
VI-B3 **Experiments** . . . 31
VI-C **Recommendations** . . . 31
VI-C1 **Design** . . . 31
VI-C2 **Prototype** . . . 32
VI-C3 **Experiment** . . . 32
VI-D **Towards clinical implementation** . . . 32

VII Conclusion 33

VIII Acknowledgements 33

References 33

Appendix A: Design Evolution interview 37

Appendix B: Design process 39

Appendix C: Needle guide trade-of 63

Appendix D: Mathematics 64
D-A Inner-cam path . . . 64
D-B Undercutting . . . 70
D-C Nitinol rod . . . 74

Appendix E: MRI compatibility design considerations 79

Appendix F: Material change 81

Appendix G: Needle system design considerations 82

Appendix H: Assembly 84

Appendix I: Technical drawings 85

MR-Conditional Wasp-Inspired Needle with Integrated Laser Functionality for Transperineal Laser Ablation

David Vainer
Biomedical Engineering, Delft University of Technology, Delft, the Netherlands

***Abstract*—TransPerineal Laser Ablation (TPLA) is a novel, minimally invasive procedure that uses accurately positioned needles through which optical fibres are inserted to ablate malignant prostate tissue, demonstrating minimal side effects in early studies. Accurate needle placement and guidance can be affected by many factors such as needle buckling, imaging modality, and needle deflection. Using the self-propelling mechanism seen in the ovipositor of parasitoid wasps, the risk of buckling can be reduced and tissue damage can be minimised. Drawing inspiration from this principle, we created a stationary, MR-conditional 3D printed device with integrated laser functionality that can propel a needle system through stationary, human-like tissue. Our results show that needle traversal through multiple gelatin phantoms (up to 15 wt%) is possible. The needle (bundle) can move through these phantoms without buckling, due to its near-zero (max $0.28\,\mathrm{N}$) net put force. The propelled needle (bundle) has an outer diameter of $1.2\,\mathrm{mm}$, which includes a centrally located needle through which the optical fibre, used for laser ablation, can be inserted. Our wasp-inspired needle design and prototype narrow the gap to the clinical implementation of wasp-inspired needles for MRI-guided TPLA. Moreover, with minimal design changes, our device may serve as a versatile platform for applications beyond its intended purpose of TPLA, such as camera positioning, drug delivery, tissue engineering, and tissue extraction.**

***Index Terms*—MRI, TPLA, Bioinspiration, Medical, Minimally invasive surgery, Laser**

I. Introduction

A. *Transperineal laser ablation*

The prostate is a part of the male reproductive system. It is situated posterior to the bladder and is located around the urethra. The prostate is similar in size to a peach pit or walnut and comprises multiple glands that secrete fluid during ejaculation [1, 2]. This fluid contributes to sperm activation and makes up around 30 to 40% of the seminal fluid [1, 3].

Prostate cancer is the most commonly diagnosed cancer in men, accounting for more than a quarter of all cancer diagnoses in men (in the United States) [4]. This makes it the second most diagnosed form of cancer in the world. Almost three percent of men diagnosed with prostate cancer die, leading to a worldwide death toll of more than 375000 men per year [5].

Current treatment consists of surgical intervention (i.e., radical prostatectomy) or radiotherapy [6]. In some cases, alternative interventions may be used that include chemical or surgical castration [1]. Radical prostatectomy and radiology, albeit effective can have life-affecting complications, such as erectile dysfunction and urinary incontinence [6–8].

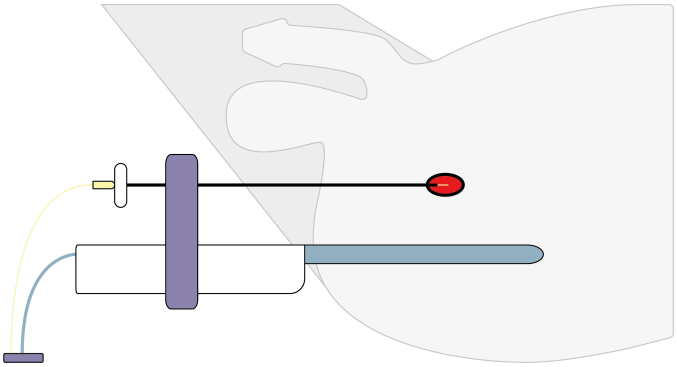


Fig. 1: *Schematic overview of the TransPerineal Laser Ablation (TPLA) approach adapted from the EchoLaser TPLA SoracteLite (Elesta SpA, Calenzano, FI, Italy) [13]. The ultrasound probe is shown in blue, the needle in black, the needle and probe holder in purple, the optical fibre in yellow (partially inside the needle), and the ablation area in red.*

An alternative treatment for selective patients with prostate cancer has been proposed in the form of a novel surgical procedure known as TransPerineal Laser Ablation (TPLA) [9]. TPLA is a procedure in which (malignant) prostate tissue is irreversibly damaged by laser light, emitted through an optical fibre. In the current procedure, a patient is positioned in the lithotomy position. Using MultiParametric Magnetic Resonance Imaging (mpMRI), a possible malignant lesion is located. Using MRI/TransRectal UltraSound (TRUS) fusion guidance, a biopsy is performed to determine the malignancy of the lesion [10]. MRI/TRUS fusion combines pre-made Three-Dimensional (3D) MRI images (with contoured regions of interest), with real-time Two-Dimensional (2D) ultrasound images [11]. With the location and malignancy of the lesion known, an ultrasound probe is inserted into the rectum. With the help of MRI/TRUS fusion guidance, a needle is inserted into the perineum at the desired location. Having reached the lesion with the needle, an optical fibre is inserted through the needle. A pullback manoeuvre follows; the needle is pulled back (around one centimetre) while the optical fibre remains in place (Figure 1). With the optical fibre tip at a safe distance from the needle tip, laser light is emitted through the optical fibre, leading to ablation of the lesion [10, 12].

TPLA may help to effectively treat prostate cancer (in

selective patients) while maintaining urinary continence and erectile function [10, 14]. Furthermore, compared to other novel minimally invasive focal methods, such as PhotoDynamic Therapy (PDT), cryotherapy, High-Intensity Focused Ultrasound (HIFU) and irreversible electroporation, TPLA appears to be the most promising procedure, based on the limited amount of available evidence and research. This comes from the fact that it offers local anaesthesia, relatively thin needles, and positive short- and mid-term complication and disease projections [15].

Nevertheless, TPLA comes with some challenges that have yet to be overcome. These challenges mainly refer to needle mis- and displacement in the target area, as a result of patient movement, prostate movement, oedema, and needle deflection due to needle-tissue interaction [16–18]. Placement accuracy is of utmost importance to ensure the pre-planned ablation area is ablated. Ablating an area different from the planned area can lead to incomplete destruction of malignant tissue or healthy tissue damage, increasing the risk of side effects such as urinary incontinence and erectile dysfunction [19].

Generally, a percutaneous intervention, such as TPLA, is performed with the use of long and slender needles to minimise tissue damage during the intervention [20]. Unsupported long and slender structures, however, are prone to buckling [21]. Buckling is the lateral bending or deformation of an object and occurs if an applied axial load (e.g. the axial load the needle experiences during insertion) surpasses the critical load. If buckling occurs in tissue, tissue damage, directly resulting from the lateral bending, may occur. Additionally, buckling can cause erratic displacement of the tip [21]. The buckling of a needle can be prevented by increasing the critical load ($\mathbf{F}_{\text{critical load}}$), the axial load at which the needle buckles, or by decreasing the penetration load (the axial force the needle exerts) [21]. The critical load can be calculated using the following equation:

$$F_{\text{critical load}} = \frac{\pi^2 EI}{(KL)^2} \tag{1}$$

In this equation, E refers to the Young's modulus (GPa) and represents the elastic property of the material of the needle. I is the area moment of inertia (m^4) concerning the cross-section of the needle. K is a dimensionless parameter called the column effective length factor and is determined by the needle fixation. At last, L represents the unsupported length of the needle (m).

B. Wasp-inspired needles

Nature has provided numerous examples of long, slender needle-like structures that can resist buckling. An especially intriguing example is the egg-laying mechanism of the parasitoid wasp [21]. The parasitoid wasp uses an ovipositor, a specialised, long, slim and hollow organ, to lay its eggs in hosts. Sometimes, these potential hosts are in hard-to-reach places, such as in trees. Fascinatingly, the wasp can reach these potential hosts by inserting its ovipositor through the wood, a relatively hard and stiff material, without buckling [22]. The ovipositor's resistance to buckling can be explained by its anatomy, which forms the basis of our bio-inspired needle system [21, 22].

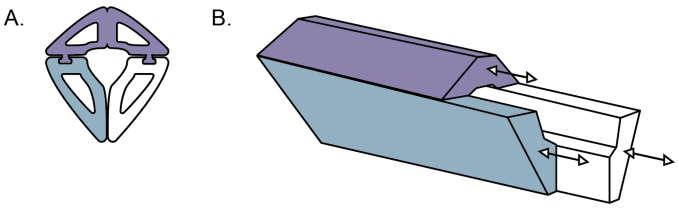


Fig. 2: *Schematic overview of the parasitoid wasp ovipositor adapted from Bloemberg et al. [28]. The dorsal valve is the purple valve on top. The blue and white valves are the ventral valves. A) Front view of the ovipositor. B) Three-dimensional schematic view of the ovipositor valve sequential movement.*

The ovipositor consists of three valves, one dorsal and two ventral [23]. These valves are interlocked similar to a dovetail mechanism. This interlocking mechanism allows for the translation of the valves relative to one another, as visualised in Figure 2 [23–25]. To insert its ovipositor through wood, the wasp forcibly pushes one valve into the substrate, while simultaneously trying to retract its other two valves in an alternating manner [26]. This movement generates forces between the three valves and between the valves and the substrate. The forces between the three valves are friction forces and cancel each other out, as a result of Newton's third law (action = -reaction) [27]. The forces between the valves and the substrate consist of a friction force between the valves and the substrate and a cutting force at the tip of the advancing valve. Applying Newton's second law, Equation 2 can be derived, where *a+r* refers to the number of advancing and retracting valves. Here, it can be seen that the sum of the friction ($\mathbf{F}_{\text{fric,i}}$), cutting ($\mathbf{F}_{\text{cut,i}}$) and external forces ($\mathbf{F}_{\text{ext,i}}$) of the advancing and retracting valves are equal to their inertial forces, represented by the mass (m_j) of each valve multiplied by its acceleration ($\mathbf{a}_\text{j}$) [27].

$$\sum_{i=1}^{a+r} (\mathbf{F}_{\text{fric},i} + \mathbf{F}_{\text{cut},i} + \mathbf{F}_{\text{ext},i}) = \sum_{j=1}^{a+r} m_j \mathbf{a}_j. \tag{2}$$

Equation 2 shows that the ovipositor can move forward without external force (and negligible inertia) if the following condition is satisfied (Eq. 3) [20, 27].

$$-\sum_{i=1}^{a} (\mathbf{F}_{\text{fric},i} + \mathbf{F}_{\text{cut},i}) \leq \sum_{j=1}^{r} (\mathbf{F}_{\text{fric},j}) \tag{3}$$

Where *a* refers to the number of advancing valves and *r* refers to the number of retracting (or stationary) valves.

If movement is achieved with approximately zero, or negative external net insertion force, the mechanism can be classified as self-propelling [20]. A self-propelling mechanism helps decrease the risk of buckling because the axial load experienced by the advancing valve is very low [20, 21]. In addition to a self-propelling mechanism, the parasitoid wasp has a further reduced risk of buckling as a result of the short unsupported length of the advancing valve [21].

Multiple minimally invasive needle systems have drawn inspiration from the self-propelling principle to reduce the risk of buckling and minimise tissue damage. [20, 27]. Various designs have been shown to enable effective tissue traversal using the reciprocal motion of (needle) segments inspired by the ovipositor [29, 30]. Frasson *et al.* [31] showed that the reciprocal movement of a segmented custom-made probe with anisotropic surfaces could be used to move tissue relative to the prope without applying external force. Building on these insights, Scali *et al.* [32] made an electrically actuated self-propelled thin needle system with a diameter of merely $1.2\,\mathrm{mm}$. Continuing upon Scali's *et al.* [32] design, Bloemberg *et al.* [28] created an MR-safe manually actuated needle system, able to self-propel through prostate tissue. Both systems [28, 32] use a stationary system to move tissue (mimicking phantoms) towards itself by applying the self-propelling principle. However, in a clinical setting, moving tissue towards a stationary system is neither feasible nor desired. Thus, drawing inspiration from Bloemberg's *et al.* [28] design, Fung-A-Jou *et al.* [25] created a stationary actuation system capable of propelling a needle system through a stationary phantom.

C. *Problem statement and research goal*

To the authors' knowledge, no wasp-inspired system exists that integrates the laser functionality required for TPLA with a stationary actuation system capable of propelling a needle system through a stationary tissue-mimicking phantom. Scali *et al.* [20] demonstrated the feasibility of replacing a needle segment with an optical fibre, whereas Bloemberg *et al.* [28] facilitated optical fibre integration by leaving an open space in the centre of the device. However, both systems still require moving tissue to achieve self-propelling needle insertion, which is not desirable in a clinical setting. Contrarily, the device developed by Fung-A-Jou *et al.* [25] can propel its needle through stationary tissue, but cannot integrate laser functionality as it has no lumen through which an optical fibre can be inserted.

Achieving precise needle insertion and accurate placement to guarantee pre-planned ablation of a malignant lesion has shown to be a challenge [16–18]. MRI/TRUS guidance has helped improve needle placement accuracy [11], but real-time MRI guidance offers multiple advantages over the combined approach [33]. These refer to improved contrast between soft tissue and improved accuracy of real-time temperature measurements [19]. To enable MRI guidance, the materials within the MR environment must be MR-safe or MR-conditional [34, 35].

Therefore, we aimed to develop and evaluate an accurate real-time guided needle system for transperineal laser ablation. To achieve this, the design must meet the following objectives:

- **MR-conditional.** The device can be used in an MR environment to allow for real-time needle and soft tissue visualisation [19].
- **Stationary.** To facilitate its use in a clinical setting the device is stationary and capable of propelling a needle system through a stationary tissue-mimicking phantom. [25].
- **Reciprocally moving needle segments.** To provide accurate needle insertion, the needle is prevented from buckling with the use of reciprocally moving needle segments [19, 20, 25, 28].
- **Laser system integration.** To enable laser functionality needed for TPLA, the device integrates a laser system.

D. *Structure*

Section II outlines the requirements and nice-to-have features for our device to achieve our goal. Following Section II, Section III describes the design process and most important design iterations. Hereafter, Section IV introduces and elaborates on the final design and the prototype. In Section V the method of testing and the final results are presented. This section is followed by a discussion of the results (Section VI) and a conclusion (Section VII).

II. Requirements

A. *Requirements*

The complete device consists of three interconnected but distinct systems: the needle, actuation, and laser system (Fig. 3). To ensure the functioning of our device and compliance with our previously stated goal, we have set up multiple sets of requirements. These requirements are subdivided based on the three distinct systems (Figure 3), with one additional subdivision comprising the general and overall requirements that every distinct system has to conform to. Table I briefly overviews all the requirements and nice-to-haves.

1) *Overall requirements*

1) *MR-safe.* The device poses no hazards when subjected to an MR environment. All parts, except for the needle and laser system, are made of electrically nonconductive, nonmetallic, and nonmagnetic materials, conforming to ASTM F2503 standard practices regarding MR-safe devices. [36].
2) *MR-conditional.* The needle and laser system are safe for use in a three-Tesla MR environment, conforming to ASTM F2503 standard practices regarding MR-conditional devices [35, 36]. This enables its use in a clinical MR environment [35, 37].

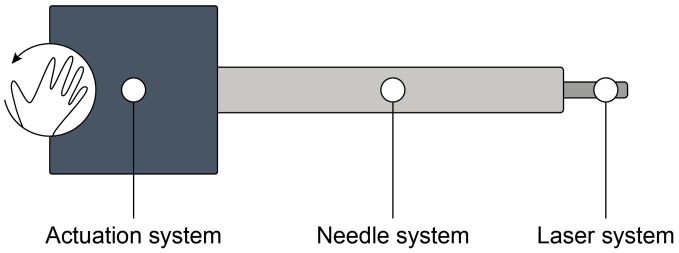


Fig. 3: *Three distinct systems comprising the device. The actuation system is shown in blue, the needle system in light grey, and the laser system in dark grey.*

3) *Manufacturable.* All parts are either bought externally or manufactured in-house. In-house manufactured parts are made using 3D printing, computer numerical controlled machining, or laser cutting.

2) Needle system requirements

4) *Six parallel needle segments.* The needle system contains six parallel needle segments. Scali *et al.* [20] have shown that six needle segments provide effective forward motion, thereby advocating its use.
5) *Sequential needle segment movement.* The needle segments move in a reciprocal movement similar to the wasp-inspired needle movement sequences shown in Scali *et al.* [20], Bloemberg *et al.* [28], and Fung-A-Jou *et al.* [25]. In these movement sequences, five needle segments retract, while one needle segment advances. The authors [20, 25, 28] showed that this wasp-inspired needle movement can be used for effective needle traversal while minimising buckling and tissue damage.
6) >$100\,\mathrm{mm}$ *Needle insertion.* The needle and laser system can traverse a distance of at least $100\,\mathrm{mm}$ in tissue. The distance between the perineum and prostate is a maximum of $97.2\,\mathrm{mm}$ as measured by Horuz *et al.* [38]. The prostate is approximately the size of a peach pit [1]. Thus to reach all areas of the prostate a distance of $100\,\mathrm{mm}$ suffices.
7) $4.0\,\mathrm{mm}$ *Stroke.* The needle segments can translate relative to one another with a maximum distance of $4.0\,\mathrm{mm}$. This exact distance is used to enable direct comparisons with similar wasp-inspired needle designs from Scali *et al.* [20], Bloemberg *et al.* [28], and Fung-A-Jou *et al.* [25].
8) $1.27\,\mathrm{mm}$ *Outer diameter.* The needle segments add up to a maximum outer diameter (O.D.) of $1.27\,\mathrm{mm}$. This maximum O.D. includes space in between the needle segments for the inclusion of a laser system. Although current TPLA procedures are performed with 21 gauge needles [12], it has been shown that the size differences between 18 and 20 gauge, and between 18 and 21 gauge needles, have limited impact on complications [39, 40]. Therefore, to enable laser system integration, the maximum O.D. is set to $1.27\,\mathrm{mm}$ (18 gauge).
9) *Self-propelling motion.* The needle segments exert a near-zero net push force below their critical load. This helps to prevent buckling and minimise tissue damage [20]. To create a near-zero net push force, the friction experienced by the needle segments should be minimised. The reason is that friction adds an external force to the needle segments, thereby affecting the push force of the needle segments [25].

3) Actuation system requirements

10) *Manual actuation.* The device is actuated with a manually applied force. Given this project's scope, the deliberate decision was made to use manual actuation instead of pneumatic actuation. Manual actuation allows for resources to be spent on laser integration and mechanism optimisation, while not interfering with the MR-safe and MR-conditional requirements.
11) *One-handed actuation.* The device can be actuated with the use of one hand. This opens up space for the urologist to perform different tasks during the TPLA procedure, such as using other instruments and responding to complications that might arise during the procedure.
12) *Concurrent laser and needle system actuation.* The actuation system connects the laser system to the needle system while enabling simultaneous and similar translation of both systems with manually applied rotational force. Similar simultaneous translation ensures that the laser system can reach the targeted area in a predictable and controlled manner.

4) Laser system requirements

13) *Replaceable optical fibre.* The optical fibre used for ablation in a TPLA procedure can be replaced during a procedure. During a TPLA procedure, some lesions require ablation twice, due to their size [41]. To comply with currently used single-use optical fibres in TPLA procedures [12], the laser system allows optical fibre replacement during the procedure.
14) > $0.3\,\mathrm{mm}$ *Inner lumen diameter.* The laser system has an inner diameter of at least $0.3\,\mathrm{mm}$. This is needed to comply with currently used optical fibres in TPLA procedures that have a diameter of $0.3\,\mathrm{mm}$ [42].
15) *Stationary optical fibre insertion point.* Although a part of the laser system is allowed to move, one part has to remain stationary to enable optical fibre insertion. This stationary part enables optical fibre insertion regardless of the laser system position.
16) > $10\,\mathrm{mm}$ *Fibre tip to laser or needle system distance.* The tip of the optical fibre can be placed at least $10\,\mathrm{mm}$ away from the nearest (most distal) part of the laser or needle system. Laser light emitted through the optical fibre tip during a TPLA procedure generates substantial heat with energy levels reaching 1800 J per emission [12]. If this energy is released too close to the needle during a TPLA procedure, it can cause heating of the needle thereby causing tissue damage. TPLA procedures therefore require a distance of at least $10\,\mathrm{mm}$ between the optical fibre tip and the needle tip [43].

B. Nice-to-haves

In opposition to the requirements, nice-to-haves are not essential in achieving our previously stated goal. Nice-to-haves illustrate the requirements that our device will need to comply with for future clinical applications. For that reason, our design does not need to comply with the nice-to-haves yet. Nonetheless, our design must not undermine the nice-to-haves as they are essential for future clinical application.

A) *Bio-compatible.* The parts that are inserted into the patient, i.e., the distal tip of the needle and laser systems, should follow the bio-compatibility guidelines described in ISO 10993 [48]. Bio-compatibility refers to a material's capability to fulfil its intended purpose and function in medical therapy without causing any undesirable effects on the recipient or beneficiary [44].

Number	Requirement	Specification	Rationale
General			
1	MR-safe	Device is made from electrically nonconductive, non-metallic, and nonmagnetic materials	Enables use in all MR environments [19, 35]
2	MR-conditional	Laser and needle system pose no known hazards during use in a three Tesla (T) MRI (ASTM F2503)	Enables use in clinical MR environments [35, 37]
3	Manufacturable	Parts can be bought or made with 3D printing, computer numerical modelled (CNC) machining, or laser cutting	Enables manufacturing at the Delft University of Technology
Needle system			
4	Parallel needle segments	6 parallel needle segments	Enables effective forward motion [20]
5	Sequential segment movement	1 advancing, 5 retracting	Enables effective needle traversal while minimising buckling and tissue damage [20, 25, 28]
6	Insertion length	$> 100\,\mathrm{mm}$	Ensures accessibility to all areas of the prostate [38]
7	Stroke	$4.0\,\mathrm{mm}$	Allows direct comparisons with similar wasp-inspired needle designs [20, 25, 28]
8	Outer diameter	$< 1.27\,\mathrm{mm}$	Enables laser system integration with minimal impact on (the number of) complications [39, 40]
9	Self-propelling	$\approx 0\,\mathrm{N}$	Helps prevent buckling and minimise tissue damage [20]
Actuation system			
10	Manual actuation	Actuation by manually applied force	Prevents interference with MR-safe and MR-conditional requirements
11	One-handed actuation	Actuation with one hand	Allows for multitasking by the surgeon
12	Concurrent system actuation	Actuation system connects the laser and needle system	Ensures predictable and controlled movement of the laser and needle system
Laser system			
13	Replaceable optical fibre	Disconnected optical fibre	Allows for compliance with currently used single-use optical fibres in TPLA procedures [12]
14	Inner diameter	$> 0.3\,\mathrm{mm}$	Ensures compatibility with currently used single-use optical fibres [12]
15	Stationary insertion point	Insertion point is independent of laser and needle system movement	Enables optical fibre insertion regardless of needle position.
16	Fibre to system distance	$> 10\,\mathrm{mm}$	Prevents heating of the needle which can cause tissue damage [12, 43]
Nice to haves			
A	Bio-compatible	Parts follow the bio-compatibility guidelines described in ISO 10993	Reduces the risk of eliciting an adverse patient reaction [44]
B	Replaceable	The laser and needle system can be removed from the device without damaging the actuation system	Improves the cost-effectiveness and sustainability of the device [45, 46]
C	MR-compatible	Sterilised parts do not significantly affect the diagnostic quality of an MR image (ASTM F2119)	Maintains clear, reliable, and stable visualisation during an MRI-guided TPLA procedure [47]

TABLE I: *Overview of the requirements and nice-to-haves of the MR-conditional device with integrated laser functionality. Abbreviations: Magnetic Resonance Imaging (MRI), TransPerineal Laser Ablation (TPLA).*

B) *Replaceable laser and needle system.* The laser and needle system can be easily removed from the device. These are the only parts that will come into direct contact with sterile tissue. Therefore, after the procedure, only these parts should be sterilised or replaced, as for the actuation system, disinfection will suffice [49]. Ensuring the actuation system can be reused without sterilisation improves the cost-effectiveness and sustainability of the device [45, 46].

C) *MR-compatible laser and needle system.* The parts in direct contact with sterile tissue are MR-compatible, following ASTM F2119. An MR-compatible part refers to an MR-conditional part that has minimal effect on the diagnostic quality of an MR image [35, 50]. Using MR-compatible invasive parts will ensure that the lesion, needle, and laser system are visualised reliably and stably during an MRI-guided TPLA procedure [47].

III. Design direction

A. *Evolution method*

We used methods derived from the Delft Design Guide as well as a Design Evolution to create our novel bio-inspired

needle system that focuses on MR-conditionality and laser integration for TPLA [51]. Using these design methods to develop our design ensured a thorough and structured design process as well as compliance with all previously determined requirements. The Delft Design Guide consists of a multitude of design methodologies that can be used in various stages of the design process. The Design Evolution communicates how activities, methods, and iterations affect the design [52]. It can be best compared to a structured and visual representation of a design logbook. A Design Evolution is divided per column and row. Each column represents a sequential step in the design process, whereas each row refers to a different information format. In a Design Evolution, the top row consists of symbols that portray the activity type. Below each symbol, in the second row, a very compressed alinea is shown to denote, explain, and evaluate the activity. If and how the activities affect the design is graphically shown below each section (alinea) in the bottom row. An example is provided in Figure 4. As a result of a conversation with Silje Dehli, a teacher at the Delft University of Technology, three main benefits of using a Design Evolution were outlined (Appendix A). These are: it helps structure the design process; it aids the communication of the design and design process to others; and it assists the decision-making regarding design choices while maintaining compliance with requirements (Appendix A). The complete Design Evolution encompassing all our iterative steps and design changes can be found in Appendix B. The most important iterations and design choices that led to the final design are discussed in the upcoming sections.

B. Ideation

Utilising insights derived from the wasp-inspired needle systems created by Fung-A-Jou *et al.* [25], Bloemberg *et al.* [28], and Scali *et al.* [20], and applying methods derived from the Delft Design Guide we started the ideation phase. We created multiple general designs based on brainstorms and How-Tos.

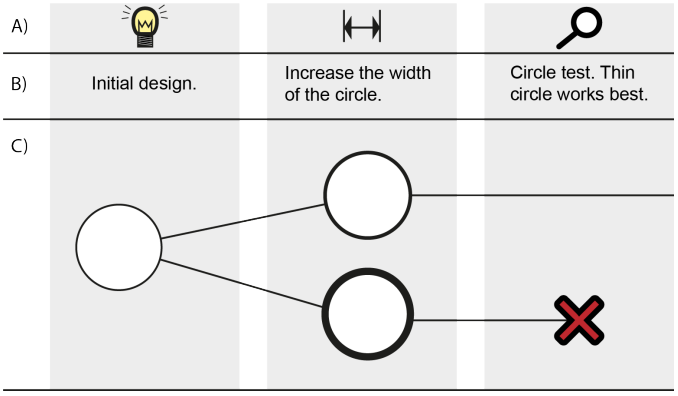


Fig. 4: *Design Evolution example. Each column (grey block) represents a sequential step in the design process. Each row (A, B, and C) represents information per sequential step in a predetermined format. A) Symbol to denote the activity. B) Textual description to explain the activity and communicate results and insights. C) Visual overview of how the activities evolve (affect) the design. The red cross represents the decision to stop with a particular design (direction).*

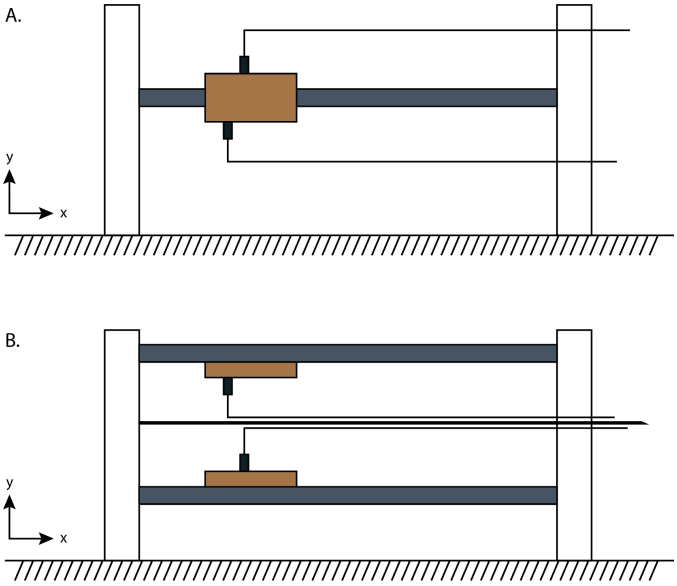


Fig. 5: *Schematic cross-section of two actuation system configurations. A) Rotating inner-axis configuration, with the inner-axis in (dark) blue, the needle rods in black, and the cam in brown. B) Rotating outer cylinder configuration, with the outer cylinder in (dark) blue, the needle rods (thin) and laser system (thick) in black, and the inner-cam in brown.*

All general designs include a rudimentary actuation, needle, and laser system and can be found in Appendix B. As per requirement, every needle system consists of multiple needle segments, called needle rods. By examining and discussing the viability of the general designs we decided on the most promising general design. The most promising general design uses a rotating outer cylinder (part of the actuation system) to rotate an inner-cam (also part of the actuation system). Upon rotation of the inner-cam, needle rods connected to the inner-cam move in a predefined sequence, necessary to reach the self-propelling wasp-inspired reciprocal motion. In this general design, the inner-cam can move freely along its cylindrical axis relative to the outer cylinder. This ensures that when the needle rods self-propel forward they will not need to pull the complete device forward, but only the inner-cam to which they are connected.

The actuation system configuration is the main difference between our chosen general design and the other proposed general designs. In contrast to the other general designs, which have a rotating inner-axis (Fig. 5 A), our proposed design has a rotating outer cylinder (Fig. 5 B). A rotating inner-axis is advantageous for including readily available parts but it provides major challenges regarding laser functionality integration (Fig. 5 A) [25]. These challenges primarily arise from the limited available space in the centre of the actuation system. Thus, to increase the available space in the centre of the device we opted for the only design that uses a rotating outer cylinder (Fig. 5 B, dark blue).

Another reason for choosing the design with the rotating outer cylinder is to facilitate needle insertion. To insert the needle, the laser system and needle rods have to be bundled (outside of the actuation system) before entering the tissue

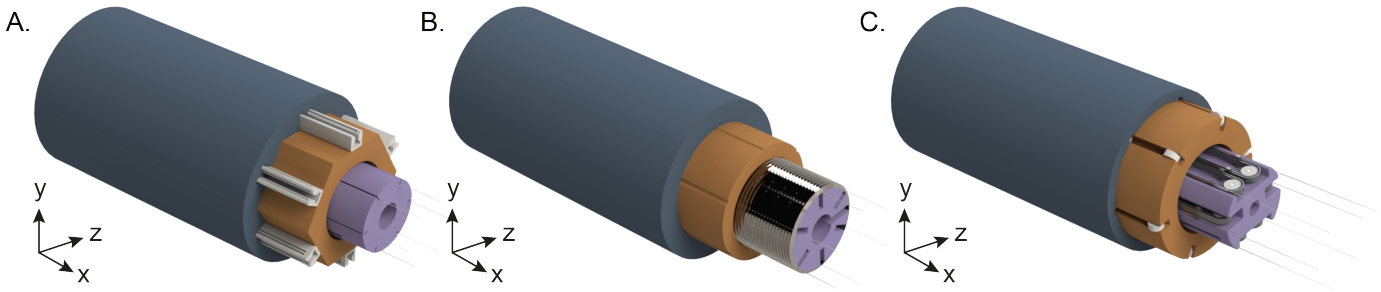


Fig. 6: *Three concepts with distinct mechanisms. The outer cylinder is visualised in dark blue, the needle rods in black, the inner-cam in brown, and the inner-axis in purple. A) Concept Rail. This concept consists of six linear guide rails (white) that glide along the outer cylinder. It has tubes in the inner-axis to prevent buckling of the needle rods. B) Concept Bearing. This concept consists of balls in the outer cylinder that enable translation of the inner-cam. Additionally, it has a harmonica-like contraption (metallic) to prevent needle rod buckling. C) Concept Roller. This concept consists of rollers (white) in the inner-cam that enable inner-cam translation. To prevent buckling of the needle rods this concept has a belt mechanism (black).*

(mimicking phantom). By adopting a rotating outer cylinder design, the needle rods and laser system are relatively close to the centre and therefore require only little bending to converge centrally to form a needle bundle (Fig. 5 B). The rotating inner-axis design, seen in Figure 5 A, would require substantial bending to converge the needle rods to form a needle bundle. Thus, by using a rotating outer cylinder the amount of bending by the needle rods is substantially reduced, eliminating the need for extreme flexibility. In addition, to bend the needle rods a bending structure or mechanism is required, in which increased bending requires increased (normal) force. Increased (normal) force leads to more friction between the needle rods and the bending structure. Thus, by using the rotating outer cylinder design, we can decrease the amount of friction between needle rods and the bending structure. This is advantageous. After all, when the needle rods experience friction outside the tissue (mimicking phantom) it can interfere with the self-propelling movement, due to the generation of external force (Section II, Requirement 9) [25].

C. *Concept design*

After deciding on the general design and design direction three concepts were created with the use of How-Tos. Each concept uses a distinct mechanism to transfer the rotation of the rotating outer cylinder to the inner-cam while allowing for horizontal movement (i.e., along the cylindrical axis) of the inner-cam. Additionally, each concept uses a distinct mechanism to allow for needle rod translation while minimising the chance of buckling. The three concepts can be found in Figure 6 and can be described as follows:

A) The first concept, Concept Rail, visualised in Figure 6 A, has six linear guide rails attached to the inner-cam that enable translation relative to the outer cylinder while allowing for simultaneous rotation of the inner-cam with the outer cylinder. To allow needle rod translation as well as minimising the chance of buckling, the needle rods are enclosed in tubes situated in grooves of the inner-axis. These tubes are not completely enclosed but have a thin opening through which the needle rods can be connected to the inner-cam. This opening is smaller than the diameter of the needle rods to ensure no buckling can occur.

B) The second concept, Concept Bearing, visualised in Figure 6 B, has an outer cylinder that is similar to a linear ball bearing. The outer cylinder includes multiple paths along which balls can roll and move. The inner-cam has grooves that slot around the balls in the outer cylinder. The balls enable translation of the inner-cam relative to the outer cylinder, whereas the grooves in the inner-cam ensure that rotation of the outer cylinder leads to similar rotation of the inner-cam. The needle rods are prevented from buckling with the use of a harmonica-like contraption. This contraption supports and encapsulates the needle rods. Additionally, it enables needle rod and inner-cam translation by ensuring the harmonica-like contraption can be compressed or extended based on the position of the inner-cam.

C) The third concept, Concept Roller, visualised in Figure 6 C, uses rollers attached to the inner-cam that allow for translation of the inner-cam relative to the outer cylinder. These rollers slot into grooves in the outer cylinder ensuring simultaneous rotation of the outer cylinder and inner-cam. The needle rods are prevented from buckling with the use of a ski-lift-inspired belt system. Fasteners that are connected to the belt system encapsulate the needle rods. The belts, each connected to two pulleys, enable translation of the fasteners that hold the needle rods. Thus when the inner-cam or needle rods translate the fasteners and with it the belts move.

To decide on the most promising design, the viability of each concept was evaluated based on the requirements. The main differences in viability between the concepts relate to the amount of friction generated during actuation, which affects the self-propelling mechanism, and the complexity of the mechanisms, which affects the manufacturability. To minimise the friction as well as the inertial forces (Section II, Requirement 9), the weight of the moving parts should be minimised (Newton's second law of motion). The inner-cam in Concept Bearing has the lowest weight, thereby being the most favourable. Nevertheless, Concept Bearing has a relatively complex buckling prevention system that introduces additional

friction into the system due to its spring-like behaviour [25]. Concept Rail, on the other hand, offers the simplest buckling prevention system. Therefore, it was decided to combine the outer cylinder and inner-cam of Concept Bearing with the buckling prevention system of Concept Rail to create a new concept, Concept Groove Bearing.

D. Design iteration

Concept Groove Bearing, visualised in Figure 7, is based on the previously mentioned Concept Rail and Concept Bearing. Concept Groove Bearing is divided into four systems that all required further optimisation, iteration and research to develop the concept into a functional device. The four systems of our concept can be listed as follows: the needle, actuation, laser, and buckling system.

1) Needle system iteration

The needle system consists of the needle rods and their connected parts (including needle rod connectors and supports). As described in Section III-B the needle rods need to converge centrally outside the actuation system to form a needle bundle.

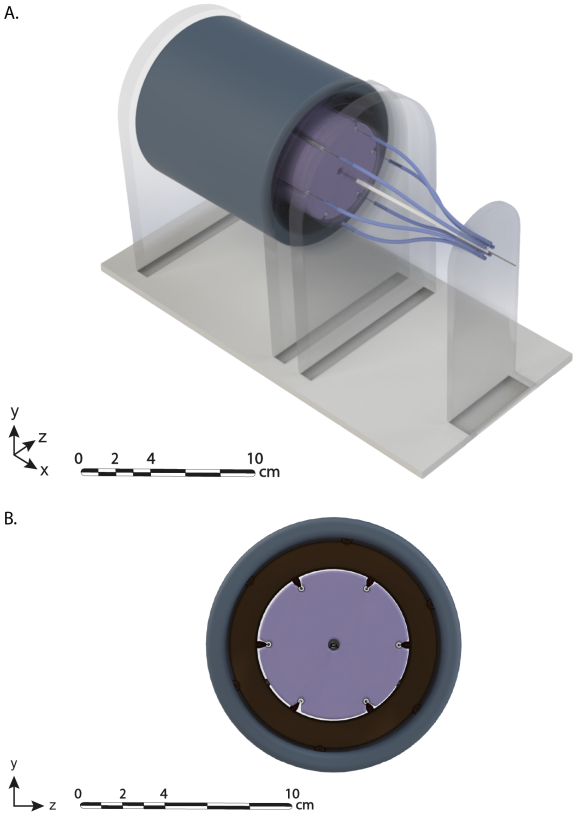


Fig. 7: *Concept Groove Bearing. The concept features an inner-axis (purple) that encloses needle rods (black) in tubes (white) each with a thin opening along its length through which the needle rods are connected to the inner-cam (brown) that surrounds the inner-axis. The inner-cam is connected to the outer cylinder (dark blue) by balls. A) Concept Groove Bearing with the bending structure (light blue). B) Front view of Concept Groove Bearing without the bending structure. The tubes and needle rods can be seen in the key-hole-shaped grooves in the inner-axis.*

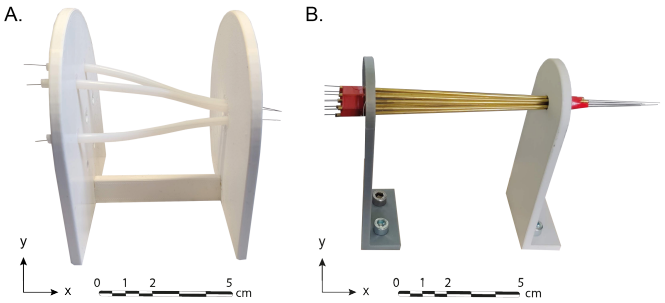


Fig. 8: *Bending system iteration. A) Bending system consisting of PolyTetraFluoroEthylene (PTFE) tubes (white) that converge centrally to enable bundling of the needle rods (black). B) Redesigned bending system consisting of straight brass tubes (gold) that slope inward to enable bundling of the needle rods (black).*

To converge the needle rods a bending structure is required. The first bending structure design consisted of curved (1 mm x 2 mm) PolyTetraFluoroEthylene (PTFE) tubes (PTFE tube shop, Breda, NB, the Netherlands) that converged centrally (Fig. 8). It was found that, even though PTFE is known for its low friction coefficient [53], due to the curve in the PTFE tubes as well as the relatively large convergence distance (radial distance between entry and exit point), the friction was high between the bending structure and needle rods. To address this, straight brass tubes (5060102458425, Albion Alloys, Bournemouth, SW, United Kingdom) were used that had a smaller convergence distance (Fig. 8). To achieve the smaller convergence distance, the grooves through which the needle rods move, similar to the grooves in the inner-axis seen in Figure 7 B, were deepened.

2) Actuation system iteration

The actuation system consists of the outer cylinder, called the linear bearing, and the inner-cam. To ensure low friction movement between the inner-cam and the linear bearing (Section II, Requirement 9) multiple experiments pertaining to the linear bearing design were performed (Appendix B). It was found that using a null-shaped path, shown in Figure 9 A, worked best to reduce friction between the inner-cam and the linear bearing. Nonetheless, due to the relatively long length (120 mm) and thinness (7 mm - 10 mm) of the part that contains the balls (Fig. 9 A), it warped. This resulted in balls falling out of these parts after assembling the linear bearing (Fig. 9 B). To prevent this, a cover encircling the linear bearing was used to apply a distributed circumferential force to the linear bearing. Following multiple experiments (Appendix B), the optimal force magnitude was found where the balls could move without much friction while remaining in the linear bearing.

3) Laser system iteration

The laser system is used to insert an optical fibre at the desired position in the prostate. To ensure the needle system moves to the desired position concurrent with the needle system (Section II, Requirement 12) it is connected to the inner-cam. To connect the laser system to the inner-cam a ring-shaped path was engraved into the inner-cam (Fig. 10 A). By placing a laser system connector, seen in Figure 10 B, in the circular

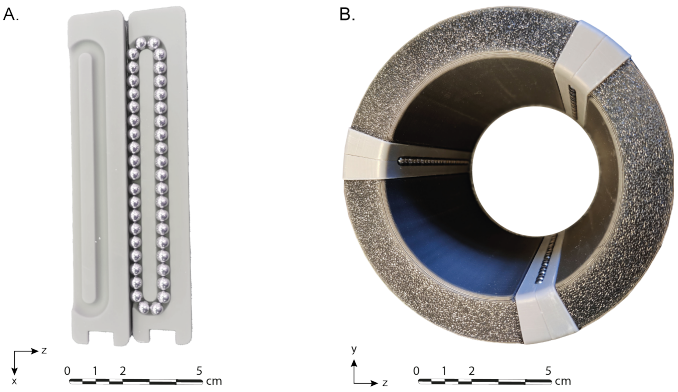


Fig. 9: *Linear bearing (outer cylinder) design. A) The linear bearing parts (light grey) that contain the balls (metallic) in a null-shaped path. B) The linear bearing assembly with the linear bearing parts containing the balls in light grey and the other linear bearing parts in black.*

path, translation of the inner-cam leads to translation of the laser system. One drawback of this approach is that translation of the laser system creates a dynamic insertion point. As stated in Section II, the device has to have a stationary insertion point (Section II, Requirement 15). For this reason, two slide-fitting tubes were used. One tube, the intermediary tube, is stationary and connected to the front (left in Figure 7) of the device, while the other tube, the laser needle, can translate along with the inner-cam.

4) Buckling prevention system iteration

To ensure the needle rods can effectively penetrate tissue they need to be prevented from buckling. Therefore, as shown by Fung-A-Jou *et al.* [25], the needle rods must be enclosed with relatively short intervals (around two centimetres). To achieve this, we tried enclosing the needle rods in PTFE tubes with an inner diameter of one millimetre (PTFE tube shop, Breda, NB, the Netherlands), situated in the inner-axis. These tubes had a thin opening along their length through which the needle rods could be connected to the inner-cam. This, however, created a dilemma. If the opening is larger than the diameter of the needle rods they can buckle, but if

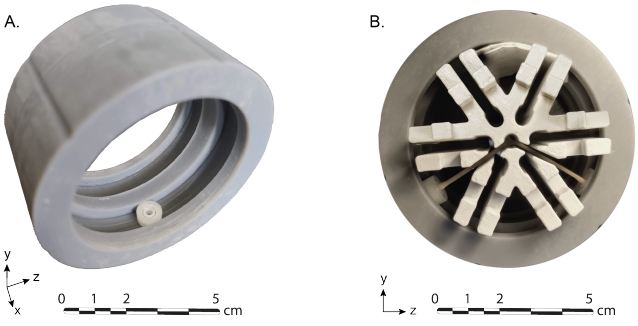


Fig. 10: *Inner-cam laser system connection. A) The inner-cam (grey) with two engraved paths and a ball bearing (white) in the ring-shaped path. B) Front view of the inner-cam (grey), the split inner-axis (white), and the laser system (triangular-shaped part connected to two white ball bearings).*

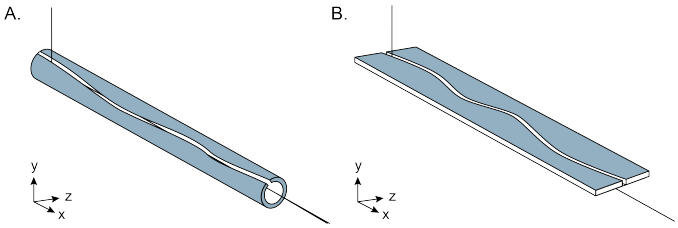


Fig. 11: *Buckling prevention system iteration. A) Schematic overview of the tube buckling prevention system. The needle rods (black) are encapsulated in tubes (light blue) that have a wave-like opening, thereby preventing buckling. B) Schematic overview of the redesigned buckling prevention system. The needle rods (black) sit below a rectangular part (light blue) with a wave-like opening, preventing buckling in the upward (positive y) direction.*

the opening is smaller than the diameter of the needle rod it requires a very thin and thus fragile connection system. Thus, either fragile connectors or large-diameter needle rods were to be used, both undesirable. With the use of multiple How-Tos, we were able to create a solution that circumvents this dilemma. Instead of enclosing the needle rods in PTFE tubes with a thin opening along the length of the tube (Fig. 7), we opted for enclosing the needle rods in tubes that have a wave-like opening, similar to Figure 11 A. This enables needle rod translation while lowering the chance of buckling. However, due to manufacturing constraints, these tubes could not be made. For that reason, we simplified the design such that it could be manufactured (Fig. 11 B). This simplified design can be inserted into the inner-axis to prevent buckling. Additional information regarding the design and its validation can be found in Appendix C.

IV. Design

A. *Overall design*

Following numerous iterative steps and design changes we made a stationary design that integrates MR-conditionality, reciprocally moving needle segments, and laser functionality for TPLA. This design is discussed by dividing it into four systems: the needle, actuation, laser, and buckling prevention system.

1) Needle system

To minimise tissue damage and the possibility of buckling, the needle system moves according to the self-propelling principle found in parasitoid wasps [20]. To achieve self-propelling movement, the needle system consists of six needle segments, called needle rods, that can translate in a sequential motion relative to one another. This sequence controls the specific movement of the needle rods, where one needle rod advances and five needle rods retract. This is visualised in Figure 12 C. The six needle rods surround one large needle, the laser needle (Figure 12 A and B). Together, they form the needle or needle bundle. The laser needle is not part of the needle rod sequence and is used to insert the optical fibre needed for TPLA [9]. To move the laser needle forward, it is indirectly connected to the needle rods via the inner-cam. The inner-cam is part of

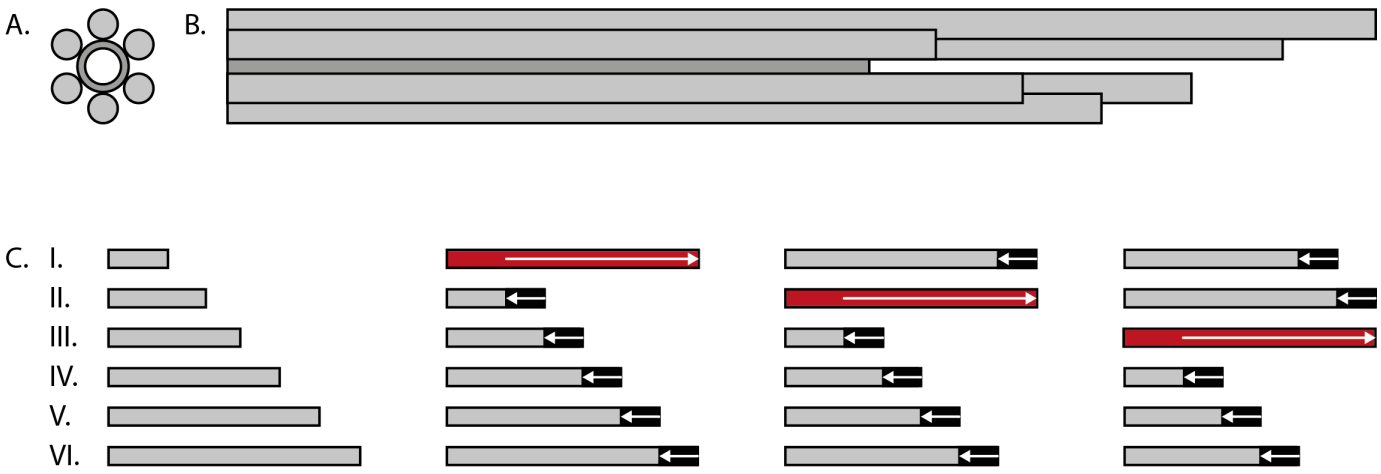


Fig. 12: *Needle system and needle rod sequence overview with light grey needle rods and a dark grey laser needle. A) Front view of the needle rods and laser needle B) Side view of the needle rods and laser needle. C) Movement sequence of the needle rods. Every cycle one needle rod advances (red) and five needle rods (grey) retract (previous position in black).*

the actuation system and moves the needle rods according to the predefined sequence upon actuation.

*2) **Actuation system***

To generate sequential rod movement a global actuation system is used, eliminating the need for individual rod actuation and simplifying the overall design. This actuation system uses one-handed rotation of the linear bearing as input. This rotational input is transferred to the inner-cam which, as its name suggests, lays within the linear bearing. The linear bearing acts as a linear bearing, meaning that even though the inner-cam and linear bearing rotate as one single unit, the inner-cam can independently translate relative to the linear bearing along its cylindrical axis, i.e., x-axis. Balls inside the linear bearing enable low friction translation of the inner-cam relative to the linear bearing along its x-axis. Grooves in the inner-cam that slot around the balls in the linear bearing eliminate rotation of the inner-cam relative to the linear bearing. This is visualised in Figure 13. Within the inner-cam, two paths are engraved. The first path is shaped like a check-mark and houses six ball bearings connected to the six needle rods (Appendix D-A). The second path is straight and contains two ball bearings, both attached to the laser needle. By limiting needle rod movement to the x-axis, rotation of the inner-cam leads to sequential movement of the needle rods along the x-axis in the first path and no movement of the laser needle in the second path. Figure 13 IV-VI shows this actuation process. For clarity, this figure (Fig. 13) does not show how the movement of the needle rods is limited to the x-axis. But, in short, the needle rods are encapsulated by a part, the inner-axis, that prohibits movement along all axes except the x-axis. This is further elaborated on in Section IV-A4.

To achieve the sequential movement needed to self-propel the needle rods, the actuation system translates all the needle rods when rotated. Translation of the needle rods results from the check-mark-shaped path, which upon clockwise rotation, retracts five needle rods while simultaneously advancing one needle rod. Figure 13 V illustrates this movement. When the needle rods are inserted into stationary tissue, they experience friction at the distal ends. If no external forces are applied and the friction generated between the stationary tissue and the retracting needle rods ($\mathbf{F}_{\mathrm{fric,j}}$) is higher than the friction and cutting forces ($\mathbf{F}_{\mathrm{fric,i}}$, $\mathbf{F}_{\mathrm{cut,i}}$) experienced by the advancing needle rod, the needle rods propel forward through stationary tissue (Eq. 4) [20, 27]. As described in Section IV-A1, the needle rods are indirectly connected to the laser needle via the inner-cam. Thus, if the needle rods propel in the forward direction, they move the inner-cam and with it the laser needle forward. However, the laser needle experiences friction and a cutting force ($\mathbf{F}_{\mathrm{laser,j}}$) when propelled forward in tissue (Fig. 14). For that reason, the needle propels forward only if the resultant force of the needle rods ($\mathbf{F}_{\mathrm{rod}}$) is larger than the opposite forces experienced by the laser needle ($\mathbf{F}_{\mathrm{laser}}$). Therefore, only after satisfying Equation 5 does the needle propel forward through stationary tissue, similar to the movement seen in Figure 13 VI and Figure 12 C.

$$-\sum_{i=1}^{a}(\mathbf{F}_{\mathrm{fric},i}+\mathbf{F}_{\mathrm{cut},i}) \leq \sum_{j=1}^{r}(\mathbf{F}_{\mathrm{fric},j}) \tag{4}$$

Where a refers to the advancing needle rod(s) and r refers to the retracting needle rods.

$$\mathbf{F}_{\mathrm{rod}}+\mathbf{F}_{\mathrm{laser}} \geq 0 \tag{5}$$

It is important to note that these equations (Eq. 4 and 5) only hold during the clockwise rotation of the actuation system. If the actuation system is rotated counterclockwise these equations (Eq. 4 and 5) do not hold. Counterclockwise rotation advances five needle rods and retracts one needle rod. The retracting needle rod experiences friction forces, whereas the advancing needle rods experience friction and cutting or pushing forces. If the pushing and friction forces of the advancing needle rods are larger than the friction force of the retracting needle rod, the needle propels backwards.

*3) **Laser system***

The laser needle, attached to two ball bearings within the inner-cam path (see Fig. 13 IV), moves concurrently with the

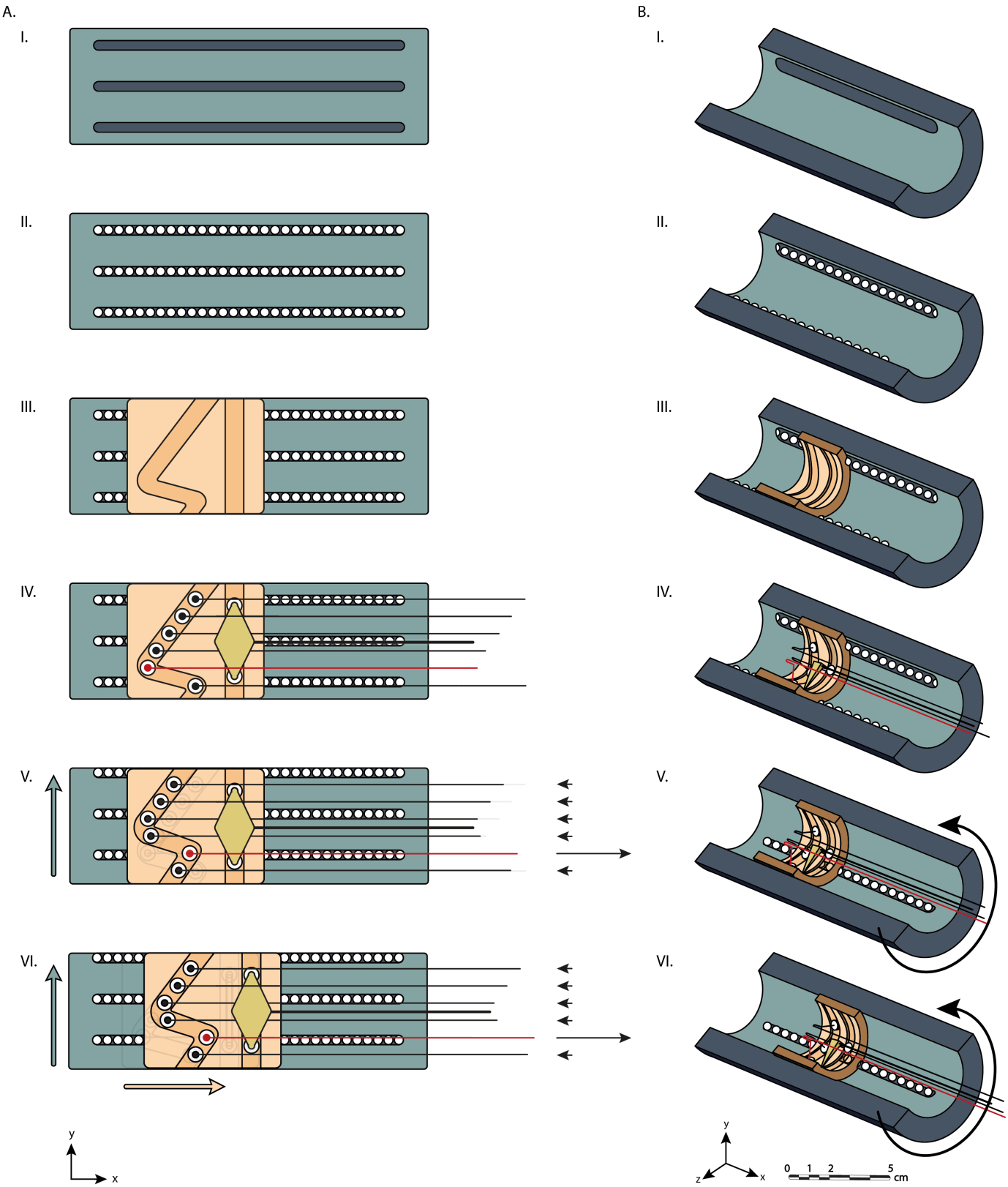


Fig. 13: *Simplified needle system overview with the linear bearing in dark blue and light blue, the balls in white, the inner-cam in orange and brown (with the inner-cam paths accentuated in darker orange), the laser needle holder in yellow, the ball bearings in white, the advancing needle rod in red, and the retracting needle rods in black. A) 2Two-dimensional schematic overview of the actuation system. B) Three-dimensional schematic cross-section of the actuation system. I) The linear bearing II) The linear bearing with incorporated balls III) The inner-cam within the linear bearing with the incorporated balls. IV) The complete actuation system. V) The actuation system and needle rod movement after turning the linear bearing when the needle rods do not experience friction. VI) The actuation system and needle rod movement after turning the linear bearing when the needles do experience friction.*

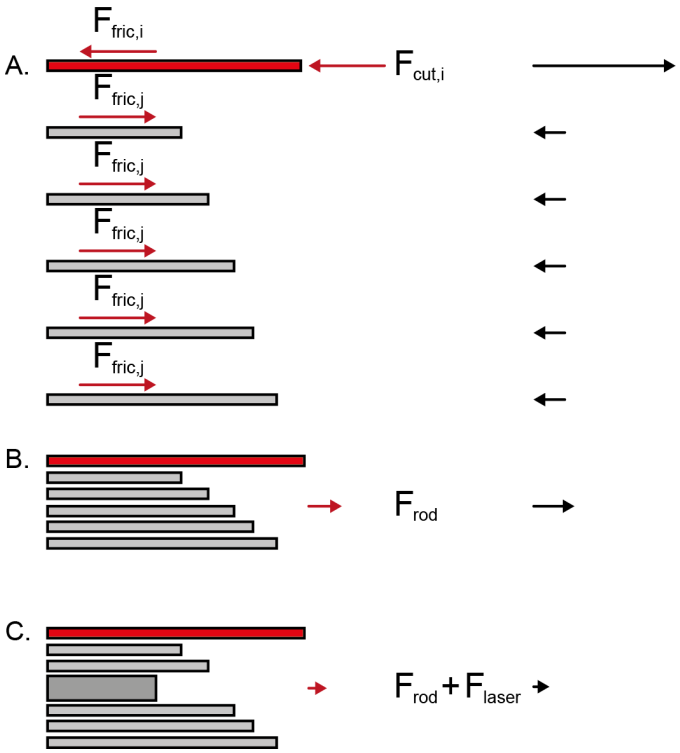


Fig. 14: *Forces acting upon the laser needle and needle rods. Red arrows represent the forces, whereas black arrows represent the movements. The top rod (red) is the advancing rod, whereas the other needle rods (grey) are retracting. A) Forces and movement per needle rod. B) Resultant movement and force of the needle rods in stationary tissue. C) Resultant movement and force of the needle in stationary tissue, if the forces acting upon the laser needle are taken into account.*

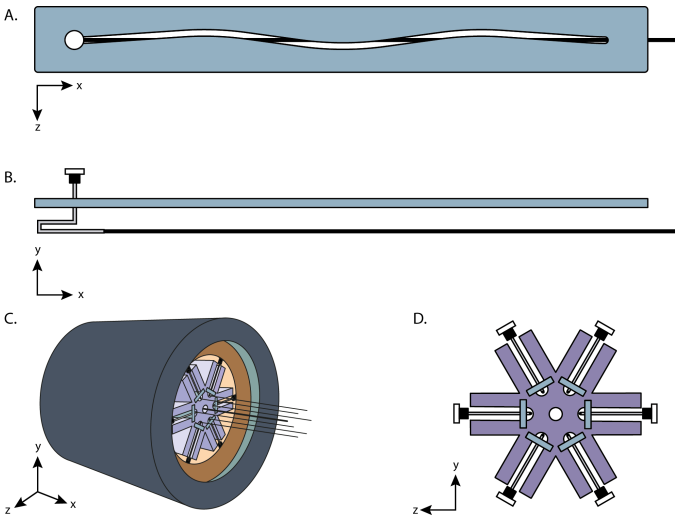


Fig. 15: *Schematic illustration of the buckling prevention system with the needle rod guide visualised in blue, the inner-axis in purple, the needle rod connectors in grey, the needle rods in black, and the ball bearing in white. A) Top view of the needle rod guide with the accompanying needle rod parts. B) Side view of the needle rod guide with the accompanying needle rod parts. C) Schematic overview of the device's core (with the inner-axis in purple). D) Front view of the inner-axis with the needle rod guide and accompanying needle rod parts.*

inner-cam. For this reason, the laser needle moves forward if the self-propelling motion of the needle rods move the inner-cam forward. When the distal end of the needle bundle is inserted into a substance, the smaller needle rods surrounding the laser needle create a lumen through which the laser needle moves. Repeated rotation of the linear bearing creates the self-propelling motion sequence of the needle rods described in Section IV-A1, which moves the actuation mechanism, and thus the laser needle, to the desired location inside the phantom. After arriving at the desired location an optical fibre can be manually inserted into the laser needle. This can be done via a funnel connected to an intermediary tube. This intermediary tube sits around the laser needle and enables the sliding of the laser needle along its cylindrical axis, i.e., the x-axis (Appendix E).

During optical fibre insertion (through the laser needle), the optical fibre moves from the intermediary tube into the laser needle. When it moves from the intermediary tube to the laser needle it experiences a slight bump (resulting from the diameter difference). It is unclear whether this damages the optical fibre tip, hence this is evaluated in the upcoming section. After moving the optical fibre through the laser needle, it has to protrude about one centimetre from the most distal needle (rod) [42]. This is done to prevent heating of the needle (rods), which could lead to tissue damage and scarring. Instead of manually pushing the optical fibre to a safe distance, the linear bearing is rotated in the opposite direction (counterclockwise). This moves the needle rods and the laser needle backwards, while the optical fibre is kept at the desired location. After reaching a safe distance, the optical fibre can be used to transmit laser light to thermally damage and ablate at the urologist's will.

4) Buckling prevention system

A buckling prevention system was developed to allow effective penetration of the needle rods through various tissues. Without this system, the needle rods would be prone to buckling, thus not penetrating the material as desired. Our system prevents buckling by limiting movement of the needle rods along the y- and z-axes, while still enabling translation along the x-axis. The system consists of two distinct parts, the needle rod guide and the inner-axis. The needle rod guide is a rectangular part with a sine-wave-shaped cut, visualised in Figure 15 A and B. This part, the needle rod guide, slots into the inner-axis and prevents movement of the needle in the y-direction in Figure 15 B. More information regarding the design of the needle guide can be found in Appendix C. The inner-axis has a hexagonal cross-section, portrayed in Figure 15 C, that restricts side-to-side and downward or upward movement of the needle rod (the z- and y-directions in Figure 15 A and B). Combined, the parts greatly lower the chance of buckling while still allowing for needle rod translation along the x-axis.

B. Prototype

To evaluate the proposed design, we made a prototype that can be seen in Figure 16 A. This prototype consists of 20

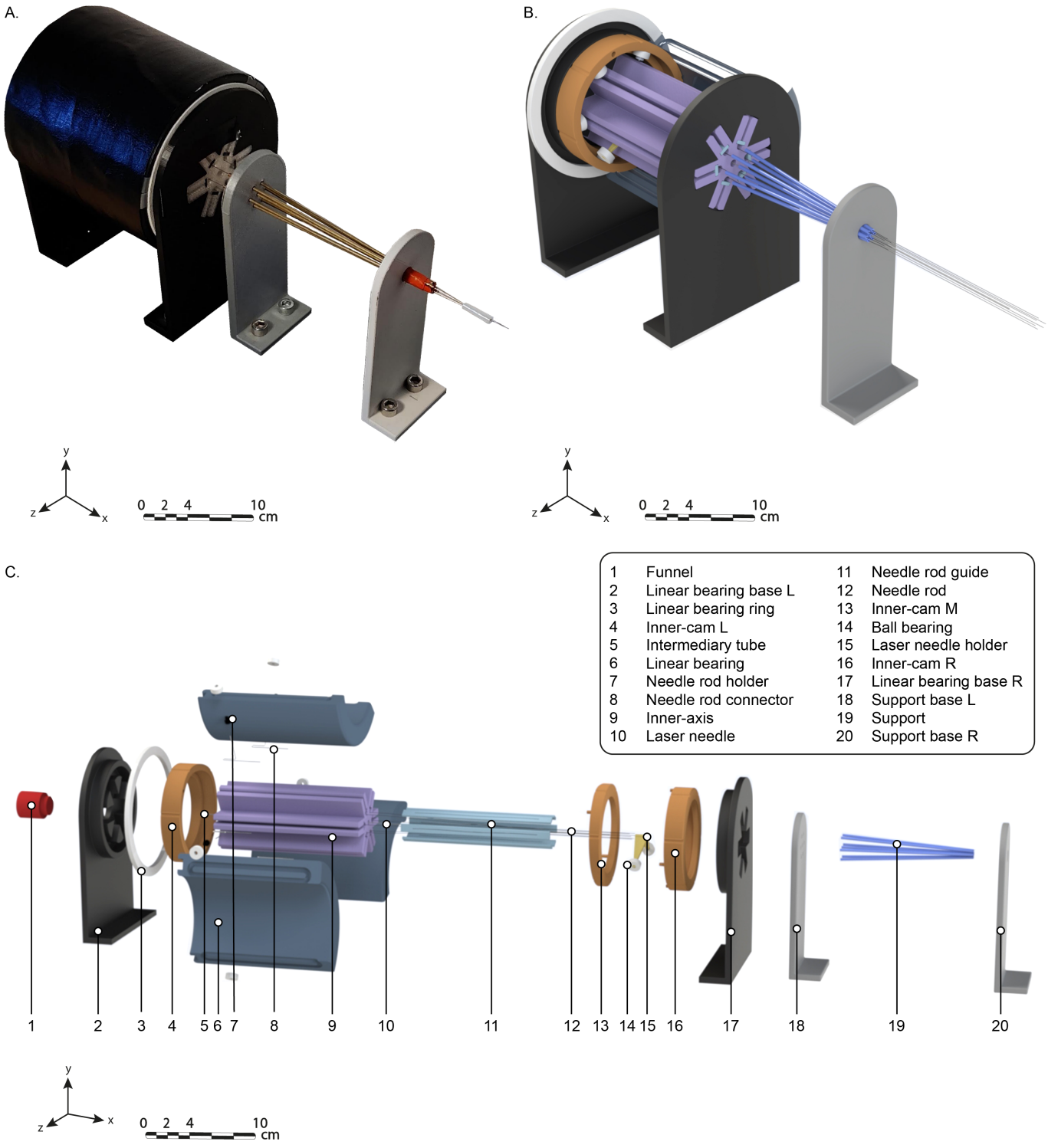


Fig. 16: *System overview of the final prototype and design. A) Final prototype. B) Final design with two linear bearing sub-assemblies (part 6), inner-cam M (part 13), inner-cam R (part 16), and support base R removed (part 20). C) Exploded view of the design where the parts are portrayed in the same colours as in B. The parts numbered in this exploded view can be found in more detail in Table II. Note: the linear bearing balls are not visualised. Additionally, the linear bearing and inner-axis are visualised as sub-assemblies.*

distinct parts, displayed in Figure 16 C and listed in Table II. The majority of the parts (i.e., 13) are custom-designed and 3D printed. Parts requiring low dimensional accuracy were printed with Fused Deposition Modelling (FDM) using an Ultimaker 5S (Ultimaker, Utrecht, UT, the Netherlands) to optimise efficiency and resource use. In contrast, parts requiring high dimensional accuracy were printed with StereoLithography (SLA) using a Formlabs 3B (Formlabs, Somerville, MA,

USA). This directly influenced the materials used. All FDM 3D printed parts were made from PolyLactic Acid (PLA) (Ultimaker, Utrecht, UT, the Netherlands) and all SLA-printed parts were made with the Form grey resin (Formlabs, Somerville, MA, USA). Both materials are non-ferrous and thus comply with the MR-safe requirement (Section II, Requirement 1). More information regarding design implications resulting from the MR-safe and MR-conditional requirements can be found in Appendix E.

*1) **Material***

To enable the use of our device in an MR environment, all long thin-walled tubes were made from materials with low magnetic susceptibility. Long thin-walled tubes are only made from selective materials, thereby severely affecting the number of material options. Brass and aluminium were the only available materials with low magnetic susceptibility and thus the only materials that complied with the MR-conditional requirement [35, 54]. The laser needle, intermediary tube, and needle rod connector were made from aluminium (5060102458739, Albion Alloys, Bournemouth, SW, United Kingdom), whereas the needle rod and laser needle support were made from brass (5060102458425, Albion Alloys, Bournemouth, SW, United Kingdom). Although these materials suffice for the non-invasive parts, the laser needle would benefit from a different material, such as titanium to enable invasive use with minimal image artefacts [55].

Part	Name	Qty	Component source	Material
1	Funnel	1	3D printed (SLA)	Form grey
2	Linear bearing base L	1	3D printed (FDM)	PLA
3	Linear bearing ring	1	3D printed (FDM)	PLA
4	Inner-cam L	1	3D printed (SLA)	Form grey
5	Intermediary tube	1	Bought	Aluminium
6	Linear bearing	3	3D printed (SLA, FDM)	Form grey, PLA
7	Needle rod holder	6	3D printed (SLA)	Form grey
8	Needle rod connector	6	Bought	Aluminium
9	Inner-axis	1	3D printed (FDM)	PLA
10	Laser needle	1	Bought	Aluminium
11	Needle rod guide	6	Lasercut	Acryl
12	Needle rod	6	Bought	Spring steel
13	Inner-cam M	1	3D printed (SLA)	Form grey
14	Ball bearing	8	Bought	Glass, Xirodur B180
15	Laser needle holder	1	3D printed (SLA)	Form grey
16	Inner-cam R	1	3D printed (SLA)	Form grey
17	Linear bearing base R	1	3D printed (FDM)	PLA
18	Support base L	1	3D printed (FDM)	PLA
19	Support	6	Bought	Brass
20	Support base R	1	3D printed (FDM)	PLA

TABLE II: *Parts overview including the name of the part, its respective source, material, and quantity. If multiple components have the same function but are different in design they are denoted with either an L, M, or R, standing for left, middle, and right, respectively. Abbreviations: Quantity (Qty), PolyLactic Acid (PLA), Fused Deposition Modelling (FDM), and StereoLithography (SLA).*

The needle guides and ball bearings are the only non-3D printed parts that were made from MR-safe materials. The needle guides were made with acryl and the ball bearings were made from glass balls in a non-magnetic housing. The needle guides were supposed to be made with PTFE, as PTFE has a remarkably low friction coefficient with metal alloys [53]. Regardless, laser cutting PTFE was prohibited due to the possible release of toxic gasses. In addition, using computer numerical controlled machining to manufacture the needle guides was discouraged due to the small scale. For that reason, it was decided to use acryl (1100060003, Astariglas, Jakarta, Java, Indonesia) instead. Acryl is a non-ferrous, cost-effective, and durable material suited for laser cutting, thereby ideal for our purposes [56]. The ball bearings were store-bought Xiros® radial deep groove ball bearings (BB-623-B180-30-GL, IGUS, Cologne NRW, Germany), consisting of glass balls in a non-magnetic Xirodur B180 housing. These ball bearings were the smallest available ball bearings made from MR-safe (or MR-conditional) materials.

Two materials were included in our prototype that are neither MR-safe nor MR-conditional. Four-millimetre steel balls (8720688100459, Neita Techniek B.V., Utrecht, Ut, the Netherlands) were used, as glass balls (HH55, CARL ROTH, Karlsruhe, BW, Germany) were out of stock. Furthermore, $0.3\,\mathrm{mm}$ diameter spring steel needle rods (4069235244937, Evek GmbH, Mülheim, NRW, Germany) were used instead of Nitinol needle rods. Nitinol is an MR-conditional superelastic shape memory alloy suitable for medical applications [57]. Nevertheless, due to its limited availability, we had to opt for spring steel in the actual prototype. Nonetheless, Nitinol needle rods can replace the spring steel needle rods if availability improves without design alterations (Appendix D-C). Similarly, the metal balls can be replaced with glass balls if availability improves. An overview of the parts that use different materials from their proposed materials can be found in Appendix IV.

*2) **Needle system***

The needle system, different from the needle (consisting of the needle rods and laser needle), consists of ball bearings (Fig. 16, Part 14), needle rod holders (Fig. 16, Part 7), needle rod connectors (Fig. 16, Part 8), supports (Fig. 16, Part 19), and the needle rods (Fig. 16, Part 12). All parts are store-bought except for the needle rod holders. Due to their small size, the needle rod holders (Fig. 16, Part 7) were made with SLA. SLA is a process in which a laser is applied to cure and solidify photo-sensitive resins layer-by-layer selectively. SLA has limited material availability, but offers high surface smoothness and precision [58]. The needle rod connectors (Fig. 16, Part 8) were made by cutting aluminium tubes to the desired length after which they were deformed to an S-shape. This is further elaborated on in Appendix G. The other store-bought parts in the needle system were not altered.

*3) **Actuation system***

The actuation system consists of the linear bearing (Fig. 16, Part 6), linear bearing ring (Fig. 16, Part 3), inner-cam (Fig. 16, Part 4, 13, and 16) and the balls (in the linear bearing).

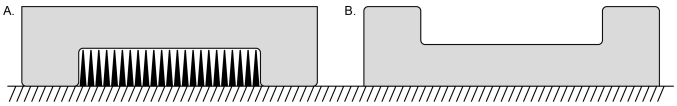


Fig. 17: *Identical parts with different print orientations. A) Shows the part with an overhang that needs support. B) Shows the same part, but with a different orientation so that it does not need support.*

The inner-cam and linear bearing were both (partially) printed using SLA. High accuracy and thus SLA was required to make the ball grooves in the linear bearing. This level of accuracy was not needed in other areas of the linear bearing. Therefore, to speed up the building process, we chose to split the linear bearing into nine parts. Six parts were printed using SLA, while the remaining three were printed using FDM. FDM is a process in which plastic is heated and extruded through a nozzle, depositing the material layer-by-layer to form a three-dimensional object [58].

The FDM-printed linear bearing parts were printed with a $0.15\,\mathrm{mm}$ resolution and orientated such that no support was needed. Using supports leads to more material usage and extends the print time [59]. More importantly, it negatively impacts the surface smoothness [60], which for a linear bearing is especially important. Supports are needed when larger overhangs or undercuts are present in the design [61]. By adjusting the orientation overhangs and undercuts can be eliminated. An example of how changing the orientation helps to eliminate support can be seen in Figure 17.

The SLA-printed linear bearing parts were printed with a $0.025\,\mathrm{mm}$ resolution and similarly designed such that no support was needed. These parts were oriented such that the majority of the grooves were parallel with the print bed. Aligning the grooves with the print bed lowers friction in the desired (x) axis [62], see Figure 18. As the SLA printed parts were made using resin, some excess fluid remained on the part after printing. For this reason, the parts were post-processed in an alcohol washing station (Formlabs, Somerville, MA, USA). Hereafter, to improve the physical properties of the parts, they were cured in a Form Cure Station (Formlabs, Somerville, MA, USA).

To assemble the linear bearing, the SLA and FDM printed linear bearing parts were first sanded to smooth out the edges and ensure a tight fit. After sanding they were assembled to form the linear bearing. After assembly, the linear bearing ring was placed into the linear bearing notches to secure everything in place. Hereafter, balls were added to the linear bearing grooves, completing the assembly.

The inner-cam was split into three parts (Fig. 16, Part 4, 13, and 16) to eliminate support usage and thus optimise surface smoothness. After following the same steps and setup as for the previously mentioned SLA printed parts, the parts were assembled using Bison super glue (8710439075990, Bison International, Goes, ZE, the Netherlands). After assembly, the parts were smoothed by sanding all surfaces. Special care was taken to deepen the grooves to ensure that they could still slide along the balls in the linear bearing. A complete list of all assembly steps needed to assemble the prototype can be found in Appendix H.

4) Laser system

The laser system consists of the funnel (Fig. 16, Part 1), intermediary tube (Fig. 16, Part 5), laser needle (Fig. 16, Part 10), and laser needle holder (Fig. 16, Part 15). The two printed parts (Fig. 16, Part 1 and 15) were printed using SLA. The funnel was printed by aligning the print bed perpendicular to the insertion hole (x-axis). Similarly to the above-mentioned SLA printed parts, the use of support was avoided. Contrarily, to ensure an effective print, the laser needle holder was printed with support. No matter the orientation, overhangs were unavoidable. For that reason, supports were added to print the laser needle holder. The needle holder was aligned similarly to the funnel, meaning that the hole (x-axis) was aligned perpendicular to the print bed. After printing, all SLA post-processing steps mentioned in Section IV-B3, as well as some additional post-processing steps were done. The additional post-processing steps consist of support removal for the laser needle holder and drilling in both the laser needle holder and funnel to guarantee the desired hole diameter.

5) Buckling prevention system

The buckling prevention system consists of two parts, the inner-axis (Fig. 16, Part 9) and the needle rod guides (Fig. 16, Part 11). The needle rod guide was made using a two-millimetre thick extruded acryl plate that was laser cut into the desired shape (Appendix C) using the Lion 900 (Lion Laser Systems, Breda, NB, the Netherlands). For post-processing, the cut was sanded and the protective covers were removed from the acryl part. The inner-axis, split into two parts to enable assembly, was printed using FDM. In theory, to minimise friction between the needle rods and the inner-axis, it would be best to print the inner-axis such that the FDM layers are parallel to the movement direction of the needle rods and laser needle (Fig. 18). However, printing in this orientation required adding lots of supports that increase surface roughness. Increased surface roughness would lead to increased friction effectively negating the friction-reducing benefit of parallel orientation. Therefore, the inner-axis was printed with the cylindrical axis perpendicular to the built plate. The technical drawings of all the parts can be found in Appendix I.

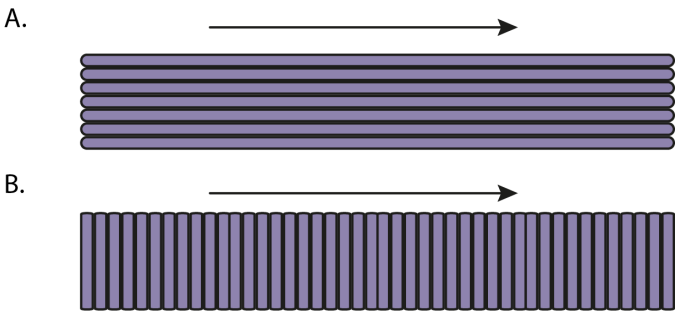


Fig. 18: *Schematic illustration of the Fused Deposition Modelling (FDM) layering. A) Movement parallel to the layer B) Movement perpendicular to the layer.*

V. Evaluation

Four experiments were conducted to evaluate the design's performance: The first experiment was used to evaluate the device's efficiency; the second and third experiments were used to perform multiple force measurements; the last experiment was used to assess optical fibre tip damage after optical fibre insertion.

A. *Slip ratio experiment*

1) *Goal*

The purpose of the experiment was to determine the efficiency of the self-propelling mechanism in three gelatin phantoms with gelatin concentrations of 5%, 10%, and 15% by weight in water. Different weight percentages result in different stiffnesses, in which higher weight percentages correspond to higher stiffnesses. The body contains a wide range of tissues, all with different stiffnesses. By testing phantoms with different stiffnesses, real-world behaviour can be better predicted. To provide a reference, the weight percentages (wt%) of 5%, 10%, and 15% of gelatin in water approximately correspond to an elastic modulus of 5, 17, and 31 kPa respectively [63].

To evaluate the efficiency of the self-propelling mechanism, the slip ratio of the needle rods relative to the gelatin phantoms was used. During a cycle, the needle rods can theoretically move a certain distance forward through the gelatin phantom. In practice, the needles can slip, thus moving a lesser distance [20]. The relationship between the measured distance (d_m) and the theoretical maximum distance (d_t) is the slip ratio (s_r) (Eq. 6). The theoretical maximum distance is based on the assumption that the gelatin phantom does not move relative to the needles. The maximum forward movement of the needles is 6/5 of the maximum stroke distance ($4\,\mathrm{mm}$) multiplied by the number of cycles. A slip ratio of zero means that there is no slip, whereas a slip ratio of one means that the needles have not moved relative to the gelatin phantom.

$$s_r = 1 - \frac{d_m}{d_t} \tag{6}$$

Eight different experiment conditions, presented in Table III, were evaluated. The device excluding the laser system, i.e., the laser needle, laser needle holder, funnel, and intermediary tube, was tested five times per experiment condition. Similarly, the device that incorporated the laser system was tested five times per experiment condition.

2) *Variables*

The independent variables were the gelatin concentration, laser system inclusion, and the number of completed cycles (5, 10, 15, and 20 rotations). The dependent variable was the measured distance of the furthest needle rod. The control variables were the room temperature (19°C), humidity (70%), initial insertion depth of the needle ($20\,\mathrm{mm}$), and the angular velocity of the linear bearing ($\frac{2\pi}{12}\ \mathrm{rad\ s^{-1}}$).

3) *Setup*

The day before the experiment, three gelatin phantoms were made. The 5 wt%, 10 wt%, and 15 wt% gelatin phantoms were made by adding $190\,\mathrm{mL}$, $180\,\mathrm{mL}$, and $170\,\mathrm{mL}$ boiling water to three different containers (200x80x50 mm^3) containing $10\,\mathrm{g}$, $20\,\mathrm{g}$, and $30\,\mathrm{g}$ of gelatin powder (8710466605023, Dr. August Oetker KG, Bielefeld, NRW, Germany), respectively. The mixtures were stirred for approximately two minutes until the gelatin powder was completely dissolved. Extra care was taken to eliminate the formation of bubbles in the mixture by careful and slow stirring. After the mixtures were cooled, they were placed in the fridge. A ten-millimetre long PTFE tube with an inner diameter of two millimetres was placed around the needle to keep the needle rods together.

On the day of the experiment, the assembled device was lubricated with WD40 (5032227312586, WD-40 Company, San Diego, CA, USA). More specifically, the supports, inner-cam, linear bearing, and inner-axis were lubricated. Hereafter, the device was placed and screwed to a breadboard (MB824, Thorlabs, Newton, NJ, USA). Millimetre paper was cut into a rectangular shape and taped to a stand with a variable height. The stand was then aligned parallel to the needle. The gelatin blocks were removed from the refrigerator and cut into 20x80x10 mm^3 blocks. A stopwatch was placed in front of the breadboard. The experiment room temperature was measured with an air purifier (Smart Air Purifier 4 Pro, Xiaomi Corporation, Beijing, China). Figure 19 shows the experiment setup.

4) *Procedure*

The procedure for each measurement was as follows:

1) A gelatin phantom was placed on the stand and aligned with millimetre paper.
2) The needle was inserted into the gelatin block up to an initial depth of $20\,\mathrm{mm}$.
3) The linear bearing was rotated clockwise until one cycle (rotation) was completed.
4) The position (mm) of the furthest needle tip was written down.
5) A timer was started, after which the linear bearing was manually turned.
6) During 12 seconds, the linear bearing was manually rotated to complete one cycle (i.e., one rotation).
7) After one minute (5 cycles), the linear bearing was stopped and the position (mm) of the furthest needle tip was written down.
8) This process was repeated three more times up until 20 cycles.
9) The needle was removed from the device and cleaned with a moist towel.
10) The gelatin block was removed.

To avoid systematic errors associated with the assembly and disassembly of the needles and the laser system in the actuation system, the device was first evaluated without the laser system and then with it. The device, both with and without the laser system, was assessed sequentially in 5 wt% gelatin phantoms, 10 wt% gelatin phantoms, 15 wt% gelatin

Experiment condition name	Laser system inclusion	Gelatin phantom	Range	Slip ratio (mean ± SD)
Air-EN	Excluding laser system	No gelatin	Cycles 0-5	0.67 ± 0.09
			Cycles 5-10	0.79 ± 0.03
			Cycles 10-15	0.83 ± 0.05
			Cycles 15-20	0.88 ± 0.02
			Total (Cycles 0-20)	**0.79 ± 0.03**
5wt-EN	Excluding laser system	5 wt%	Cycles 0-5	0.87 ± 0.06
			Cycles 5-10	0.89 ± 0.03
			Cycles 10-15	0.92 ± 0.01
			Cycles 15-20	0.92 ± 0.03
			Total (Cycles 0-20)	**0.90 ± 0.03**
10wt-EN	Excluding laser needle	10 wt%	Cycles 0-5	0.91 ± 0.04
			Cycles 5-10	0.88 ± 0.06
			Cycles 10-15	0.91 ± 0.03
			Cycles 15-20	0.94 ± 0.02
			Total (Cycles 0-20)	**0.91 ± 0.03**
15wt-EN	Excluding laser system	15 wt%	Cycles 0-5	0.93 ± 0.02
			Cycles 5-10	0.93 ± 0.02
			Cycles 10-15	0.95 ± 0.03
			Cycles 15-20	0.96 ± 0.01
			Total (Cycles 0-20)	**0.94 ± 0.02**
Air-IN	Including laser system	No gelatin	Cycles 0-5	0.72 ± 0.07
			Cycles 5-10	0.83 ± 0.03
			Cycles 10-15	0.90 ± 0.05
			Cycles 15-20	0.91 ± 0.03
			Total (Cycles 0-20)	**0.84 ± 0.02**
5wt-IN	Including laser system	5 wt%	Cycles 0-5	0.88 ± 0.05
			Cycles 5-10	0.92 ± 0.06
			Cycles 10-15	0.90 ± 0.02
			Cycles 15-20	0.95 ± 0.05
			Total (Cycles 0-20)	**0.91 ± 0.02**
10wt-IN	Including laser system	10 wt%	Cycles 0-5	0.90 ± 0.03
			Cycles 5-10	0.91 ± 0.03
			Cycles 10-15	0.92 ± 0.04
			Cycles 15-20	0.99 ± 0.02
			Total (Cycles 0-20)	**0.93 ± 0.00**
15wt-IN	Including laser system	15 wt%	Cycles 0-5	0.92 ± 0.01
			Cycles 5-10	0.91 ± 0.01
			Cycles 10-15	0.94 ± 0.03
			Cycles 15-20	0.93 ± 0.03
			Total (Cycles 0-20)	**0.93 ± 0.01**

TABLE III: *Slip ratio results from the slip ratio experiment. The slip ratios are represented per experiment condition and range.*

phantoms, and finally in air. Each experiment condition was repeated five times.

5) *Test results*

The slip ratio results per experiment condition are portrayed in Table III and shown in Figure 20. The slip ratio per five cycles became progressively higher in both systems in the air (Table III Air-EN, AIR-IN). Similar behaviour is seen in 5 wt% gelatin without the laser system (Table III 5wt-EN) and in 10 wt% gelatin with the laser system (Table III 10wt-IN). The other four conditions did not have an upward or downward trend regarding travelled distance per five cycles.

The mean slip ratio of the needle without the laser system was 0.90 (SD = 0.02), 0.91 (SD = 0.03), and 0.94 (SD = 0.02) in the 5 wt%, 10 wt%, and 15 wt% phantom, respectively. The mean slip ratio of the needle with the laser system was 0.91 (SD = 0.02), 0.93 (SD = 0.01), and 0.93 (SD = 0.03) in the 5 wt%, 10 wt%, and 15 wt% phantoms, respectively. The mean slip ratio of the needle when not inserted into gelatin was 0.79 (SD = 0.03) and 0.84 (SD = 0.02) with and without the laser system, respectively.

B. *Push force experiment*

1) *Goal*

Rotating the linear bearing can generate a push force at the needle rod tips. Although the parts were designed to minimise friction when sliding, manufacturing imperfections likely cause surface roughness and slight dimensional deviations that increase friction [60]. If this is the case, the resulting friction exerts a force on the needle system. For this reason, a resultant force in the form of a push force at the end of the needle rod tips is likely present. The purpose of this measurement was to determine the magnitude of the push force generated when turning the linear bearing and to evaluate a potential difference between the exerted force of the needle with and without the laser system. Additionally, this force measurement was used to better understand the self-propelling mechanism's behaviour. This was done by performing linear bearing rotations and measuring the net push force behaviour over time.

Two experiment conditions were created to evaluate the push force and its behaviour over time. The difference between the conditions was the exclusion of the laser system. Five

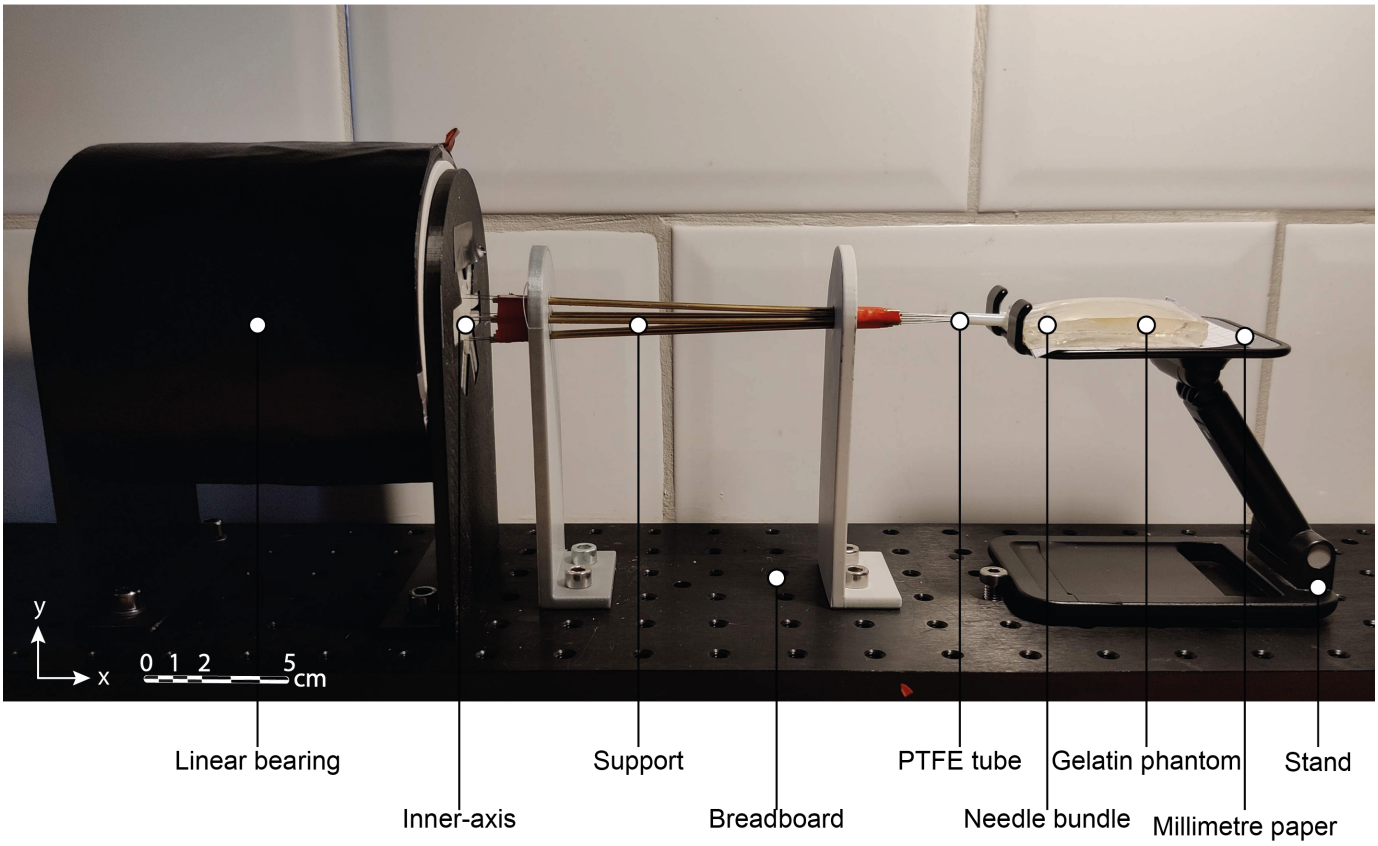


Fig. 19: *Slip ratio experiment setup.*

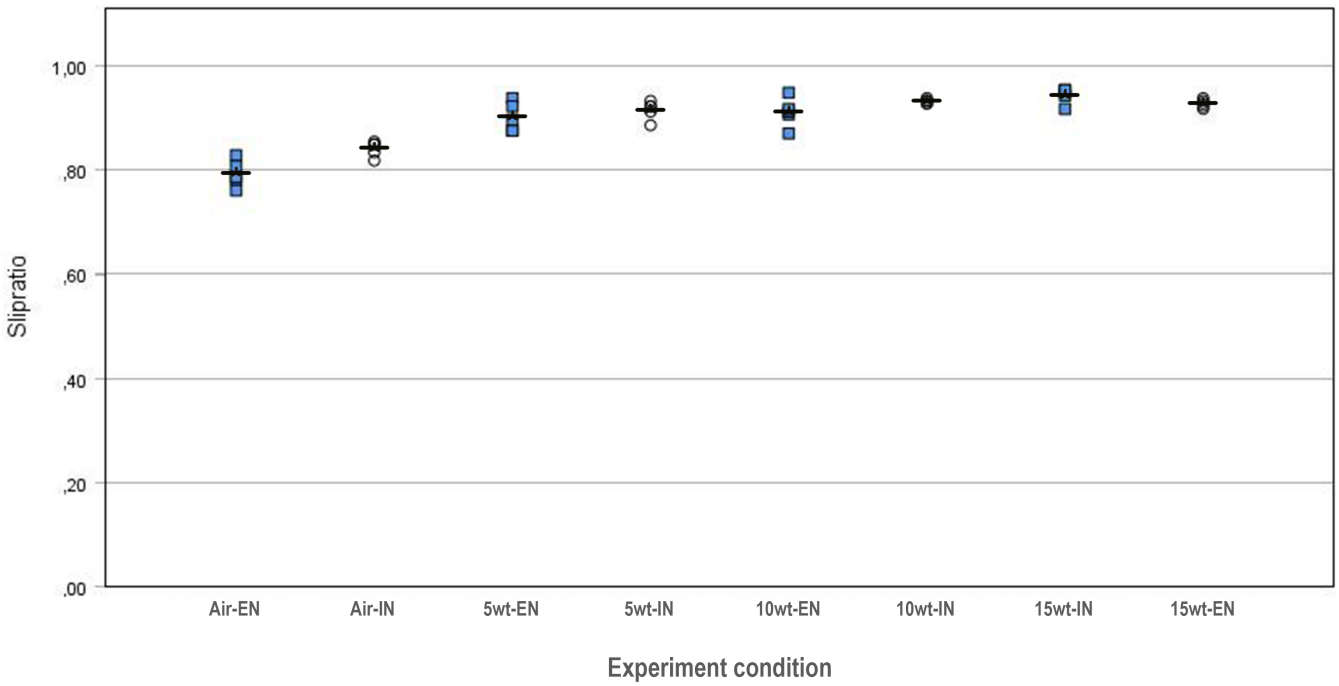


Fig. 20: *Scatter plot of the slip ratio per gelatin weight percentage: no gelatin (Air), 5 wt% (5wt), 10 wt% (10wt), and 15 wt% (15wt). A distinction was made between the device tested with (IN) and without the laser system (EN). The slip ratio results from the device with the laser system are illustrated with blue squares, whereas the results from the device without the laser system are illustrated with white circles. The average slip ratio per experiment condition is illustrated with a bold horizontal line.*

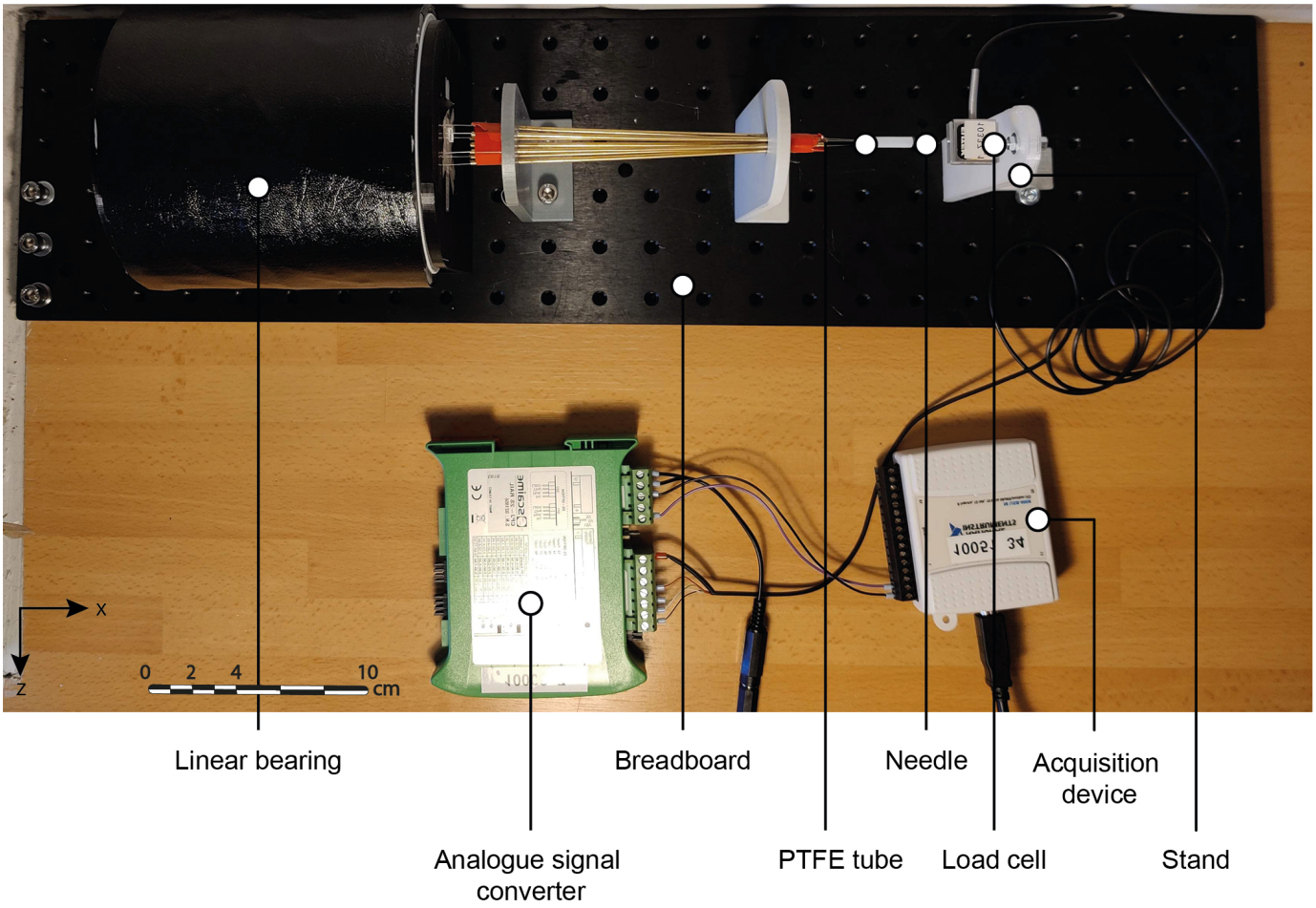


Fig. 21: *Push force experiment setup.*

measurements were conducted per experiment condition, with each measurement consisting of one continuous push force recording during 20 contiguous linear bearing cycles.

*2) **Variables***

The independent variable was the inclusion of the laser system. The dependent variable was the measured force (per period, i.e., $0.1\,\mathrm{s}$) of the furthest needle rod. The control variables were the room temperature (20°C), humidity (70%), number of cycles (20), and the angular velocity of the linear bearing ($\frac{2\pi}{12}\ \mathrm{rad\ s^{-1}}$).

*3) **Setup***

The assembled device excluding the laser system was attached to a breadboard (MB824, Thorlabs, Newton, NJ, USA). A 3D printed stand with a calibrated $2.0\,\mathrm{N}$ load cell (FSH00091, FUTEK Advanced Sensor Technology, Irvine, CA, USA) attached, was screwed to the same breadboard. The stand was placed in such a way that it aligned with the needle. The load cell was connected to an analogue signal conditioner (CPJ2S, Feteris Scaime, Orsay, LR, France). This conditioner was attached to a data acquisition device (NI USB-6008, National Instruments Corp., Emerson Electric Co., Ferguson, MO, USA) which itself was connected to a laptop. The setup can be seen in Figure 21. A force measurement programme was installed and run in LabView (NI LabVIEW 2018, National Instruments Corp., Emerson Electric Co., Ferguson, MO, USA). In addition, a stopwatch was placed in front of the breadboard.

*4) **Procedure***

The procedure for each measurement was as follows:

1) We placed the needle in contact with the load cell.
2) The linear bearing was rotated clockwise until one cycle (rotation) was completed.
3) The needle was pulled backwards until the real-time force seen in the software fell to zero, or just below zero. This was the point at which the needle was not in contact with the load cell.
4) The software was started concurrently with a four-minute timer.
5) During 12 seconds, the linear bearing was manually rotated, completing one cycle.
6) This was done continuously until 20 cycles were completed (in 4 min).
7) The results were saved to an Excel file.

To avoid systematic errors associated with the assembly and disassembly of the needles and the laser system in the actuation system, the device was first evaluated without the laser system and then with it. Each experiment condition was repeated five times.

5) *Test results*

The mean maximum force in the experiment condition without the laser system was $0.23\,\mathrm{N}$ (SD = $0.02\,\mathrm{N}$), where the mean maximum force refers to an average of the maximum forces measured in an experiment condition. The mean maximum force measured in the experiment condition with the laser system was $0.28\,\mathrm{N}$ (SD = $0.06\,\mathrm{N}$). In both experiment conditions, the maximum forces were reached at different times and no clear trends were observed. Additionally, in both experiment conditions, the needles did not generate a measurable force spike per cycle. That is to say, an advancing needle rod is expected to generate a push force in every cycle, but this was not measured.

C. *Friction force experiment*

1) *Goal*

This experiment consisted of one setup with two different sets of variables, goals, and protocols. The first goal was to characterise the net friction force between the linear bearing and inner-cam relative to the position of the linear bearing. The experiment's second goal was to evaluate the net friction force between the linear bearing and inner-cam with two different constant accelerations and velocities.

In the first experiment, the Position Experiment, the net friction force was measured at six different linear bearing positions (see Fig. 22). The experiment was carried out by attaching the needle to a load cell and moving the linear bearing (along its cylindrical axis) with a constant acceleration ($0.1\,\mathrm{mm\ s^{-2}}$) until a predetermined velocity ($2\,\mathrm{mm\ s^{-1}}$) was reached. After reaching the predetermined velocity, the acceleration was set to zero and the linear bearing moved at a constant velocity ($2\,\mathrm{mm\ s^{-1}}$). This was done five times for every linear bearing position.

The second experiment, the Movement Experiment, was carried out by attaching the needle to a load cell and performing the same linear bearing movements mentioned above. This was done five times. Hereafter a similar movement sequence was performed, but with a higher constant acceleration ($0.3\,\mathrm{mm\ s^{-2}}$) and velocity ($6\,\mathrm{mm\ s^{-1}}$). This was repeated five times. During this experiment, the linear bearing was placed in Position 1 (Figure 22).

2) *Variables*

For the first experiment, the Position Experiment, the position of the linear bearing was the independent variable. The dependent variable was the force measured (per period, that is, $0.1\,\mathrm{s}$), and the control variable was the distance moved ($50\,\mathrm{mm}$), along with the accompanying velocity and acceleration.

For the second experiment, the Movement Experiment, the velocity and acceleration of the linear bearing were the independent variables. The dependent variable was the same as in the first experiment, the force measured (per period, that is, $0.1\,\mathrm{s}$). The control variables were the distance travelled ($50\,\mathrm{mm}$) and the position of the linear bearing (Position 1).

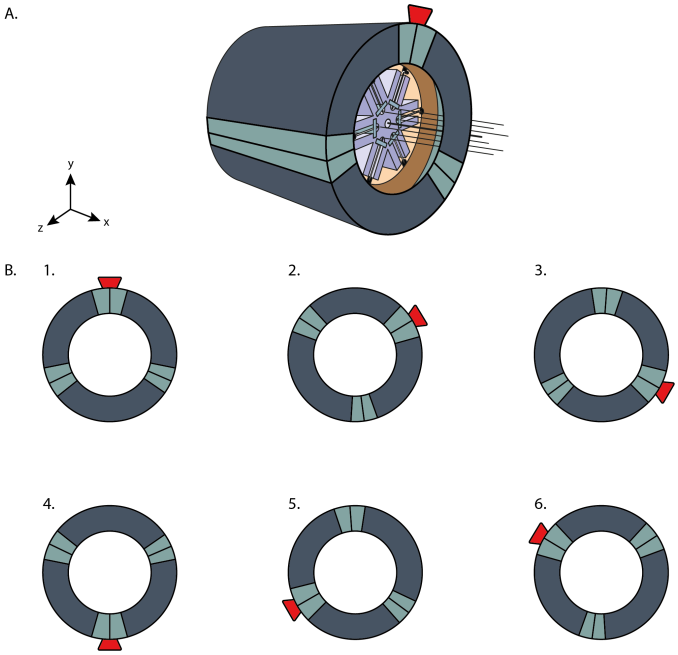


Fig. 22: *Linear bearing positions. A) Schematic overview of the device's core with the linear bearing parts shown in dark blue and light blue. B) Six different linear bearing positions. Each position represents a rotation of $\frac{\pi}{3}$ radians relative to the prior position. For example, Position 2 is rotated $\frac{\pi}{3}$ radians relative to Position 1. The individual bearing parts that house the balls are portrayed in light blue, which together with the dark blue housing parts make up the linear bearing. The red label is used as a mark to visualise the different positions.*

3) *Setup*

The assembled device that included the laser system was attached to a custom-made poplar triplex plate. The triplex plate (with the device on top) was attached to a $150\,\mathrm{mm}$ motorised linear translation stage (NRT150/M, Thorlabs, Newton, NJ, USA), which itself was attached to a breadboard (MB12D, Thorlabs, Newton, NJ, USA). The proprietary Kineses software (1.14.49.23058, Thorlabs, Newton, NJ, USA) was used to control the motorised linear translation stage.

A 3D printed stand with a calibrated ($2.0\,\mathrm{N}$) load cell (FSH00091, FUTEK Advanced Sensor Technology, Irvine, CA, USA) attached, was screwed to the same breadboard. The stand was placed in such a way that it aligned with the needle. The load cell was connected to an analogue signal conditioner (CPJ2S, Feteris Scaime, Orsay, LR, France). This conditioner was attached to a data acquisition device (NI USB-6008, National Instruments Corp., Emerson Electric Co., Ferguson, MO, USA), which itself was connected to a laptop (similar to Figure 21). The friction force experiment setup can be seen in Figure 23. A force measurement program was installed and run in LabView (NI LabVIEW 2018, National Instruments Corp., Emerson Electric Co., Ferguson, MO, USA.).

4) *Procedure*

The procedure in the Position Experiment for each measurement was as follows:

1) Movement function Slow was added to the Kineses software. This function moved the linear stage $50\,\mathrm{mm}$ with

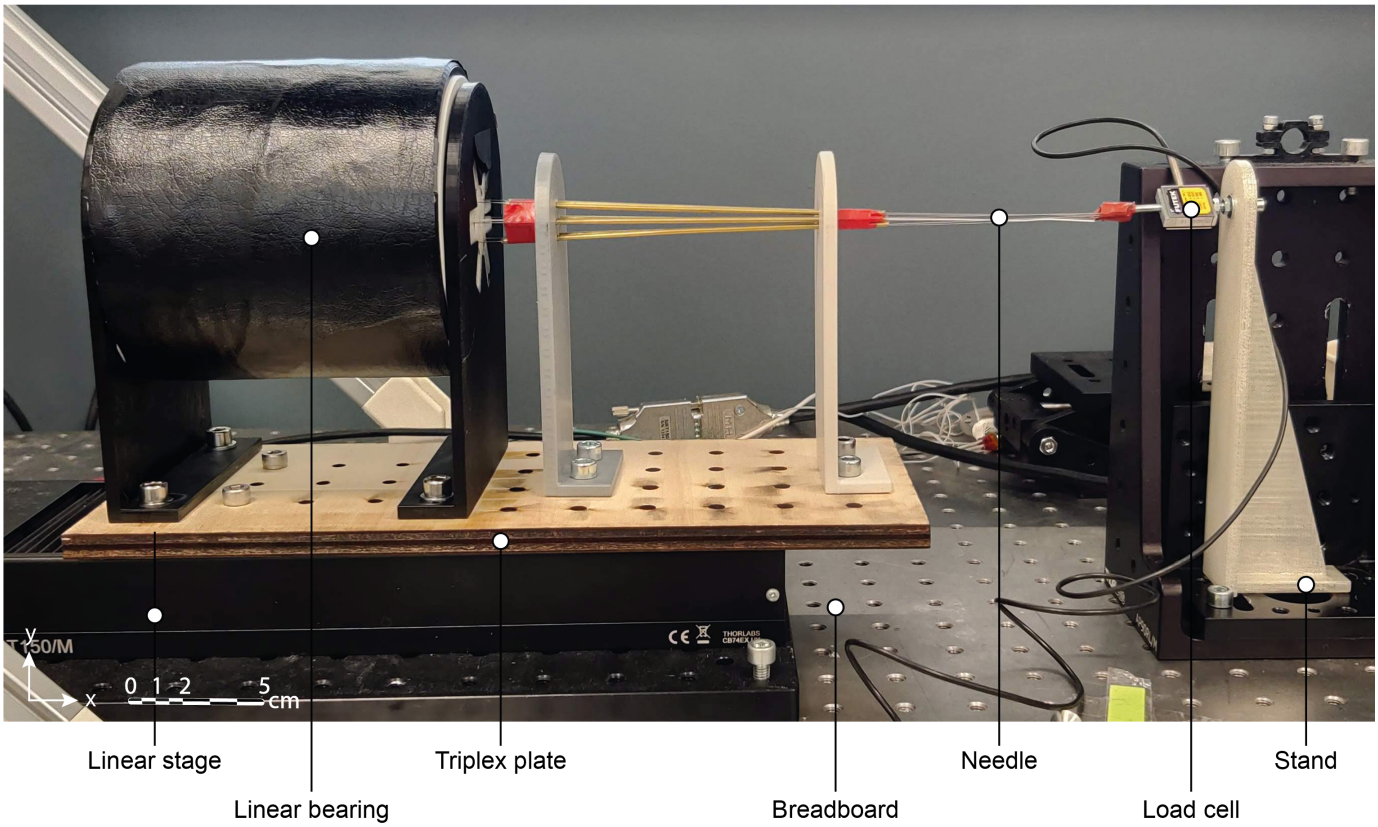


Fig. 23: *The friction force experiment setup.*

a constant acceleration of $0.1\,\mathrm{mm\ s^{-2}}$ and a maximum velocity of $2\,\mathrm{mm\ s^{-1}}$.

2) Movement function Reset was added in the Kineses software. This function moved the linear stage back to its starting location.
3) The linear bearing was rotated until it aligned with a position seen in Figure 22.
4) The linear stage was moved to the starting place using the Reset movement function.
5) The needle rods were attached to the load cell using tape.
6) The force exerted by the needle rods was checked. The maximum force had to be less than $|0.01\,\mathrm{N}|$. If the force was too high, the needles had to be reattached.
7) The load cell software in LabView and the Slow movement function in Kineses was started.
8) After the movement function was finished the data was saved to an Excel file.

The device (with laser system) was assessed sequentially in Positions 1, 2, 3, 4, 5, and 6. Each experiment condition was repeated three times.

The procedure in the Movement Experiment for each measurement was as follows:

1*) Movement function Reset was added in the Kineses software. This function moved the linear stage to its start location.
2*) Movement function Slow was added to the Kineses software. This function moved the linear stage $50\,\mathrm{mm}$ with a constant acceleration of $0.1\,\mathrm{mm\ s^{-2}}$ and a maximum velocity of $2\,\mathrm{mm\ s^{-1}}$.
3*) Movement function Fast was added in the Kineses software. This function moved the linear stage $50\,\mathrm{mm}$ with a constant acceleration of $0.3\,\mathrm{mm\ s^{-2}}$ and a maximum velocity of $6\,\mathrm{mm\ s^{-1}}$.
4*) The linear bearing was rotated until it aligned with Position 1 in Figure 22.
5*) The linear stage was moved to the starting place using the Reset movement function.
6*) The needle rods were attached to the load cell using tape.
7*) The force exerted by the needle rods was checked. The maximum force had to be less than $|0.01\,\mathrm{N}|$. If the force was too high, the needles were reattached.
8*) The load cell software in LabView and the movement function Slow, or Fast were started.
9*) After the movement function was finished the data was saved to an Excel file.
10*) The Reset function moved the linear stage back to the starting place.

The device (with laser system) was assessed using the movement function Slow first, hereafter the device was assessed using the movement function Fast. Each experiment condition was repeated five times.

5) Test results

Following the Position Experiment the following results were found. The mean maximum force (MeanMax) within the first ten seconds was $0.49\,\mathrm{N}$ (SD = $0.15\,\mathrm{N}$, n = 18). The mean

maximum force refers to an average of the maximum forces measured in an experiment condition. This result probably corresponds to the stiction, i.e., the friction force needed to overcome to initiate (sliding) movement [64]. These results appear to be biased, as positions one and six show close to double the force (MeanMax = $0.68\,\mathrm{N}$, SD = $0.08\,\mathrm{N}$, n = 6) in the first 10 seconds compared to Positions 2-5 (MeanMax = $0.39\,\mathrm{N}$, SD = $0.06\,\mathrm{N}$, n = 12). Maximum forces were reached around the 30 to 35-second mark in Positions 2-6 (MeanMax = $1.14\,\mathrm{N}$, SD = $0.15\,\mathrm{N}$, n = 15) and in the first ten seconds in Position 1 (MeanMax = $0.70\,\mathrm{N}$, SD = $0.05\,\mathrm{N}$, n = 3).

The maximum force measured with a constant acceleration of $0.1\,\mathrm{mm\ s^{-2}}$ and a maximum velocity of $2\,\mathrm{mm\ s^{-1}}$ was $0.72\,\mathrm{N}$ (SD = $0.05\,\mathrm{N}$, n = 5). Similarly, the maximum force measured with a constant acceleration of $0.3\,\mathrm{mm\ s^{-2}}$ and a maximum velocity of $6\,\mathrm{mm\ s^{-1}}$ was $0.73\,\mathrm{N}$ (SD = $0.05\,\mathrm{N}$, n = 5).

D. *Laser damage experiment*

1) *Goal*

The laser damage experiment aimed to evaluate the damage to the optical fibre tip after inserting the optical fibre through the laser system. In this setup, a second-hand optical fibre (19S medium optical fibre, Diamond SA, Losone, TI, Switzerland) was used. The damage to the optical fibre tip was evaluated using a microscope (AM73915MZTL, Dino-Lite Digital Microscopes, AnMo Electronics Corporation, New Taipei City, Taiwan).

2) *Variables*

The independent variable was the insertion of the optical fibre. The dependent variable was the damage to the optical fibre tip. The control variables were the magnification and position of the microscope and the position of the optical fibre tip during the measurement.

3) *Setup*

The microscope with proprietary software was set up by placing the tip of the 19S medium optical fibre (Diamond SA, Losone, TI, Switzerland) next to a ruler within the field of view of the microscope. After applying a magnification of 140, the height was adjusted to focus on the optical fibre tip and the ruler. This was saved as a calibration profile in the software.

The device was assembled with the laser system (excluding the laser needle holder), but without the actuation system (Section IV-B3). After assembly, the device was screwed onto a breadboard (MB824, Thorlabs, Newton, NJ, USA).

4) *Procedure*

The procedure in the laser damage experiment was as follows:

1) Two pieces of tape were added to the optical fibre. One triangular piece to the front and one rectangular piece to the back. This was used to distinguish the front from the back of the optical fibre tip to enable accurate evaluation.
2) The microscope was set to the saved calibration profile.
3) The optical fibre tip was placed within the field of view of the microscope, with the triangular piece of tape visible (on top).
4) A picture was taken (and labelled) using the proprietary software.
5) The optical fibre was rotated Π radians so that the rectangular piece of tape became visible (on top).
6) The optical fibre tip was placed within the field of view of the microscope.
7) A picture was taken (and labelled) using the proprietary software.
8) The optical fibre was inserted into the laser system via the funnel.
9) The optical fibre was pushed as far as possible (approximately $15\,\mathrm{cm}$).
10) The optical fibre was pulled back.

This experiment condition was done twice.

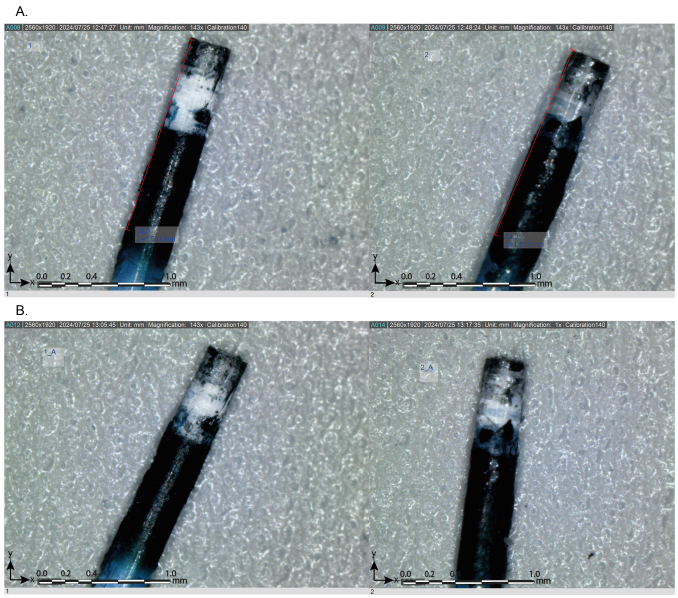


Fig. 24: *Optical fibre tip before and after insertion. A) laser tip before insertion. On the left, the front of the optical fibre tip can be seen. On the right, the back of the optical fibre tip can be seen. B) Optical fibre tip after insertion. On the left, the front of the optical fibre tip can be seen. On the right, the back of the optical fibre tip can be seen.*

5) *Test results*

No clear damage was observed (Figure 24). The optical fibre tips before insertion are shown in Figure 24 A, and the optical fibre tips after insertion are shown in Figure 24 B. It can be seen that only some charred material was moved and the tip roughened.

VI. Discussion

A. *Main findings*

1) *Slip ratio*

In this study, we created an MR-conditional wasp-inspired needle with an incorporated laser system for transperineal

laser ablation, narrowing the gap to clinical implementation of wasp-inspired needles. Our stationary actuation system is capable of transforming manually applied torque into linear needle motion (of the individual needle rods) while allowing for optical fibre insertion into the centre of the propelled needle. Evaluation of the device's performance showed that the needle, consisting of the needle rods and laser needle, was able to propel through multiple gelatin phantoms with varying stiffnesses. Our tests showed that the needle could travel through 5 wt%, 10 wt%, and 15 wt% gelatin phantoms, with slip ratios of 0.91 (SD = 0.02), 0.93 (SD = 0.00), and 0.93 (SD = 0.01), respectively. This is comparable to recent studies performed by Bloemberg *et al.* [28] and Scali *et al.* [63] with slip ratios of 0.86–0.96 and 0.87–0.90, respectively. It is however higher compared to the studies performed by Fung-A-Jou *et al.* [25] and Scali *et al.* [20], who reported slip ratios of 0.29-0.35 and 0.45-0.8, respectively.

To evaluate the propelling mechanism of the needle rods, the slip ratio, friction forces, and push forces need to be taken into account. Here, a slip ratio of one indicates that the slip occurs to such an extent that no relative movement occurs between the needle rods and the gelatin phantom, while a slip ratio of zero indicates that there is no slip. Interestingly, the slip ratios were lower in lower gelatin wt% concentrations (lower stiffnesses), and lowest when suspended in air, not in gelatin. This implies that the propelling mechanism of the needle rods was in large a result of the friction between the needle rods and the device and less of the friction generated between the needle rods and gelatin. This is further supported by the fact that the needle rods exerted a maximum non-zero push force of around $0.28\,\mathrm{N}$ (SD = $0.06\,\mathrm{N}$) with the laser system and $0.23\,\mathrm{N}$ (SD = $0.02\,\mathrm{N}$) without the laser system. This indicates that the needle rods were indeed subject to friction within the device, as no push forces would have been measured without friction. That is because friction within the device exerts an external force, a push force, on the needle system. A prerequisite for a self-propelling mechanism is that it has to propel through a substrate with a negative external net force (i.e., pulling force) or an approximately zero external net force. For that reason, the propelling mechanism of our device cannot be classified as self-propelling according to the definition provided by Scali *et al.* [20].

The friction force experiment showed that the maximum friction force to overcome when pulling the needle bundle was $1.14\,\mathrm{N}$ (SD = $0.15\,\mathrm{N}$) in our device, which includes a laser system. This is lower, albeit comparable to the WASP, a similar device without a laser system, which experienced a maximum friction force of $1.27\,\mathrm{N}$ [25]. In the same study, a push force of $0.18\,\mathrm{N}$ was mentioned, which is also comparable to our results without the laser system [25]. Yet, our slip ratios presented under both conditions, with and without the laser system, are substantially higher compared to the slip ratios in the aforementioned study. This, in part, might be explained by a lower turning velocity and thus a lower needle velocity. In a velocity experiment performed by Fung-A-Jou *et al.* [25] increased velocity of the needle bundle corresponded with lowered slip ratios. This suggests that a lower velocity could lead to higher slip ratios. Nonetheless, it should be noted that research regarding force-velocity dependence for needles in tissue remains inconclusive [65].

Although lowered velocity might be part of the reason for the increased slip ratio compared to Fung-A-Jou *et al.* [25], we suspect that the needle rod connectors also add to the increased slip ratios. The needle rod connectors are relatively thin ($0.6\,\mathrm{mm}$) tubes that connect the needle rods to the inner-cam. During rotation of the inner-cam the needle rod connectors, and with it the needle rods, translate according to the self-propelling movement sequence (Section IV-A2). Because the needle rod connectors are not rigid and instead prone to bending due to their small diameter, a translation of the needle rod connector likely does not result in a one-to-one translation of the needle rod. Additionally, bending of the needle rod connectors likely leads to tilting of the needle rods which may lead to increased friction. Therefore, when the needle rod connectors move $4.0\,\mathrm{mm}$ (stroke distance), the needle rods probably move a smaller distance. This directly impacts the slip ratio, as the measured distance at the needle rod tips is lower.

*2) **Push force***

The push force experiment showed that the maximal push forces were higher in the device with the laser system compared to without. This increased push force did not correspond to an increased slip ratio, compared to the device without the laser system. This is a positive result because it shows that the inclusion of the laser system does not severely impact the performance of our device in terms of its slip ratio. Moreover, a high push force without a negative impact on slip would enable the device to move through materials with higher stiffnesses, thereby opening up the possibility for applications within a wider range of tissues. Tissue stiffness directly impacts the cutting force [66]. A higher cutting force is therefore needed to cut through tissue with higher stiffnesses compared to tissue with lower stiffnesses. Nevertheless, a high push force increases the risk of buckling (i.e., bending of needle rod along its length), which can lead to needle deformation or worse tissue damage [20]. The push force at which the needle bundle buckles in prostate tissue has yet to be defined.

Conducting the push force experiment over time, provided information about the push force behaviour throughout the experiment. The maximal push force per measurement was reached in seemingly arbitrary actuation cycles, that is to say, in each measurement the maximum push force was reached during a different actuation cycle. Additionally, and rather remarkably, in multiple cycles within multiple measurements maximum push forces of merely $0.05\,\mathrm{N}$ were recorded. One would expect a similar peak push force in every cycle over multiple measurements, but in reality, our results show more variability. We suspect that inconsistent bending of the needle rods caused force components to vary in the x, y, and z-direction. Since push force is only measured along the x-axis, inconsistent force direction could be the reason for the high variability. Additionally, needle rod connector (sideways) movement likely added to this variability.

3) *Friction force*

The friction force experiment, more specifically the Position Experiment, provided an insight into the force needed to move the needle bundle (and inner-cam). In this experiment, the linear stage movement caused the linear bearing to move relative to the inner-cam, which was connected to the load cell via the needle. The friction force between the linear bearing and the inner-cam was thereby evaluated. We evaluated the force per linear bearing position to avoid bias in the interpretation of the results. Four linear bearing positions (2-5) showed similar force behaviour over time. During the first ten seconds in which the linear stage moved a distance of $5\,\mathrm{mm}$, the force gradually increased to a force of $0.39\,\mathrm{N}$ (SD = $0.06\,\mathrm{N}$), after which it remained fairly constant and even decreased a little. Around the 20-second mark, the measured force began to increase again, reaching a mean maximum force of $1.09\,\mathrm{N}$ (SD = $0.06\,\mathrm{N}$) at the 30 to 35-second mark. Following this peak, the force decreased slightly until the linear bearing travelled a total distance of $50\,\mathrm{mm}$. The other positions, Position 1 and 6, showed different force behaviour, which was especially noticeable in the first 10 seconds. For Positions 1 and 6, the force gradually increased to $0.68\,\mathrm{N}$ (SD = $0.08\,\mathrm{N}$) during the first ten seconds, which is substantially higher than the force measured for the other four linear bearing positions (2-5). This difference is likely the result of manufacturing inconsistencies. Positions 1 and 6 are located next to each other, which means that the inner-cam applied the majority of the gravitational force on the same linear bearing sub-parts.

Further analysis of the measurements from the friction force experiment showed that the force changed from an increasing to a constant force, while the linear stage (and thus the linear bearing) continued accelerating (relative to the inner-cam). This suggests that the force of $0.39\,\mathrm{N}$, and $0.68\,\mathrm{N}$ correspond to the initial friction forces (stiction) that the inner-cam needs to overcome to move relative to the linear bearing in Position 2-5, and 1 and 6, respectively. The maximum forces in Positions 2-6 were reached when the linear bearing moved with a constant velocity. The reason for the increased force could thereby be due to an increase in the friction between the linear bearing and the inner-cam, but it could also represent an accumulation of forces acting upon the needle, such as additional friction between the needle rods and the inner-axis due to deformation of the needle rod connectors. Nevertheless, the Friction force results are promising, as it shows that friction between the inner-cam and linear bearing can remain fairly constant and relatively low ($0.39\,\mathrm{N}$). Thus, translating the inner-cam over balls in the linear bearing seems to be a viable option for future applications if the current force spike (i.e., the force increase after 20 seconds) can be mitigated.

Examination of the measurements taken in the Movement Experiment showed similar force magnitudes in both experiment conditions (different acceleration and velocity). The results indicate that the velocity and acceleration do not affect the force magnitude. Additionally, both conditions exhibit very similar force progression and behaviour, albeit sped up. This further suggests that the maximum force at the beginning of the measurements indeed corresponds to the initial friction (stiction) between the linear bearing and inner-cam, as even with higher acceleration the force values remain the same.

4) *Laser damage*

To guarantee the laser functionality of the device, the optical fibre cannot be damaged during insertion into our device. Our laser damage experiment showed no clear scratches or damage after optical fibre insertion. However, because the optical fibre had been used for laser ablation before this experiment, the optical fibre could not be used for laser ablation again to verify the laser functionality.

B. *Limitations*

1) *Design*

To allow for repeated and comfortable usage of our device our actuation system should be ergonomic. Currently, prolonged usage of our device can cause cramps and substantial discomfort. The discomfort is likely a cause of the large diameter of the linear bearing ($115\,\mathrm{mm}$). The recommended diameters for cylindrical handles vary widely but are generally below $60\,\mathrm{mm}$ [67]. Some have created slightly larger handles with diameters in the vicinity of $70\,\mathrm{mm}$ [25], but none come close to our linear bearing diameter. Thus for our device to be ergonomic the diameter of the actuation system should be lowered.

2) *Prototype*

To enable the use of our device within an MR environment it must be evaluated based on the General Safety and Performance Requirements (GSPRs) to comply with the European Union Medical Device Regulation (MDR) [35]. As MRI scanners generate magnetic fields, objects may behave differently and pose greater risks as opposed to their usage outside an MR environment. How objects behave in an MR environment greatly depends on their material [68]. To ensure parts are used that pose no or negligible risk in an MR environment, they should be made of electrically nonconductive, nonmetallic, and nonmagnetic materials, conforming to ASTM F2503 standard practices regarding MR-safe devices and material [36]. Some materials, however, are not inherently MR-safe, but MR-conditional. In short, this means that the materials can be used safely in an MR environment only if certain conditions are met [69]. Because these materials are not inherently MR-safe, they can create image artefacts [70]. The materials proposed for the needle rods (Nitinol) and laser needle (titanium) are MR-conditional and could cause image artefacts in an MR environment [70]. Although Bloemberg *et al.* [28] evaluated the MRI artefacts of Nitinol needle rods, it is unclear to what extent the laser needle creates image artefacts.

Our prototype has seven parts, six needle rods and one laser needle, that were inserted into gelatin during the slip ratio experiment. These seven parts were not sharpened. Not sharpened, or blunt needles are generally undesirable as they require more force to puncture through tissue than bevelled or conically tipped needles [71]. Using a blunt laser needle and blunt needle rods likely led to an increase in slip ratio and increased chance of buckling, as the needle rods required greater cutting forces to cut through the gelatin phantoms.

Hence, sharpened needles and sharpened needle rods are desired for future applications.

*3) **Experiments***

The slip ratio experiment was performed at a velocity of 20 cycles in four minutes. If these velocities are converted to $\mathrm{mm/s}$, this results in an average velocity (v) of $0.4\,\mathrm{mm/s}$, see Equation 7.

$$v = \frac{d_t \times c}{t} \tag{7}$$

In the velocity equation (7) d_t describes the theoretical maximum distance (mm) and is calculated using the stroke distance ($4\,\mathrm{mm}$) multiplied by $\frac{6}{5}$. The $\frac{6}{5}$ results from the assumption that the backwards-moving needle rods remain stationary with respect to the tissue. c represents the total number of cycles (20) and t represents the time (s) in which a total number of cycles (c) is completed. A velocity of $0.4\,\mathrm{mm/s}$ is substantially lower compared to the velocity used in similar experiments in previous studies [20, 25, 28]. The size of the cam was the main cause of the lowered velocity. If a velocity of $2\,\mathrm{mm/s}$ was to be reached, the linear bearing had to complete a rotation every 2.4 seconds. This was not feasible in the current experiment, as manual actuation of the relatively large linear bearing prohibited a fast, yet controlled, velocity. A prior study has shown that velocity does influence the slip-ratio [25]. For that reason, this difference in velocity and its effects on the slip ratio should be kept in mind when directly comparing the slip ratio results to Bloemberg *et al.* [28], Fung-A-Jou *et al.* [25], and Scali *et al.* [20].

The laser damage experiment showed no obvious signs of surface damage to the optical fibre tips. Nevertheless, it is possible that the optical fibre tip sustained internal damage that is not detectable with a surface inspection. We suggest that future studies evaluate damage to the optical fibre tips through performance evaluations. A possible (nondestructive) method could be by emitting low-energy light through the optical fibre and evaluating the change in light refraction at the needle tip after an insertion.

C. Recommendations

*1) **Design***

To improve upon the efficiency and slip ratio of the device a redesign of the needle rod connector is suggested. The slip ratio results are likely influenced by the design of the needle rod connector. As described in Section VI-A, the needle rod connectors are prone to bending due to their small diameter. As a result, the needle rod connectors are unable to transfer their movement to the needle rods in a one-to-one ratio. Eliminating, or at least lowering the amount of bending will likely improve the movement transfer, thereby lowering the slip ratio. Additionally, this might lead to less tilting of the needle rods thereby decreasing friction. We suspect that a slight alteration of the needle rod connectors will be sufficient to minimise its bending during actuation. A schematic overview of a possible solution is shown in Figure 25 B. In this solution, the top half of the needle

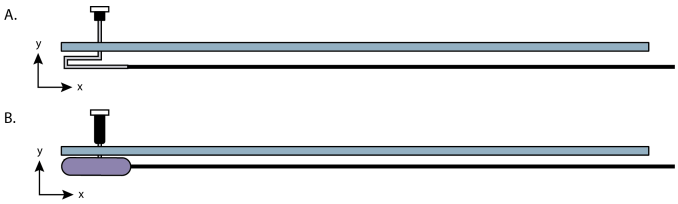


Fig. 25: *Needle rod connector redesign. The needle rods and connection parts are indicated in black, the needle rod connectors in grey, the ball bearings in white, and the needle guides in blue. A) Schematic overview of the current needle rod connector. B) Schematic overview of the needle rod connection redesign, where the purple part eliminates sideways movement (z-axis) and the connection part (black) limits the bending of the needle rod connector.*

rod connector is made with a larger diameter (Fig. 25 B, black part). This increases the area moment of inertia, which increases the bending stiffness and thereby lowers the (elastic) deformation (Eq. 1). Encapsulating the needle rod connector in the bottom half (Fig. 25 B, purple part) better controls sideways rotation (z-axis), as less sideways movement can occur. Additionally, it improves upon the fixation of the needle rod, likely lowering the column effective length factor (K) and increasing its critical load, as shown by the Euler equation (Equation 1).

To further improve the efficiency and slip ratio of the device we propose a redesign of the bearing mechanism. Our device is relatively large compared to similar wasp-inspired needle systems [25, 28]. The increased size is a result of using off-the-shelf ball bearings in the inner-cam. This is explained in detail in Appendix E. Increased size leads to increased weight and thus increased gravitational force. The increased gravitational force of the inner-cam will inevitably lead to higher friction forces between the inner-cam and linear bearing. Additionally, the large diameter of the inner-cam leads to the need for long connection parts between the inner-cam and the needle rods. Longer connective parts, i.e., needle rod connectors, are more prone to flexion and bending than short connective parts. This is because length directly impacts the deformation of a beam, due to the internal bending moment (Eq. 1). As previously described, increased bending likely results in a less efficient transfer of movement from the needle rod connectors to the needle rods. For these reasons, it is beneficial to decrease the size of the inner-cam. Replacing the ball bearings with smaller diameter cylindrical sleeve bearings allows for a decrease in size of the inner-cam, but might also increase the inner-cam's resistance to rotation. The sleeve bearings could be placed directly around the needle rod connector or, as an alternative, the sleeves could be placed around an intermediary cylindrical part, as shown in Figure 26 C. This would be similar to a ball bearing without balls around the needle rod connector (Fig. 26 B and C). Depending on the friction coefficient between the sleeve bearing and the part with which it will come into contact, the sleeve bearing might introduce a non-negligible torque onto the needle rod connector. This can lead to disturbed movement along the inner-cam paths. Therefore, it would be interesting to investigate the effect of replacing ball bearings with small-diameter sleeve bearings in our device in

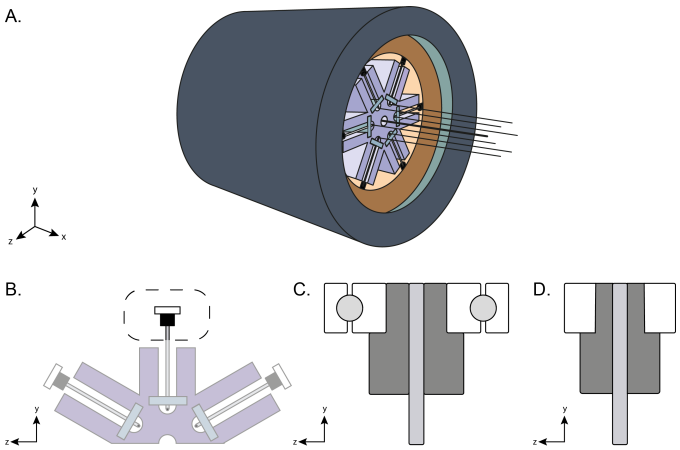


Fig. 26: *Redesign of the bearing mechanism to decrease its diameter. A) Schematic overview of the device's core with the inner-axis visualised in purple. B) Schematic front view of the inner-axis with the bearing mechanism accentuated. The inner-axis is shown in purple, the needle guides in blue, the needle rod connectors in grey, the needle rods and connection parts in black, and the ball bearings in white. C) Cross-section of the current bearing mechanism. The needle rod connector and balls are shown in light grey, the connection part in dark grey, and the ball bearing in white. D) Cross-section of the redesigned bearing mechanism. The needle rod connector is shown in light grey, the connection part in dark grey, and the sleeve bearing in white.*

practice.

It is recommended to investigate the optical fibre positioning in the laser ablation procedure. Currently, the optical fibre must be inserted into the laser needle after which the urologist has to manually hold the optical fibre in place while turning the linear bearing to retract the needle rods. First, the risk of damaging the optical fibre tip should be evaluated, as described in Section VI-A. Second, laser insertion while turning the linear bearing requires two hands, which might be undesired in a clinical setting. An urologist might want to keep one hand free to perform various other tasks, such as using other instruments and responding to complications that might arise during the procedure. To eliminate the need for double-handed control, motorised actuation could be used. Even though manual actuation offers greater control, it negatively affects ergonomics and velocity. Motorised actuation, on the other hand, will require only one hand, offer improved ergonomics, and generate a constant velocity, but will increase costs and raise safety concerns. These safety concerns mostly pertain to loss of power, lack of force feedback and possible decreased accuracy [72]. Besides motorised actuation, another option would be to adjust the device such, that only one hand is needed for manual actuation. For example, using a clamp to hold the optical fibre will greatly benefit the goal of one-handed actuation.

2) *Prototype*

Six needle rods made from spring steel (4069235244937, Evek GmbH, Mülheim, NRW, Germany) were used to propel the needle. Spring steel, however, has a serious disadvantage. It cannot be used safely in an MR environment due to its magnetic susceptibility. For that reason, different material needle rods should be used in future applications. We propose the use of Nitinol needle rods to replace spring steel needle rods, as Nitinol has a relatively low magnetic susceptibility and is superelastic [73, 74]. If the spring steel needle rods are replaced by Nitinol needle rods, we recommend a re-evaluation of the needle rod behaviour to ensure their safety and functionality during insertion in tissue. This is because Nitinol has different elastic properties compared to spring steel rods. According to the manufacturer the spring steel rods have an elastic modulus of $206\,\mathrm{GPa}$ [75], whereas Nitinol has an elastic modulus between 40 and 70 GPa depending on its state [76]. This difference in elastic moduli will affect the risk of buckling, according to the Euler equation; see Equation 1. According to Equation 1, if E decreases, the critical load decreases as well. If the critical load is exceeded, the needle rod will buckle.

3) *Experiment*

It is recommended to evaluate the effect of increased push force on the slip ratio and tissue damage. Previous papers [19, 20, 25, 28], have all used, or tried to use the self-propelling principle for their needle movement mechanism. The self-propelling principle is based on moving a needle through tissue using a net external push force of zero, which means that the user and the actuation mechanism should not exert a net external push force onto the needle rods [20]. Reasons for using self-propelling needle mechanism are mostly linked to avoiding buckling and minimising tissue damage [28]. However, in our design and the design made by Fung-A-Jou *et al.* [25] we have seen that a small net push force may help the needle to cut through (stiff) tissue and improve slip ratios [25]. For that reason, we recommend performing a study in prostate tissue to determine the maximum push force at which ($0.25\,\mathrm{mm}$ diameter) Nitinol rods do not buckle. This can be used to determine the critical load. Hereafter, we suggest performing a study to evaluate the effect of increased push force on slip ratio and tissue damage and compare this to a similar device with a self-propelling mechanism.

D. *Towards clinical implementation*

To move our prototype toward medical application multiple aspects will need resolving, starting with sterilisation. In its current form, the device cannot be sterilised in an autoclave, i.e., sterilised with the use of steam, the most common method of sterilisation in hospitals [77, 78]. The materials cannot withstand the heat and due to all the nooks and crannies, residue is likely to remain in the device [79, 80]. Making the needle single-use or reusable and easy to replace will eliminate the need for complete sterilisation of the device. In both solutions, single-use or reusable, the needle should be designed with the ISO 11737-2 (sterility) norm in mind. If minimal safety concerns are present, it is suggested to use a life cycle analysis (LCA) to decide on whether to use a single-use or reusable needle system.

To enable clinical application of our device it will have to comply with the MDR as well as additional country-specific legislation [81]. A major part of MDR compliance

is related to risk management and mitigation. To evaluate the risks of our device, a risk assessment should be performed, conforming to requirements derived from ISO 14971. This risk assessment should cover all aspects of the device, but in particular, the optical fibre and laser needle interaction should be reviewed. Currently, the urologist has to rotate the linear bearing counterclockwise, while holding the optical fibre in place until a distance of $10\,\mathrm{mm}$ is reached between the optical fibre tip and the most distal needle tip [12]. If the optical fibre tip is too close to the needle tip, heating of the needle may occur during ablation, which can lead to irreversible tissue damage. On the other hand, having too much distance between the optical fibre tip and the most distal needle tip can lead to bending of the optical fibre leading to inaccurate placement. Inaccurate placement might lead to ablation of healthy tissue, or incomplete ablation of malignant tissue. We therefore suggest looking into the use of a fail-safe mechanism to create inherent safety by design. As an added benefit this will aid the usability of the device (according to IEC 62366-2), thereby moving closer to meeting the requirements set in IEC 62366-1:2015.

Furthermore, it could be interesting to incorporate current research on steerable needles into our device. An example could be to implement the discrete bevel tip method described by Scali *et al.* [32]. A steerable needle offers greater control and would allow more precise ablation of tumours [32]. Current procedures sometimes require multiple attempts due to needle misplacement resulting from tissue deformation and respiratory motion [82]. Steerable needle rods can alleviate those issues. Additionally, steerable needle rods open up the opportunity for use in different clinical fields, such as, but not limited to, deep brain stimulation, drug delivery in the brain, neurological aspiration, and brachytherapy [83].

We foresee that with minimal design adaptions, our device could be used to accompany a wide range of medical procedures. Our device might serve as a platform with which various functional elements can be inserted and positioned in a patient. Instead of inserting an optical fibre through the laser needle, various tools such as fibre Bragg gratings (FBG) for shape detection in steerable needles [84] and cameras could be inserted and positioned. Additionally, the device may be used for localised drug delivery, tissue engineering and tissue extraction. This versatility and adaptability make the device a promising tool for advancing minimally invasive procedures.

VII. Conclusion

This study presents a methodologically designed device that incorporates a laser system into an MR-conditional wasp-inspired needle for TransPerineal Laser Ablation (TPLA) to treat prostate cancer. Our aim was to integrate a laser system in a stationary device, capable of transforming manually applied torque into linear needle motion that propels the needles through stationary tissue without buckling. Our results show that the needle bundle, consisting of six needle rods and one (hollow) needle for the optical fibre, was able to travel through multiple gelatin phantoms, with gelatin concentrations of 5 wt% up to 15 wt% and slip ratios ranging from 0.91 to 0.93. Our needle could propel itself by transforming the manually applied torque into linear needle motion. The propelling mechanism is not considered self-propelling, as external forces related to friction in the mechanism (max $1.14\,\mathrm{N}$) generated a non-zero push force (max $0.28\,\mathrm{N}$) at the tips of the needles. Nonetheless, this low net push force did not result in buckling or noticeable bending of the needle rods. Furthermore, inserting the optical fibre through the propelled needle did not cause obvious surface damage to the optical fibre tip. In conclusion, our wasp-inspired needle design and prototype narrow the gap to the clinical implementation of wasp-inspired needles for MRI-guided TPLA. Additionally, with minimal design changes, our device may serve as a versatile platform for applications beyond its intended purpose of TPLA, such as camera positioning, drug delivery, tissue engineering, and tissue extraction.

VIII. Acknowledgements

I want to express my sincere gratitude to Mostafa Atalla for his assistance with the data collection and setup for the friction force experiment. Additionally, I would like to thank Jacques Brenkman for providing me with the necessary tools and software to perform the push force experiment. Last, I am thankful to the staff from the Instrument Werkplaats Medewerkers (IWM) and Practicum Modelbouw en Bewerkingen (PMB) for their help in manufacturing most of the parts.

References

[1] Elaine Nicpon Marieb and Katja Hoehn. *Human anatomy & physiology / Elaine N. Marieb, Katja Hoehn.* 2016.

[2] La Tayia Aaron, Omar E. Franco, and Simon W. Hayward. *Review of Prostate Anatomy and Embryology and the Etiology of Benign Prostatic Hyperplasia*. 2016.

[3] Matthew J. Roberts et al. *Seminal fluid: A useful source of prostate cancer biomarkers?* 2015.

[4] Rebecca L. Siegel et al. "Cancer Statistics, 2021". In: *CA: A Cancer Journal for Clinicians* 71.1 (2021). ISSN: 0007-9235.

[5] Le Wang et al. "Prostate Cancer Incidence and Mortality: Global Status and Temporal Trends in 89 Countries From 2000 to 2019". In: *Frontiers in Public Health* 10 (2022). ISSN: 22962565.

[6] Robert K. Nam et al. "Incidence of complications other than urinary incontinence or erectile dysfunction after radical prostatectomy or radiotherapy for prostate cancer: A population-based cohort study". In: *The Lancet Oncology* 15.2 (2014). ISSN: 14702045.

[7] Kristian D. Stensland et al. "National Long-term Survival Estimates After Radical Prostatectomy for Prostate Cancer". In: *Urology* 184 (2024). ISSN: 15279995.

[8] Christopher J.D. Wallis et al. *Survival and Complications Following Surgery and Radiation for Localized Prostate Cancer: An International Collaborative Review*. 2018.

[9] Valerio Iacovelli et al. “50 - TransPerineal Laser Ablation for low- and intermediate risk prostate cancer: Short-term functional outcomes”. In: *Continence* 6 (2023). ISSN: 27729737.

[10] Guglielmo Manenti et al. “Transperineal laser ablation (TPLA) with ultrasound/MRI fusion guidance in the treatment of localized radiotherapy-resistant prostate cancer”. In: *BJR|Open* 5.1 (2023).

[11] Andrea Benelli et al. “The role of MRI/TRUS fusion biopsy in the diagnosis of clinically significant prostate cancer”. In: *Therapeutic Advances in Urology* 12 (2020). ISSN: 17562880.

[12] Iacopo Meneghetti et al. “A single-operator experience using EchoLaser SoracteLite™ for focal laser ablation of prostate cancer: One more arrow in the quiver for the conservative management of the disease”. In: *Archivio Italiano di Urologia e Andrologia* 94.4 (2022). ISSN: 22824197.

[13] Elesta SpA. *SoracteLite is the EchoLaser Thermal Ablation treatment for urological disorders*. 2020.

[14] Luigi A.M.J.G. van Riel et al. “Safety and Feasibility of Soractelite Transperineal Focal Laser Ablation for Prostate Cancer and Short-term Quality of Life Analysis from a Multicenter Pilot Study”. In: *European Urology Open Science* 39 (2022). ISSN: 26661683.

[15] Gugliemo Manenti et al. “Transperineal Laser Ablation (TPLA) Treatment of Focal Low-Intermediate Risk Prostate Cancer.” In: *Cancers* 16.7 (Apr. 2024). ISSN: 2072-6694.

[16] Richard Taschereau et al. “Seed misplacement and stabilizing needles in transperineal permanent prostate implants”. In: *Radiotherapy and Oncology* 55.1 (2000). ISSN: 01678140.

[17] Marek Wartenberg et al. “Closed-Loop Active Compensation for Needle Deflection and Target Shift During Cooperatively Controlled Robotic Needle Insertion”. In: *Annals of Biomedical Engineering* 46.10 (2018). ISSN: 15739686.

[18] Annie D.R. Li et al. “Needle deflection and tissue sampling length in needle biopsy”. In: *Journal of the Mechanical Behavior of Biomedical Materials* 104 (2020). ISSN: 18780180.

[19] Jette Bloemberg et al. “Therapeutic prostate cancer interventions: a systematic review on pubic arch interference and needle positioning errors”. In: *Expert Review of Medical Devices* 21.7 (July 2024), pp. 625–641. ISSN: 1743-4440.

[20] M. Scali, P. Breedveld, and D. Dodou. “Experimental evaluation of a self-propelling bio-inspired needle in single- and multi-layered phantoms”. In: *Scientific Reports* 9.1 (2019). ISSN: 20452322.

[21] Aimée Sakes, Dimitra Dodou, and Paul Breedveld. *Buckling prevention strategies in nature as inspiration for improving percutaneous instruments: A review*. 2016.

[22] Uroš Cerkvenik et al. “Mechanisms of ovipositor insertion and steering of a parasitic wasp”. In: *Proceedings of the National Academy of Sciences of the United States of America* 114.37 (2017). ISSN: 10916490.

[23] Hany K.M. Dweck, Neveen S. Gadallah, and Essam Darwish. “Structure and sensory equipment of the ovipositor of Habrobracon hebetor (Say) (Hymenoptera: Braconidae)”. In: *Micron* 39.8 (2008). ISSN: 09684328.

[24] Noraly M.M.E. van Meer et al. “The ovipositor actuation mechanism of a parasitic wasp and its functional implications”. In: *Journal of Anatomy* 237.4 (2020). ISSN: 14697580.

[25] Zola Fung-A-Jou et al. “WASP: a Wasp-inspired Surgery needle for Prostate cancer procedures”. PhD thesis. Delft: Delft University of Technology, 2023.

[26] Marcus King and Julian Vincent. “The mechanism of drilling by wood wasp ovipositors”. In: *Biomimetics* 3.4 (1995). ISSN: 1059-0153.

[27] Uroš Cerkvenik et al. “Functional principles of steerable multi-element probes in insects”. In: *Biological Reviews* 94.2 (2019). ISSN: 1469185X.

[28] Jette Bloemberg et al. “Design and evaluation of an MRI-ready, self-propelled needle for prostate interventions”. In: *PLoS ONE* 17.9 September (2022). ISSN: 19326203.

[29] L. Frasson et al. “STING: A soft-tissue intervention and neurosurgical guide to access deep brain lesions through curved trajectories”. In: *Proceedings of the Institution of Mechanical Engineers, Part H: Journal of Engineering in Medicine* 224.6 (2010). ISSN: 09544119.

[30] Alexander Leibinger, Matthew J. Oldfield, and Ferdinando Rodriguez Y Baena. “Minimally disruptive needle insertion: A biologically inspired solution”. In: *Interface Focus* 6.3 (2016). ISSN: 20428901.

[31] Luca Frasson et al. “Early developments of a novel smart actuator inspired by nature”. In: *International Journal of Intelligent Systems Technologies and Applications* 8.1-4 (2010). ISSN: 17408873.

[32] M. Scali et al. “Ovipositor-inspired steerable needle: design and preliminary experimental evaluation”. In: *Bioinspiration & Biomimetics* 13.1 (Dec. 2017), p. 016006. ISSN: 1748-3190. URL: https://iopscience.iop.org/article/10.1088/1748-3190/aa92b9%20https://iopscience.iop.org/article/10.1088/1748-3190/aa92b9/meta.

[33] Olivier Wegelin et al. *Comparing Three Different Techniques for Magnetic Resonance Imaging-targeted Prostate Biopsies: A Systematic Review of In-bore versus Magnetic Resonance Imaging-transrectal Ultrasound fusion versus Cognitive Registration. Is There a Preferred Technique?* 2017.

[34] Gregor Schaefers. “Testing MR safety and compatibility”. In: *IEEE Engineering in Medicine and Biology Magazine*. Vol. 27. 3. 2008.

[35] Simon Lidgate, Gregory Griffin, and Gregory Martin. *Magnetic Resonance Conditionality applications: EU Requirements and supporting Standards*. Tech. rep.

[36] U.S. Department of Health et al. *Testing and Labeling Medical Devices for Safety in the Magnetic Resonance*

(MR) Environment. Tech. rep. Food and Drug Administration, 2023.

[37] Yue Chen et al. "MR-conditional steerable needle robot for intracerebral hemorrhage removal". In: *International Journal of Computer Assisted Radiology and Surgery* 14.1 (2019). ISSN: 18616429.

[38] Rahim Horuz et al. "Simple preoperative parameters to assess technical difficulty during a radical perineal prostatectomy". In: *International Urology and Nephrology* 45.1 (2013). ISSN: 03011623.

[39] Hye Shin Ahn et al. "Comparison of the diagnostic efficacy of ultrasound-guided core needle biopsy with 18-versus 20-gauge needles for thyroid nodules". In: *Journal of Ultrasound in Medicine* 37.11 (2018). ISSN: 15509613.

[40] Ping Liang et al. "US-guided percutaneous needle biopsy of the spleen using 18-gauge versus 21-gauge needles". In: *Journal of Clinical Ultrasound* 35.9 (2007). ISSN: 00912751.

[41] Lazaros Tzelves et al. *Transperineal laser ablation as a new minimally invasive surgical therapy for benign prostatic hyperplasia: a systematic review of existing literature*. 2023.

[42] Gaetano De Rienzo et al. "Transperineal interstitial laser ablation of the prostate, a novel option for minimally invasive treatment of benign prostatic obstruction". In: (2020). URL: https://doi.org/10.1016/j.eururo.2020.08.018.

[43] Claudio Maurizio Pacella et al. "Transperineal laser ablation for percutaneous treatment of benign prostatic hyperplasia: a feasibility study. Results at 6 and 12 months from a retrospective multi-centric study". In: *Prostate Cancer and Prostatic Diseases* 23.2 (2020). ISSN: 14765608.

[44] David F. Williams. "On the mechanisms of biocompatibility". In: *Biomaterials* 29.20 (2008). ISSN: 01429612.

[45] Ashmith Relia Da Cruz and Aileen J. "Optimisation of Processes by Recommending Cost Reduction Strategies in Central Sterile Supply Department (CSSD) in a Tertiary Care Hospital". In: *Journal of Health Management* 24.2 (2022). ISSN: 09730729.

[46] Forbes McGain, Graham Moore, and Jim Black. "Hospital steam sterilizer usage: Could we switch off to save electricity and water?" In: *Journal of Health Services Research and Policy* 21.3 (2016). ISSN: 17581060.

[47] Tobias Penzkofer et al. "How mri compatible is "mRI compatible"? A systematic comparison of artifacts caused by biopsy needles at 3.0 and 1.5 T". In: *CardioVascular and Interventional Radiology* 36.6 (2013). ISSN: 01741551.

[48] ISO. *ISO 10993-1:2018*. Oct. 2018.

[49] S. Mohapatra. "Sterilization and Disinfection". In: *Essentials of Neuroanesthesia*. 2017.

[50] Glenn N. Levine et al. *Safety of magnetic resonance imaging in patients with cardiovascular devices: An American heart association scientific statement from the committee on diagnostic and interventional cardiac catheterization, council on clinical cardiology, and the council on cardiovascular radiology and intervention*. 2007.

[51] A.G.C. van Boeijen et al. *Delft Design Guide*. Amsterdam: BIS Publishers, 2013.

[52] Stefan Persaud et al. *BEP Manual 2020 2021 Q4*. Delft, 2021.

[53] Matthieu Fischer et al. "Friction testing of tube-guided electrically heated Nitinol shape-memory alloy wires". In: *Tribology International* 191 (2024). ISSN: 0301679X.

[54] John F. Schenck. "The role of magnetic susceptibility in magnetic resonance imaging: MRI magnetic compatibility of the first and second kinds". In: *Medical Physics* 23.6 (1996). ISSN: 00942405.

[55] Georg C. Feuerriegel and Reto Sutter. *Managing hardware-related metal artifacts in MRI: current and evolving techniques*. 2024.

[56] Eshwar Pawar. "A Review Article on Acrylic PMMA". In: *IOSR Journal of Mechanical and Civil Engineering (IOSR-JMCE) e-ISSN* 13.2 (2016).

[57] Deepak Kapoor. *Nitinol for Medical Applications: A Brief Introduction to the Properties and Processing of Nickel Titanium Shape Memory Alloys and their Use in Stents*. 2017.

[58] Aleksa Milovanović et al. "Experimental dimensional accuracy analysis of reformer prototype model produced by FDM and SLA 3D printing technology". In: *Lecture Notes in Networks and Systems*. Vol. 54. 2019.

[59] Paul Alexander, Seth Allen, and Debasish Dutta. "Part orientation and build cost determination in layered manufacturing". In: *CAD Computer Aided Design* 30.5 (1998). ISSN: 00104485.

[60] Christin Arnold et al. "Surface quality of 3D-printed models as a function of various printing parameters". In: *Materials* 12.12 (2019). ISSN: 19961944.

[61] Christina Schmidleithner and Deepak M. Kalaskar. "Stereolithography". In: *3D Printing*. InTech, Oct. 2018.

[62] Antonio Pavone, Gianni Stano, and Gianluca Percoco. "On the Fabrication of modular linear electromagnetic actuators with 3D printing technologies". In: *Procedia CIRP*. Vol. 110. C. 2022.

[63] Marta Scali. "Self-propelling needles: From biological inspiration to percutaneous interventions". PhD thesis. Delft: Delft University of Technology, 2020.

[64] Bharat Bhushan. "Adhesion and stiction: Mechanisms, measurement techniques, and methods for reduction". In: *Journal of Vacuum Science & Technology B: Microelectronics and Nanometer Structures Processing, Measurement, and Phenomena* 21.6 (2003). ISSN: 1071-1023.

[65] Torben A. Lenau et al. "Mosquito inspired medical needles". In: *Bioinspiration, Biomimetics, and Bioreplication 2017*. Vol. 10162. 2017.

[66] Allison M. Okamura, Christina Simone, and Mark D. O'Leary. "Force modeling for needle insertion into soft tissue". In: *IEEE Transactions on Biomedical Engineering* 51.10 (2004). ISSN: 00189294.

[67] Gregor Harih and Bojan Dolšak. “Comparison of subjective comfort ratings between anatomically shaped and cylindrical handles”. In: *Applied Ergonomics* 45.4 (2014). ISSN: 18729126.

[68] Lawrence P. Panych and Bruno Madore. *The physics of MRI safety*. 2018.

[69] Qingyu Xiao et al. *MR-Conditional Actuations: A Review*. 2020.

[70] L.J. Erasmus et al. “A short overview of MRI artefacts”. In: *South African Journal of Radiology* 8.2 (2004). ISSN: 1027-202X.

[71] Shan Jiang et al. “Experimental study of needle-tissue interaction forces: Effect of needle geometries, insertion methods and tissue characteristics”. In: *Journal of Biomechanics* 47.13 (2014). ISSN: 18732380.

[72] Russell H. Taylor and Dan Stoianovici. *Medical Robotics in Computer-Integrated Surgery*. 2003.

[73] Andreas Melzer et al. “Nitinol in magnetic resonance imaging”. In: *Minimally Invasive Therapy and Allied Technologies* 13.4 (2004). ISSN: 13645706.

[74] A. Szold. “Nitinol: Shape-memory and super-elastic materials in surgery”. In: *Surgical Endoscopy and Other Interventional Techniques* 20.9 (2006). ISSN: 09302794.

[75] Evek GmbH. *Veerstaaldraad 0,3mm-2,25mm Veerstaaldraad EN 10270-1 Grade DH Staaldraad*. Oct. 2024.

[76] Petr Šittner et al. “Young’s modulus of austenite and martensite phases in superelastic NiTi wires”. In: *Journal of Materials Engineering and Performance*. Vol. 23. 7. 2014.

[77] Cynthia Spry. *Understanding current steam sterilization recommendations and guidelines.* 2008.

[78] Mubarak Taiwo Mubarak, Ilker Ozsahin, and DIlber Uzun Ozsahin. “Evaluation of Sterilization Methods for Medical Devices”. In: *2019 Advances in Science and Engineering Technology International Conferences, ASET 2019*. 2019.

[79] L. K.O. Lopes et al. “Complex design of surgical instruments as barrier for cleaning effectiveness, favouring biofilm formation”. In: *Journal of Hospital Infection* 103.1 (2019). ISSN: 15322939.

[80] Gopal Panta, Ann K. Richardson, and Ian C. Shaw. *Effectiveness of autoclaving in sterilizing reusable medical devices in healthcare facilities*. 2019.

[81] J. Malvehy et al. *New regulation of medical devices in the EU: impact in dermatology*. 2022.

[82] C. N. Riviere et al. “Predicting respiratory motion for active canceling during percutaneous needle insertion”. In: *Annual Reports of the Research Reactor Institute, Kyoto University*. Vol. 4. 2001.

[83] Michel A Audette, Stéphane PA Bordas, and Jason E Blatt. “Robotically Steered Needles: A Survey of Neurosurgical Applications and Technical Innovations”. In: *Robotic Surgery: Research and Reviews* Volume 7 (2020).

[84] Abdulhamit Donder and Ferdinando Rodriguez Y. Baena. “Kalman-Filter-Based, Dynamic 3-D Shape Reconstruction for Steerable Needles With Fiber Bragg Gratings in Multicore Fibers”. In: *IEEE Transactions on Robotics* 38.4 (2022). ISSN: 19410468.

APPENDIX A
DESIGN EVOLUTION INTERVIEW

This Appendix provides the interview taken on 30-09-2024 with Silje Dehli, a teacher at the Delft University of Technology industrial design faculty, about the Design Evolution method.

Design Evolution Interview - Silje Dehli – 30-09-2024:

Short introduction:

1. Who are you? (experience and academic credentials in short)
    a. Industrial Design Engineering (IDE) teacher. Has more than 15 years of teaching experience at the IDE faculty at the technical university of Delft.
    b. Was part of the team that redesigned the IDE bachelor.
2. What is your expertise?
    a. Educational design. More specifically, how to teach design, design processes and design methodologies to students.

General understanding:

3. Can you explain a Design Evolution in the context of product development?
    a. It is a method that helps to communicate and structure the design process. Moreover, it can be used as a tool to decide on what steps to take to improve the design, while maintaining a structured design process and compliance with the previously set goal.
4. Where does the Design Evolution originate from?
    a. It is a method created by multiple teachers at the IDE faculty to help students understand design processes. It is inspired by methods used by NPK design, a design agency focused on product development.

Process:

5. What are the typical stages or phases involved in the Design Evolution process?
    a. Typically a Design Evolution encompasses one or multiple concepts phases. However, it can be used for a wide range of phases.

Pros and cons:

6. When should one use a Design Evolution?
    a. From the beginning of the concept phase until the end. Or, if there is limited time, when a decision has to be made regarding the design direction.
7. What are the benefits of using a Design Evolution?
    a. First, it helps in structuring the design process.
    b. Second, it can helps in communicating the design and design process to others.
    c. Third, it helps with deciding on what steps to take to improve the design, while maintaining a structured design process and compliance with requirements.
8. When not to use a Design Evolution?
    a. When there is very limited time. A Design Evolution can be time consuming to create and maintain.
9. What are the cons of a Design Evolution?
    a. Large file size, time consuming, and cannot be represented easily in a A4 (portrait) format.

Practical application:

10. Is the Design Evolution methodology used in the design industry?
    a. No, at least not like it is taught at IDE. NPK, however, uses a similar method to communicate their designs with clients.

APPENDIX B
DESIGN PROCESS

This Appendix provides an overview of the design process. To ensure a thorough and structured design process, as well as compliance with all requirements a Design Evolution was used. A Design Evolution is a tool used to communicate the design process through visual representations as well as textual descriptions. It is used to communicate how activities, methods, and iterations have led to the final design. With the use of the Design Evolution, every (iterative) step has been documented, evaluated and communicated.

How it works in detail:

The Design Evolution is structured using sequential steps. It therefore shows how the different activities have evolved the design. The visual symbols in the top row of the Design Evolution are used to portray the type of activity and what tools were used to perform this activity (e.g. Solidworks, Illustrator, Maple, hand tools, etc.). Below each symbol, a very compressed alinea is written to denote, explain and evaluate the activity. If and how the activities affected the design is graphically shown below each alinea. It is important to note that all visual and textual elements per column are connected and represent the same activity. The Design Evolution is presented in the next 23 pages or can be accessed by clicking the link below. The pages are organised sequentially and should be read in order from the first to the last page. For the best experience, it is recommended to read the Design Evolution in its dedicated PDF format by clicking the link below.

Link:

The Design Evolution is attached as a PDF, as its format makes it challenging to portray in a LaTeX file accurately. To download the Design Evolution (subdivided into four different PDF files) click the link below.

https://filesender.surf.nl/?s=download&token=
c2f87ad4-0f47-4eb2-b7cd-1c8530b3e1e4

MR-conditional WASP-inspired needle with integrated laser functionality.

Context

TPLA UROLOGY

Target group

Urologists

Ideation phase

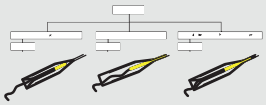


From this point on I will focus on the ideation. This means I will ideate, prototype, experiment and validate to improve my design.
I will write down the most important things I have done, and which have given me insights. Some continuous processes, such as updating my planning, or the requirements and wishes lists will, generally speaking, not be mentioned.

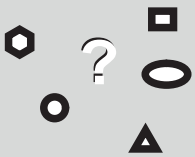
Brainstorm global solutions



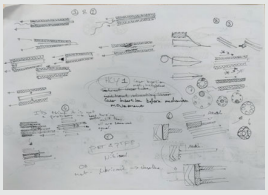
Identified possible global solutions (3 laser classes), and investigated their sub-problems to create “How-Tos”.

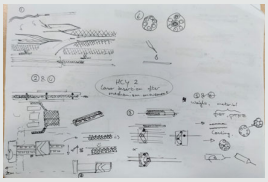


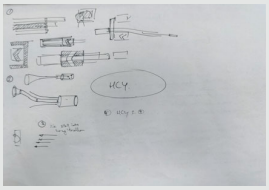
How-Tos

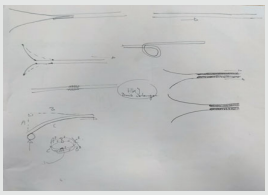


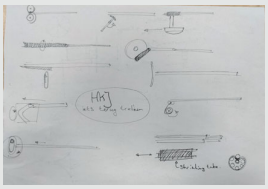
I created How-Tos of the previously identified sub-problems per laser class.







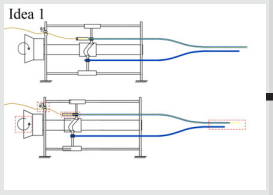


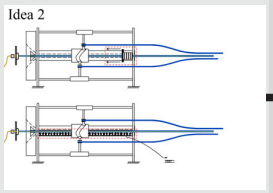


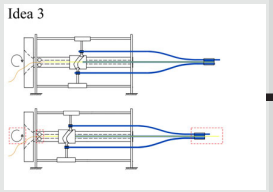
7 idea creation

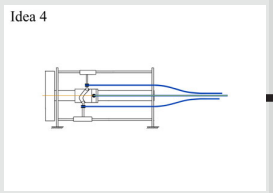


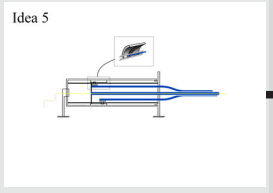
Used the sub-solutions to create 7 ideas

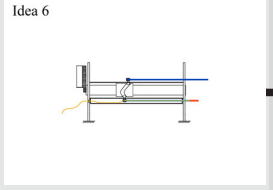


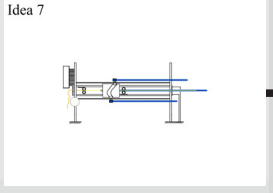








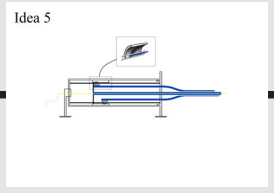




Meeting



Had a meeting with Jette and Aimée to brainstorm about the ideas. Idea 5 - inverse camshaft - was the preferred idea. However, some issues need to be resolved in order to make it a viable option, namely: low friction of the cam to enable translation; securing and retracting the cam; integration of the mechanism and inner needle; and ensuring the inner needle does not stick out of the device.



MR-conditional WASP-inspired needle with integrated laser functionality.

Context

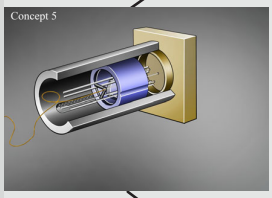
TPLA UROLOGY

Target group

Urologists

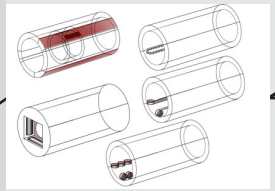
3D sketch concept

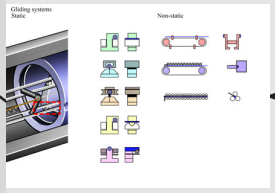
I drew a 3D sketch to enable discussion and integration of sub-solutions, thereby minimising errors (resulting from 2D image discussions) and ensuring solutions are being created within a 3D space.



Sub-solutions needle and cam

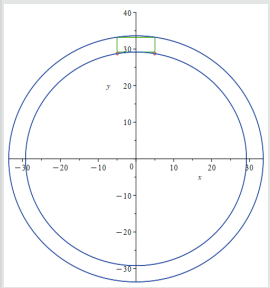
I drew multiple 3D sketches to enable discussion and integration of sub-solutions, thereby minimising errors (resulting from 2D image discussions) and ensuring solutions are being created for a 3D space.





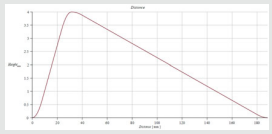
Maple - undercutting

I determined the minimum radius to prevent undercutting for MR-safe ball bearings (10mm outer diameter).



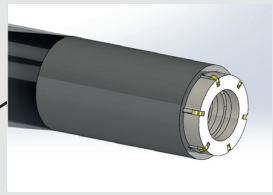
Maple - cam path

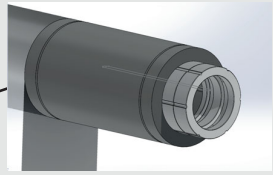
I made a Maple model to determine the path the ball bearings have to take.

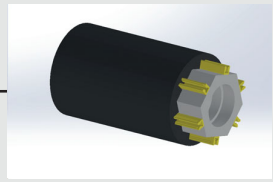


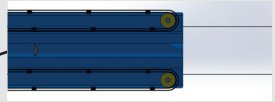
Solidworks - 6 sub-solutions

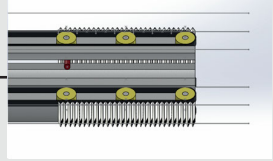
I made Solidworks models based on the outer mechanism sub-solutions. I took the minimum radius to prevent undercutting into account.

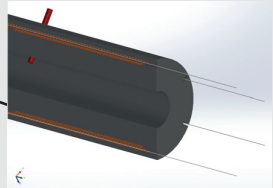












MR-conditional WASP-inspired needle with integrated laser functionality.

Context

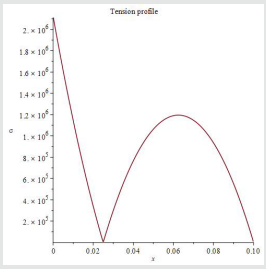
TPLA UROLOGY

Target group

Urologists

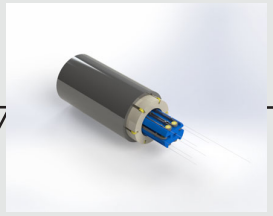
Maple - deflection, tension

I calculated the maximum deflection of a 300mm long nitinol rod. Surprisingly, the nitinol rod does not need to be supported at all if a rod length of 300mm is used.
However, when taking into account buckling, the rod needs to be supported.



SW - 3 concept creation

I created 3 concepts based on sub-solutions following the How-Tos.







Ball bearing print

I printed ball bearings to evaluate the tolerances of the Ultimaker.
The tolerances that I chose were too little, which resulted in non-functioning ball bearings.
Tolerances ball-bearing (print on 2mm metal ball)
r = 0.05 mm
- Too small, I will need around 0.25 mm extra due to the small size and print inaccuracies with curvatures at that size.

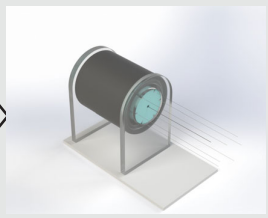
Tolerances holders (print on print)
r = 0.05 mm
- Fits, but barely. r = 0.1 would probably be better while still maintaining a tight fit.

Meeting Concepts

I discussed the concepts with my supervisors. This resulted in the following takeaways.
- Make the cam as light as possible to minimise force needed to move the device (friction & inertia).
- Minimise moving parts i.e., ball bearings and belts - they make it more intricate and are not necessarily lower friction at the desired speed and size.
- Prototype with balls and the gliding of the rods. Additionally evaluate whether a thin needle inside a tube will work with low friction.
- Evaluate whether the laser needle will have horizontal forces acting upon it.

SW - Redesign

- Based on comments from both supervisors I decided to create a redesign taking the previously mentioned comments into account. By redesigning the model now, I could determine what parts I need to experimentally evaluate.
- The redesign focusses on minimising moving parts and aims for lower inner cam weight instead.



MR-conditional WASP-inspired needle with integrated laser functionality.

Context

TPLA UROLOGY

Target group

Urologists

Render - sub-problems

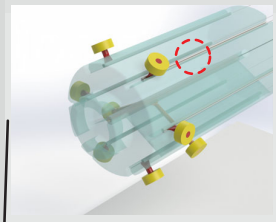
I created multiple renders to highlight the sub-problems.

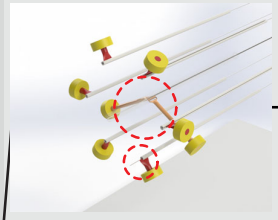
1 Laser needle holder
- Tip too fragile?
- Connection with needle strong enough?
- Friction with Teflon side too high?

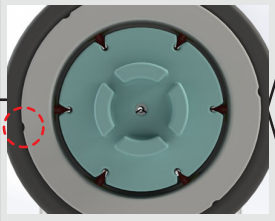
2 Needle rod within Teflon tube
- Friction too high
- How to ensure it does not buckle & fall

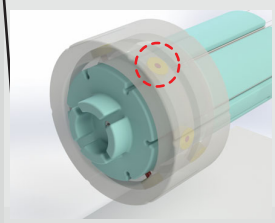
3 Balls to enable gliding
- Closed or open path for the balls?

4 Plastic ball bearings
- How to hold the bearings in place?





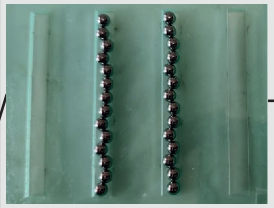




Prototype - Linear bearing

I created a test to evaluate if I needed a closed loop for the gliding balls.

Materials:
- Lasercut acryl (2mm)
- 4mm metal balls
- Glue/tape





Evaluate - Linear bearing

Not using a closed loop led to more friction compared to using a closed loop. The balls within the straight paths (no loop) would not roll, whereas the balls in the closed loop would.
Of course this experiment has some major limitations, but it did show that (even with a lot of pressure) the balls were not willing to rotate in the straight paths, thereby leading to sliding balls instead of rolling balls.

Note: it is very important to create a well rounded path with minimal tolerances to ensure the balls line-up well.

Maple - Needle friction

Nitinol might experience high friction when sliding along a surface. To evaluate the friction I have chosen to use a material with the lowest theoretical friction coefficient with Nitinol. This is PTFE (also known as Teflon). It has a friction coefficient of 0.056 (see paper in the analysis map).
To evaluate the effect sliding will have, I need to create a full test setup measuring the friction of the needle. This is, however, quite cumbersome and unnecessary as some sources provide a friction coefficient which can be used to evaluate the theoretical effect.
Note: I will reconsider this statement.
The friction force will be 2.52*10^-5 N.

$$Ff := 0.00002523216118$$

Needle holder problem

Using laser needle holders might be too fragile, but to evaluate this I need to either make a 3D model and evaluate the effects, or print it at a place able to print that small and accurate. This takes up valuable time and effort, so I will have to take this in to consideration.

MR-conditional WASP-inspired needle with integrated laser functionality.

Context

TPLA UROLOGY

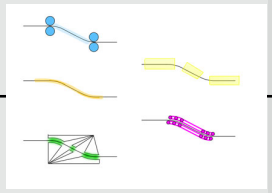
Target group

Urologists

Ideation - needle support



Create sub-solutions which can support and guide the needle rods such that they come together in the middle, without too much friction.



Prototype - needle support



I created sub-solutions which guide the needles in such a way that they come together in the middle.
Evaluate friction and determine whether they can be an effective solution.

- The friction in a straight Teflon tube is 6x higher than mentioned in the paper. This can be a result from the Teflon tube not being straight enough. It could also be a result from surface roughness.

Evaluate with real world tests whether a Teflon tube can indeed keep shape, and guide the Nitinol needle rods.

- Yes they can, but ensuring they follow the exact path is challenging.

$\mu := evalf\left(\frac{Ff}{Fn}\right);$

0.32



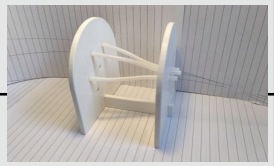
Prototype - needle support



I created sub-solutions which support and guide the needles such that they come together in the middle.
Evaluate the friction and determine whether it can be an effective solution.

- The friction within a curved PTFE tube is really high. The gravitational force of the rod does not overcome the friction within the PTFE tube, meaning the friction is higher than in the straight tube.

Solve this by placing the needle rods closer to the middle and minimising the angle of attack.

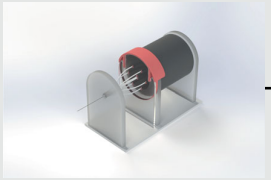


SW - retraction mechanism



The retraction mechanism

- Connecting the laser needle to the innercam will enable retraction by simply rotating the linear bearing in the opposite direction.
- It needs, however, an additional mechanism to hold the inner-cam/needles in place. This is to make sure that when the laser is pushed through the laser needle, the cam and thus the needle rods do not move forward.
  - A possible solution is shown in red in the render.



Meijer en Blessing



- I checked the materials and tubes readily available at the store for prototyping purposes.
  - They have no small diameter plastic tubes.
  - They do have small diameter brass, aluminium (both MR-conditional), and metallic tubes. All can perfectly fit a Nitinol needle rod.
    - 5 rods = 8eu

MR-conditional WASP-inspired needle with integrated laser functionality.

Context

TPLA UROLOGY

Target group

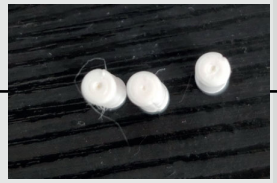
Urologists

FDM nitinol holders



Can I print a Nitinol rod holder with a 'basic' fused deposition modelling (FDM) printer?

- No, the printer could not reliably make a 0.3, 0.4, or 0.5mm hole.

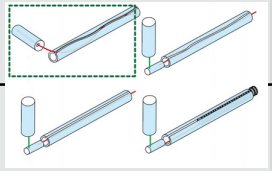


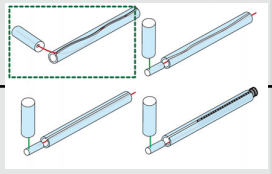
Needle guidance solutions



How can I ensure that the needle rods can translate with minimal friction, while making sure that buckling does not occur/ create problems?

- Placing a Nitinol needle rod into a 90 degree angled Nitinol needle rod holder, ensures connection to the cam. Placing this into a PTFE tube with a wavelike incision ensures the needle can translate without buckling (in theory).

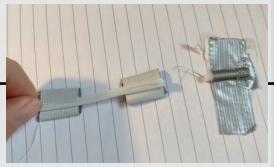


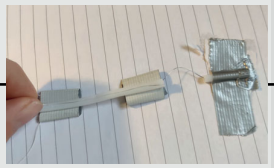


Prototyping needle guidance



- I evaluated the previous needle translation sub-idea, with a quick prototype. I found that the principle of a curvy guide works well. However, when inserting the rod with an angle, as shown in the picture below, it can create problems. For that reason it might be advisable to combine the curvy guide sub-solution with a different sub-solution.
- A potential problem might be on how to ensure movement of the ball bearing will lead to effective translation in the path parallel to the PTFE tube and the Nitinol needle rod.

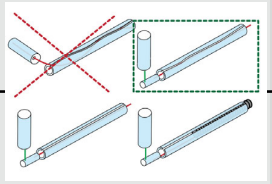


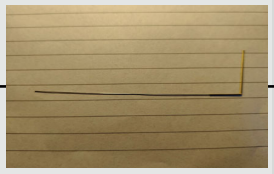


SW sub-solution prototype



I made different sub-solution combinations. The green rod in the picture can be made from brass.





Prototype meeting



I showed them the presentation "*25_4_2024*", and they were quite satisfied with the progress. Some important remarks were:

1 - Does it really matter if the ball bearings are supported by the Nitinol/brass tubes?
2 - Watch out for plastic deformation when trying to stop the needles
3 - Evaluate the best curve for the PTFE tube, by making prototypes (IWM).
4 - What performance metrics do I want to test?
Interaction with surgeon? - Handle
5 - Lowering friction by using "talk" powder or lubricants.
6 - Place the PTFE tubes closer to the middle to decrease the radius, and thus friction.

MR-conditional WASP-inspired needle with integrated laser functionality.

Context

TPLA UROLOGY

Target group

Urologists

Call 123-3D



I called 123-3D to inquire about the friction coefficient of the PTFE tube. He told me that I bought a no-name PTFE tube for 3D printing, so although it should have a low friction due to its material (PTFE), the manufacturing is likely to be cheap. Therefore, the PTFE is probably not optimised for low friction. He advised me to buy Capricorn PTFE tubes, as these are optimised for friction.

Prototype - needle support



I reran the previous tests with a shorter tube, this led to a lower friction coefficient, but the results vary quite a bit during different measurements. Most are between 10 and 20 degrees, with a spike around 13 degrees. As this is not a methodological approach this experiment can only provide an indication for the actual friction coefficient. Although the assumption that the shape might lead to differences cannot be debunked, it is likely that differences in surface roughness lead to the majority of differences in friction coefficients and therefore in the heightened friction coefficient compared to the theoretical value mentioned in the paper before.

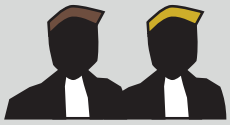
$Ff := evalf(w \cdot g \cdot \sin(\theta))$;

$Ff := 0.00007285046261$

$\mu := evalf\left(\frac{Ff}{Fn}\right)$;

0.23

IWS & IWM



I talked with Damien from IWM and Sam from IWS, to discuss possible manufacturing options for the Teflon needle guidance. The main takeaways from the conversation were:
1 - Likely too small & too thick for CNC machining. Might be possible, but wont give the smooth finish
2 - Lasercutting is best, if they cut Teflon
- Spoiler: They don't - it does not lead to good results and is toxic.
- They do have polystyrol (PVC alike)

3 - D printing is possible. The best option would be Formlabs without supports.
4 - Try to adjust the shape, such that it becomes manufacturable.
- Basically, make the curve/ incision in 2D, as this will lead to better results.

Prototype - ball slider



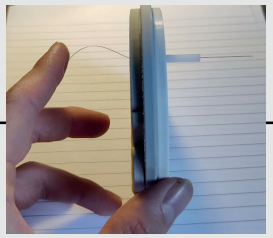
I created a stereo-lithography (SLA - formlabs 3) print of a linear ball bearing. I wanted to evaluate whether the balls would roll when a glider was placed upon them. If the balls roll I want to evaluate whether the printer can create a smooth enough path to ensure low friction and smooth ball movement.
Experiment:
- The balls roll. However, it does take some normal force to roll, instead of slide.
- Applying WD40 improves rolling, and leads to less normal force being needed.
- Tolerances were ok. But clamping too hard led to more rolling resistance.
- Conclusion: It works, but there is some room for improvement.



Prototype - needle rod stop



I created an FDM (Ultimaker) printed retraction mechanism. I wanted to find out whether this mechanism would hold the needles in place, while not leading to plastic deformation of the Nitinol needle rods. The mechanism works by pushing the middle part down, thereby clamping the needles, and thus (hopefully) ensuring no needle movement when the laser is inserted.
Experiment:
- It works. The needle rods experience significantly greater friction, meaning they buckle before they move/translate (photo 3).
- After a visual inspection no visible plastic deformation has taken place (photo 5)
- Remark: redo tolerances middle part.



MR-conditional WASP-inspired needle with integrated laser functionality.

Context

TPLA UROLOGY

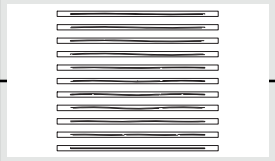
Target group

Urologists

IWS



I talked with IWS regarding laser cutting possibilities to evaluate the effect of different curve lengths, radi, and intersections. They advised me not to use Teflon, because it is toxic, difficult to laser cut, and can lead to undesired deformation and heat damage. For that reason, they advised me to use a thin plastic material (polystyrol) that can be cut easily. This hopefully assures smooth paths, likely leading to less friction compared to using a low friction material (PTFE) that cannot be laser cut.



Meeting Jette



I had a meeting with Jette to discuss the experimental design outcomes. All in all, the results were promising and I should move on to print the actual parts.
When printing the parts I should focus on minimising the material needed and I should use the printers wisely.
Additionally, I can experiment with PTFE plates attached to the inner-axis. This will ensure low friction

IWM



Talked with IWM about printing the inner-cam and linear bearing. Decided on resin printing the inner-cam and the ball bearing parts of the linear bearing due to need of a smooth surface. The remaining parts will be printed with FDM (fused deposition modelling) to lower costs. This is also taken account in the design of the linear bearing.

Experimental setup Ideation



While waiting for my 3D printed and laser cut parts, I will focus on the test setup. What performance criteria do I want to evaluate and how? I will make multiple proposals and discuss those in the future with Aimée and Jette.

Meeting Jette



Talked about many things, most importantly the following:

- One needle rod moves forward while the others retract. This leads to friction forces between the needle rods and the tissue (already known). However, friction forces between the cam and needle will also add to the forward movement, and likely generate a net force.
- Need to determine my independent and dependent variables.
- Both agree that the laser needle can be made from a different material (look to Soloman).

MR-conditional WASP-inspired needle with integrated laser functionality.

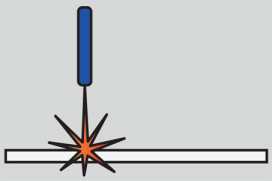
Context

TPLA UROLOGY

Target group

Urologists

Laser cutting



The material IWS recommended to me, turned out to be a thermoplast. So after waiting two weeks my laser cut part turned out to be unusable, because the material melted. I will have to laser cut again. From now on I will try to laser cut at PMB, in the industrial design faculty (IDE).



3D printing laser holder

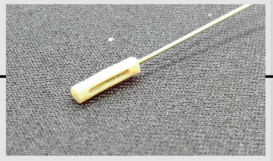


The parts were printed to find out whether it is possible to print at this scale and to examine the “strength” and flexibility of the parts.

- The prints seem to be rigid enough.
- The functionality and rigidity will have to be tested.

Remark:

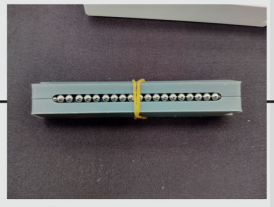
- Due to the small diameter, but long length, the prints are a little warped. It is unsure whether this will lead to problems in the assembly.



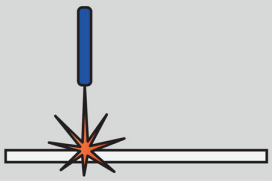
3D printing linear ball bearing



With half of the linear ball bearing prints done I examined the functionality of the parts. Using the same parameters as in the previous print (DesignEvolutionThesis.), I expected the results to be similar.
The results were similar, but due to the long length, the prints were a little warped. This led to balls falling out if too little pressure was applied to the parts. If too much pressure was applied, the balls experienced too much friction and would not move. A balance will have to be found to circumvent these problems.



Laser cutting



After laser cutting at IWS went wrong, I went to the PMB (IDE). At PMB they laser cut one 1mm acryl plate and one 2mm acryl plate. The 1mm plate was noticeably warped, whereas the 2mm plate showed only little deformation. For this reason, I will use 2mm thick acryl plates in the future. The right curvature/ angles still need to be validated.





Testing needle guides



After testing the needle guides on their ability to limit buckling the following curves were deemed to be a success:
2, 6, 7, 8, 10
Except for number two, these are splines that cross the middle twice, or four times.
Two seems to be an outlier as similar splines with the same shape, but different curvatures do allow buckling.
It has to be noted that it is only a preliminary test. Therefore the results are not 100% conclusive. Nevertheless, it provides a good starting point for the final design.



MR-conditional WASP-inspired needle with integrated laser functionality.

Context

TPLA UROLOGY

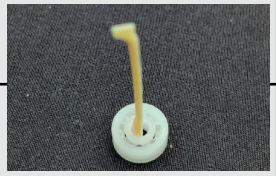
Target group

Urologists

Needle holder & ball-bearing



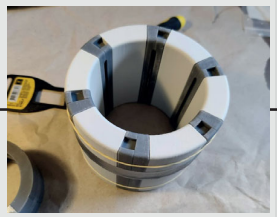
Due to warping of the laser needle holder, only one fits in the ball-bearer. The ball bearer seems to work fine though.

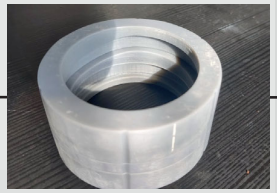


Linear bearing - inner-cam



Due to a misunderstanding with IWM the resin printed parts resulted in 12 A parts instead of 6 A and 6 B parts. Nevertheless, with some elastic bands and ducktape it was made into a viable prototype. Generally speaking the fit is good, that is, the prints need limited sanding and tolerances are good. There is, however, a problem with making sure all the parts stay in the exact same position. The elastic bands keep everything together, but allow for too much wiggle room, which could result in decreased performance.
The 3 parts making up the inner-cam fit perfectly together and are very smooth.

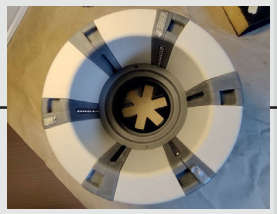




Linear bearing prototype



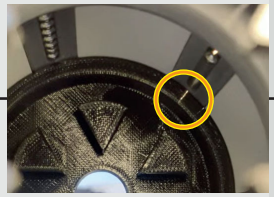
After assembling the prototype and inserting 300 balls greased with a synthetic greaser called "Super Lube" some test were performed. The fit with the balls was tested. adly some balls fell out when picking up the linear bearing. The balls fell from the end and the beginning of the ball bearing path. The friction when entering the corner, was higher compared to breaking out from the part. After applying WD40 this problem became less of an issue and the inner-cam was placed into the linear bearing. Sadly the inner-cam did not fit into the linear bearing. The inner-cam needed a lot of sanding. After sanding the inner-cam fitted in the linear bearing, but it was still quite tight.



Linear bearing prototype



This tightness resulted again in balls falling out of the linear bearing. Interestingly, almost all balls fell out of one ball bearing part. As the inner-cam was made up out of three parts, I placed the bottom part of the inner-cam at the bottom of the device. This ensured that the ball would not fall out of the ball-bearing part when trying to go around the corner. This helped. Nevertheless, when placing the outer cam with the inner-cam horizontal and turning the linear bearing, balls fell. This time the balls fell from the other end.
I will have to find a solution for this.



Inner-axis fit in (back)plate



I printed the inner-axis with FDM and the results were good. The design is stronger than expected and fits in the front and backplate. The different design compared to earlier is to minimise material. Additionally the inner-axis was adapted to hold Teflon plates.



MR-conditional WASP-inspired needle with integrated laser functionality.

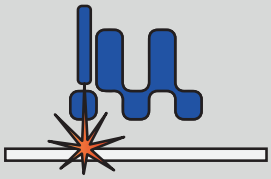
Context

TPLA UROLOGY

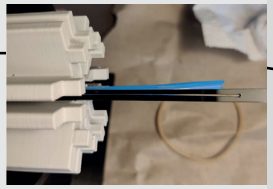
Target group

Urologists

PTFE tube needle guide fit



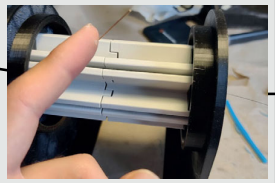
I cut the PTFE tube through the middle. This was quite hard and led to the tube needing a lot of sanding and shaving with a knife. When finished, I put the halved PTFE tube into the inner-axis and placed the needle guide on top. This worked perfectly. The needle guide fitted perfectly in the inner-axis.
The only issue was that the lasercut needle guides were pushed towards the middle (this can be seen in the picture). This will likely lead to more friction when moving the needle rod holder forward. This will be tested.



Needle guide prototype



As expected, due to the increasing tightness of the needle guiders towards the middle of the prototype, the friction is indeed higher. Interestingly in the left halve friction is significantly lower than in the right halve. This might be a result of the irregular cut PTFE tube. The cut tube is not precisely cut in the middle, thereby probably pushing the needle guides inwards. Correspondingly increasing needle rod connector friction.



Inner-cam prototype



The ball bearings fit perfectly into the inner-cam, and slide freely following the cam path. No adjustments need to be made!



Laser needle holders in axis



The laser needle holders are too tight to fit into the inner-axis, and thus need to be redesigned. Additionally, it is difficult to keep everything together in one place, without using glue. In the next iteration I have to change the dimensions and make everything in one piece.

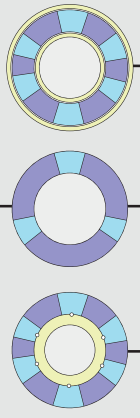


Linear bearing ideation



I created thee different ideas to prevent the balls falling out of the ball-bearing parts.

1. Decrease the number of ball-bearing parts and slightly change the dimensions.
2. Place inner and outer cylindrical parts to tighten the current prototype.
3. Place an inner cylinder with notches at the beginning and end of the ball bearing parts. This ensures the balls will move around the corner without falling out .



MR-conditional WASP-inspired needle with integrated laser functionality.

Context

TPLA UROLOGY

Target group

Urologists

Midterm & meeting



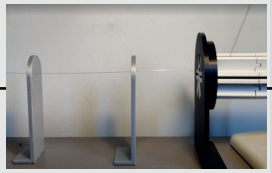
Had my midterm, and everyone was satisfied with how its going up until now. So I am happy.

Meeting remarks:
First print the surrounding circles from the linear bearing ideation (picture 2) and afterwards, print idea 1.
Jette will ask DEMO whether they can make the PTFE tubes with an incision.
If it is not possible I might disregard the PTFE tubes in the inner-axis.
I will redesign the laser holders
Jette will check for materials.

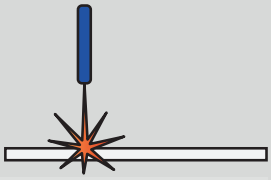
Needle guide prototype



In this prototype experiment I tried to find the biggest friction contributor. The main contributor of the increased friction seems to be the needle guides. By widening the needle guide path, the friction should be significantly less (in the future). Nevertheless, there are also other contributors. Without PTFE there is slightly increased friction. With PTFE the friction decreases, but only if they are perfectly cut, otherwise friction increases. Another friction contributor is the inner-axis. Due to the shape of the hole of the inner-axis the needle guides are pushed inside. This can be solved, by either changing the inner-axis or by changing the PTFE tube.



Laser cutting



I decided to use needle guide 6 (see *testing needle guider*) as a template. I used the exact same measurements, except for the width of the path. I created 7 needle guides with a 0.6 mm thick path, and 7 needle guides with a 0.7 mm thick path.
The actual laser cutting went ok. For some reason the laser cut parts were a little deformed, but with some post processing this was taken care of. The post processing included sanding, and the application of a constant load to straighten the guides.



Testing new needleguides



IT WORKS! The needle guider with a path of 0.7 mm thick leads to almost no increase in tangible friction, compared to not using a guide at all. Concurrently, the Nitinol needle rod does not seem to be able to buckle in the inner-axis. All in all, great!
The path of 0.6 mm thick leads to more friction than the 0.7 mm thick path. For that reason the 0.7 mm thick will be the desired path thickness.
Remark: when placing the Nitinol needle rod in the inner-axis no buckling can be seen. The only issue is that the needle rod holder can fall out of the inner cam. This will likely not be an issue.



PTFE plates



I added PTFE plates to the side of the inner-axis to lower the friction. In total there should be 1 mm space for the 0.5 mm needle rod holder.

Sadly, the friction is significantly higher with the inclusion of the PTFE plates, compared to without PTFE plates. This is a result from too little space for the needle rod connector.





MR-conditional WASP-inspired needle with integrated laser functionality.

Context

TPLA UROLOGY

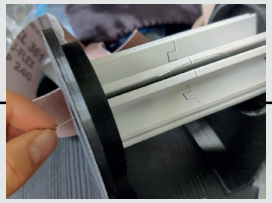
Target group

Urologists

Test guides & PTFE plates



I tested the needle guides to see if the needle rods can buckle if I really try. The short answer is: Yes, they can buckle. The chances of buckling are low, but it is possible. I have to make a choice between either low friction and higher chance of buckling, or higher friction and lower chance of buckling.
Adding PTFE plates will increase costs and complexity, while the benefits are deemed insignificant due to the low sideways force during forward and backward movement of the rods.





Redesign laser needle holder



I redesigned the laser needle holder by combining the three parts into one rigid part. This concept works. However, I need to print it again, as the hole was not cleared with high pressured air. For that reason the prototype cannot be used for the final prototype. I tried to heat it, to soften the plastic and than put a tube through the softened plastic, but this did not work.



Issues list

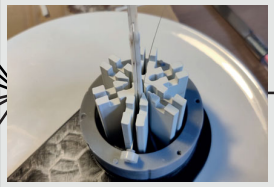


I made a list of possible issues and dilemmas I had to make during the process. This will be useful when writing the discussion. This will be updated continuously.

Assembling the system



While waiting for the linear bearing I decided to test the system as is. This resulted in some useful knowledge. I used a PTFE plate, instead of PTFE tubes, to create the halved PTFE tubes. On top of the halve PTFE tubes I assembled the needle guides. At first I wanted to leave the PTFE tube out, but due to the design of the inner-axis combined with the inclusion of a laser holder it could not be left out (see picture). I then assembled everything. I placed the ball-bearings with the needle rod holders in to the assembled inner-axis. Hereafter I filled the linear bearing with balls. I placed the inner-cam into the linear bearing which I then placed around the inner-axis.

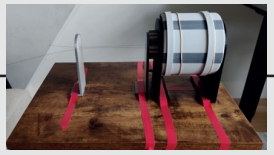


Testing the system



After assembling the prototype some tests could be done. Note: only one needle rod was used instead of 6.
Experiment:
I pulled the needles to move the inner-cam. Here I found multiple problems.

- The needle rods can come out of the needle rod connectors, because this friction is less than the friction needed to move the inner-cam.
- The inner-cam experiences some frictions spikes. This is likely directly linked to the linear bearing, and should be solved in the redesign.



MR-conditional WASP-inspired needle with integrated laser functionality.

Context

TPLA UROLOGY

Target group

Urologists

Testing the system



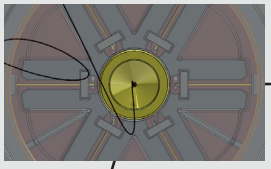
- If the needle rods are pushed, they can buckle. The chance of this happening is low, but it did happen, so I will need to redesign this part.
- I should use WD40 to lubricate all surface in case they touch.

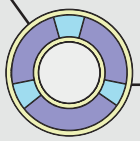


Redesign

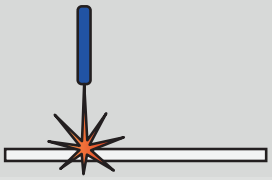


I redesigned the linear bearing, inner-axis and needle guides. As a result I had to redesign and reconfigure multiple components, which I will have to print (again).
The redesign mostly focused on ensuring the inner-axis could hold the needle guides better, and it focused on ensuring the needle rod connectors, could in fact hold the needle rods reliably.
Consequently, I had to move the tubes through which the Nitinol rods travel 3mm in the distal direction. This will increase friction in the tubes guiding the Nitinol rods to the middle.
The linear bearing was redesigned according to the explanation earlier.

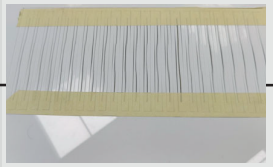




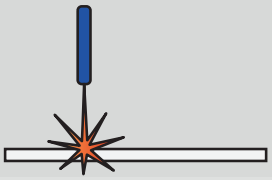
Needle guides



I laser cut three different needle guides. By making them wider they should be stiffer and thus move less to the middle. Additionally, I have made them with different tolerances, so that they fit better.
Something went wrong during the cutting, so sadly I will have to cut them again.



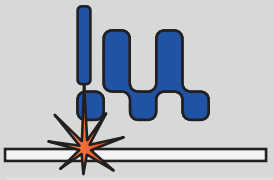
Needle guides



I laser cut the three different needle guides again. This time it was successful.



Needle guides test inner-axis



The fit is perfect. The needle guides maintain their desired shape and ensure that the two inner-axes are perfectly aligned.
Additionally it seemed that no, or atleast less bending occurs in the middle of the needle guiders compared to previous attempts.
The 0.5 mm needle guide led to too much friction. The 0.6 and 0.7 mm needle guides did not have more noticable friction compared to not using needle guides. Too minimise the chance of buckling the 0.6 mm needle guide was chosen.



MR-conditional WASP-inspired needle with integrated laser functionality.

Context

TPLA UROLOGY

Target group

Urologists

Meeting Jette & Aimée



Interesting points:

- For testing it would be interesting to evaluate if the optical fibre is damaged during insertion. This can be seen with a microscope.
- I should test conditions 3 or 5 times.
- Redesign for breadboard alignment.
- It might be more useful to use a load cell instead of a veerunster, as the veerunster is less precise.
- Last, I should keep all my receipts to be able to get some of the costs covered.
- I should make 3 big gelatin blocks and divide them in 3 smaller blocks each.

Needle support testing



I tested whether tubes with lesser angle, meaning less difference in radial distance, worked better. The conclusion is yes, they do work better compared to when the holes are further apart. However, there is something important to note here. The experienced friction also depends on the way the PTFE tubes are shaped. Ideally one would want to straighten the PTFE tubes. Only after this they should be placed into the inner-axis.
This could be achieved manually, with a mould, or by being clamped between two solids.



Needle support straightening



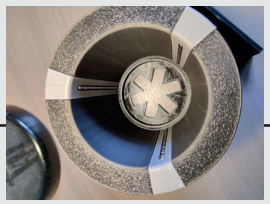
I tried to straighten the tubes using a laser cut mould and I tried it manually. Manual adjustment worked best. I can always clamp the PTFE tubes in the end, but by manually adjusting them, I maintain a bit more control.

To test the straightness I inserted needle rods. If the needle rod easily moves through the needle supports, it is deemed straight enough. I also evaluated multiple tube diameters. The most promising inner diameter is 1 mm as it is less prone to manual errors. The smallest diameter does not work, due to small straightening errors impacting the friction.

New linear bearing



I printed the new linear bearing using SLA and FDM printers. The prints turned out fine. They nicely fit together and only had to be sanded to remove some sharp outer edges. The linear bearing securely holds balls, if enough pressure is put on the individual SLA printed parts (the ball-bearing parts). To ensure enough pressure is provided two FDM printed rings are lined with tape on the inside. Hereafter they are placed around the linear bearing. The added tape compensates for the slightly larger diameter and helps to keep the ring in place.



MR-conditional WASP-inspired needle with integrated laser functionality.

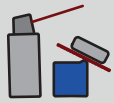
Context

TPLA UROLOGY

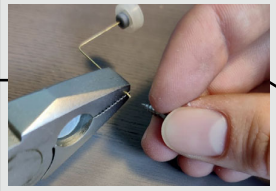
Target group

Urologists

Preperation



1- I placed balls in the linear bearing. Noteworthy: I placed slightly less balls than possible to minimise initial friction of the inner-cam.
2- I sanded the inner-cam and needle guides.
3- I placed tape on the outer diameter rings.
4- I placed the Nitinol needle rods into the brass needle rod connectors, which were then inserted into the ball bearings using a coupling part. Noteworthy: to ensure the needle rod does not slide out of the needle rod connector, the needle rod connector containing the needle rod is clamped using a wire cutter.
5- I placed double sided tape on the 3 parts of the inner-cam for non-destructive (dis)assembly.



Assembly

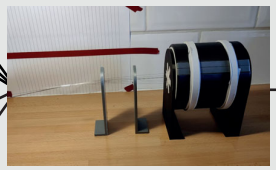


1. Placed the linear bearing around the backplate.
2. Placed 2 rings around the linear bearing.
3. I placed the needle guiders halfway into the inner-axis.
4. I placed the prepared needle guides in the inner-axis with the needle rods put through the needle guides.
5. I assembled the inner-cam and kept it at the same height as the inner-axis.
6. I placed the ball bearings into the inner-cam path and I placed the assembled laser needle holder into the second inner-cam path.
8. I placed the inner-cam into the linear bearing around the inner-axis.
9. I closed the linear bearing and placed it horizontally.

Prototype setup 1



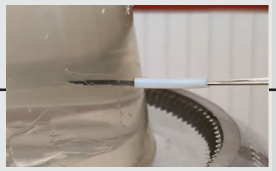
This is the first setup. The assembled prototype is fixed using tape, and the needle rods (and laser needle) are inserted through the vertical stands seen in grey in the picture.



Experiment 1



I made a 15%wt gelatin mixture the day prior to the experiment.
In this experiment I manually inserted the 5 (40cm long) Nitinol needle rods into the gelatin mixtures. One Nitinol rod had a length of 20 cm and the aluminium laser needle was 30 cm long, so they could not be inserted. I tested the device by turning clockwise for 3 minutes, after which I removed the needle rods and inserted them into a different spot. Hereafter I turned anti-clockwise for 3 minutes. Clockwise rotation led to the needle moving out of the gelatin mixture as expected. Anti-clockwise led to the needles moving out (unexpected) of the gelatin mixture, albeit slow and irregularly.



Prototype setup 2



This is the second setup. As the first prototype showed unexpected behaviour the aim of the second prototype was to address this behaviour. I tried to minimise buckling options for the needle rods, as I expected this to be the reason for the unexpected behaviour. I placed the needle rods through the PTFE support tubes (white), which I taped together. I also added a long PTFE tube at the end (blue) to try to eliminate buckling behaviour of the needle bundle.



MR-conditional WASP-inspired needle with integrated laser functionality.

Context

TPLA UROLOGY

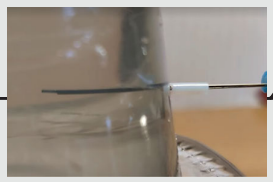
Target group

Urologists

Experiment 2



I manually inserted the needle bundle into the same gelatin mixture. The main difference being the prototype adaptation and the insertion depth. I inserted the needles a couple of centimetres further. I tested the device by turning clockwise for 3 minutes. Hereafter I removed the rods and inserted them into a different spot. After this I turned anti-clockwise for 3 minutes. This resulted again in unexpected behaviour. The Nitinol rods barely moved.



Meeting Jette

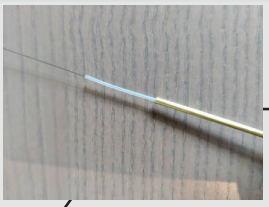


I suspected that the unexpected behaviour was due to buckling again, but I was not 100% sure. I discussed with Jette, and see agreed that this would be the most likely cause. To address this, I will use shorter (spring steel) rods. Nitinol is too expensive and hard to get, so altering the Nitinol rods was not an option. Additionally, I will use more WD40 around the inner-cam. Moreover, will make the PTFE supports more rigid, and I will test in more gelatin mixtures.

Redesign needle supports



I redesigned the needle supports by using 6 brass tubes in which PTFE tubes could be placed. These brass tubes should minimise buckling, while the inner PTFE should ensure low friction.



Prototype needle supports



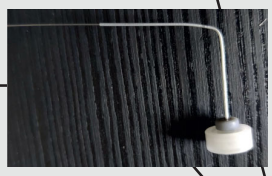
I prototyped the needle supports. I inserted 15cm PTFE tubing into 15 cm long brass tubes. I enlarged the holes of the vertical plates with a nail to adjust for the larger outer diameter (2mm) of the brass tubes. I placed the brass tubes one by one into the plates. They were fixed using friction of the plates and tape.



Prototype rod connector



I used spring steel instead of Nitinol, because I could not alter the Nitinol rods, due to their price and availability. The spring steel needle rods, were exactly 0.3 mm I.D., which did not fit into the 0.5 mm O.D. brass needle rod connectors. For that reason I used 0.6 mm O.D. aluminum tubes.
The design remained the same



MR-conditional WASP-inspired needle with integrated laser functionality.

Context

TPLA UROLOGY

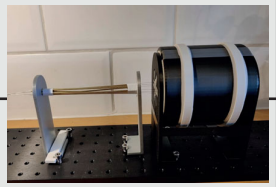
Target group

Urologists

Prototype setup 3



This is the third setup. The assembled prototype was fixed using screws, and the spring steel rods were inserted through the brass tubes seen in gold in the picture.



Experiment 3



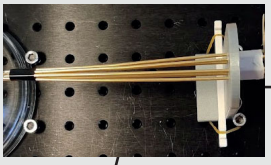
I tested the prototype into 3 different gelatine wt% (5, 10, and 15) mixtures. Sadly compared to earlier prototypes there was not much difference. A little bit of movement could be seen, but no expected forward or backward trends could be seen



Prototype needle support



I changed the needle supports, to ensure they end more centrally, as I suspected that a lot of friction was created at the end of the brass-PTFE tubes (needle supports). By doing so, I had to eliminate the stand most distal to the system. To ensure no further movement of the rod support ends (left in picture), I taped it secure at a predetermined height. Additionally, I moved the right stand a bit more to the left, in order for the supports to stick out at the beginning. This was done to better match the location where the needle rods leave the inner-axis. Hereafter I taped everything together.



Prototype rod connector



I shortened the needle rod connectors to limit the force placed on the inner-axis. In addition, I reshaped the needle rod connector bend angle, and ensured the rod connector had an angle of 90 degrees (or a little less), not more! If the rod connectors have an angle of more than 90 degrees they might cause extra friction. The reason for this would be that they put pressure onto the inner-axis, increasing the friction generated when sliding along the inner-axis.

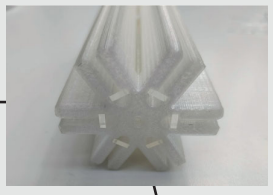


Preperation

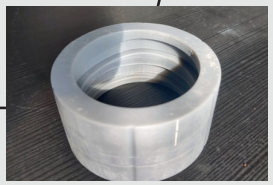


I prepared the parts for assembly, by doing multiple things:

1. I sanded the needle guides.
2. I used WD40 to lubricate the inner-axis.
3. I sanded the inner-cam, and reassembled the inner-cam parts using glue.
4. I cleaned and dried the inner-cam.
5. I used WD40 to lubricate the inner-cam and linear bearing. I also lubricated the cam paths of the inner-cam.







MR-conditional WASP-inspired needle with integrated laser functionality.

Context

TPLA UROLOGY

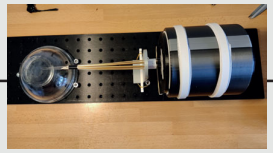
Target group

Urologists

Prototype setup 4



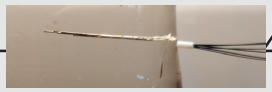
This is the fourth setup. The assembled prototype is fixed using screws, and the spring steel needle rods were inserted through the brass tubes seen in gold in the picture.



Experiment 4



I tested the prototype into 3 different gelatine wt% (5, 10, and 15).
Good news! There is a noticeable difference in performance, compared to experiment 3. Within 10 wt% gelatine very clear movement of the needle rods can be seen. The rod movement seemed to move the inner-cam backward (sadly, only backward). When testing in 15 wt% gelatine movements could be seen, but no general moving trend could be derived. All in all, positive results, but the device needs further optimisation. The problem seemed to lie within the new brass-PTFE needle supports, so I will need to alter those.



Meeting Jette

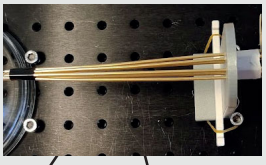


I suspected that the unexpected behaviour was due to the brass-PTFE needle supports, but I was not 100% sure. I discussed with Jette, and she agreed that this would be the most likely cause. To address this, I will remove or alter the brass-PTFE needle supports. Additionally, Jette provide me with an interesting remark. I could perform tests with the needle fully put through the gelatine. By doing so I can eliminate the cutting forces, and thereby perform the experiment if I cannot lower the friction enough. In addition, I will need to find the friction range of the inner-cam movement in the linear bearing.

Prototype rodguider



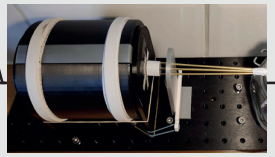
I noticed that the brass needle support tips were bent, thereby increasing friction. To resolve this , I removed the end of the brass tubes with a saw. This ensured the tips remained cylindrical and open. I quickly tested with a needle rod if I should keep or remove the PTFE tubes from the needle supports. The PTFE tubes increased friction, because more pressure was put on the needle rods as a result of the bent brass rod and smaller diameter PTFE tube.



Prototype setup 5



This is the fifth setup. The assembled prototype is fixed using screws, tape, and elastic rubbers. The spring steel needle rods were inserted through the brass needle supports seen in gold in the picture.



MR-conditional WASP-inspired needle with integrated laser functionality.

Context

TPLA UROLOGY

Target group

Urologists

Experiment 5



I tested the prototype into 3 different gelatine wt% (5, 10, and 15).
Interestingly the behaviour is similar to experiment 4. A little more movement can be seen, especially in the 15 wt% gelatine, which resulted in some (barely noticeable) trends. All in all, an OK result, but it needs further optimisation to produce reliable, repeatable and more noticeable results. The needle still does not move forward, only backward.
I also tested the prototype excluding the cutting forces. This showed considerable more movement (trends), but weirdly, the needle no matter the turning direction moved backwards.



Problem ideation



There was still too much friction in the device, and weirdly the needle could only move backwards (even without the cutting forces). I checked whether the system was levelled - it was; I checked whether the cam was straight or cone shaped - it was straight; I checked whether the linear bearing was straight - it was. What could it be? Then I noticed that by moving the rings surrounding the linear bearing, the friction changed. If I moved the rings to the right, the cam moved significantly easier to the left, without balls falling out of the bearers. If I moved the rings to the left, the opposite happened. This let me to the new prototype.

Prototype linear bearing



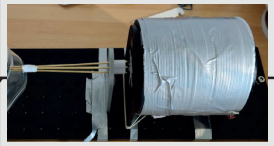
It might seem like a mess, but taping the linear bearing was actually a deliberate choice. By taping the linear bearing, I could distribute the load more evenly, thereby removing pressure points caused by the rings. With the distributed load the balls move smoother and faster, while remaining inside the linear bearing.



Prototype setup 6



This is the sixth setup...! The assembled prototype is fixed using screws, tape, and elastic rubbers. The spring steel rods were inserted through the brass needle supports seen in gold in the picture.



Experiment 6



I tested the prototype into 3 different gelatine wt% (5, 10, and 15).
Good news! Clear movement trends can be seen! Especially in the 5 and 10 wt% gelatine, very noticeable trends could be seen. All in all, a very positive result. But again, the needle does not move forward. No matter what direction I turned the cylinder, it always moved backwards. I tested this with and without the cutting forces, but the backward movement direction remained.



MR-conditional WASP-inspired needle with integrated laser functionality.

Context

TPLA UROLOGY

Target group

Urologists

Problem explanation

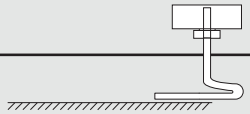


The friction was so low in the linear bearing, that even with 5 wt% gelatine, very clear movement trends could be seen. So why, even without cutting forces, does the inner-cam not move forward. As stated before I tested all boundary conditions, but the issue remained. I put the device on a ramp, to see if this helped, it did, but not by as much as I expected. For that reason I expected it to be an issue with the needle rod connectors. I think the aluminium rod connectors (elastically) deform before they pull the inner-cam forward, while this deformation happens less during backward movement.

Problem ideation



The problem is likely related to the created torque. During backwards movement torque leads to minimal/ negligible deformation, as its design restricts movement in the anti-clockwise direction. When the needle is pulled forward by the friction in the gelatin, torque in the aluminium rod connector leads to noticeably less forward movement than expected. This can be seen in the figure below. To combat this I will aim to restrict deformation resulting from torque in the aluminium rod connector system. I plan to do this by proposing an S shape, which can be seen below.



Meeting Aimée



Meeting went fine. No mentionable remarks. I will wait for the prints and then test again.

Post-processing



After IWM printed my parts, I had to post-process them. Using a 0.5 mm drill bit I drilled through every T-shaped coupling part, to ensure the aluminium needle rod connectors would fit perfectly (see picture below) into the ball bearings. Additionally I drilled and sanded the laser needle holder and cone (through which the laser will be inserted).



Connector manufacturing setup



I created a setup with which I could reliable make the previously designed S shaped aluminium needle rod connector.
An interesting remark: to limit movement of the spring steel rods relative to the aluminium rod connector I first inserted the spring steel needle rods into the aluminium needle rod connectors, only then I bent the holder into the S shape.



MR-conditional WASP-inspired needle with integrated laser functionality.

Context

TPLA UROLOGY

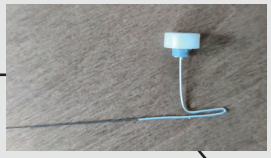
Target group

Urologists

Needle part creation



I assembled all the needle rod parts into 6 needle rod assemblies.



Prototype setup 7



This is the seventh setup. The assembled prototype is fixed using screws, tape, and elastic rubbers. The assembled needle rods were placed into the inner-cam, similar to previous prototypes. These were then inserted through the brass needle supports, seen in gold in the picture.



Experiment 7



I tested the prototype into 3 different gelatine wt% (5, 10, and 15).
Good news! Clear forward movement trends can be seen! Especially in the 5 and 10 wt% gelatine very noticeable trends could be seen. Contrary to the previous experiments, the needles move forward instead of solely backwards. When turning the opposite direction the needles move backwards in 5 wt% and 10 wt% gelatin. In the 15 wt% gelatine the needle does not move backwards, at least I was unable to observe clear backward movement.



Laser needle integration



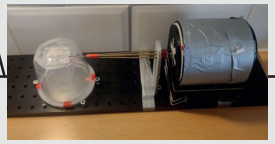
I placed a seventh brass needle support tube in the system, through which the laser needle could be inserted.



Prototype setup 8



This is the eight setup. The assembled prototype is fixed using screws, tape, and elastic rubbers. The assembled needles were placed into the inner-cam. After this the laser needle with the laser needle connectors were inserted into the inner-cam. The 7 needles were then inserted through the brass needle supports, seen in gold in the picture.



MR-conditional WASP-inspired needle with integrated laser functionality.

Context

TPLA UROLOGY

Target group

Urologists

Experiment 8



I tested the prototype into 3 different gelatine wt% (5, 10, and 15).
Good news! Clear forward movement trends can be seen! In the 5, and 10 wt% gelatine, noticeable trends could be seen. In the 15% a forward trend can be seen, but the movement is minimal. Contrary to the previous experiments, the needle system can only move backward in the 5 wt% gelatine sample. From experiment 7 and 8 it can be seen that forward movement is now considerable easier, than backwards movement. This likely has to do with the aluminium rod connector design. Nevertheless this design suffices for the final tests and evaluations.



Meeting Jette

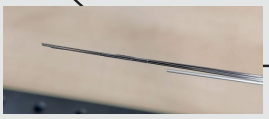


Was a nice dense meeting in which I showed the result of my preliminary tests. The most important points/answers are written below:
She can get me a longer laser, but I will have to check the diameter.
I will measure the length after 5, 10, 15, and 20 cycli (create an excel file).
First I measure the order of magnitude with a 'veerunster', only then I use a load cell.
Jette will help me to attach the krimpkous.
I will need to make device prettier.

Attaching a shrinking tube



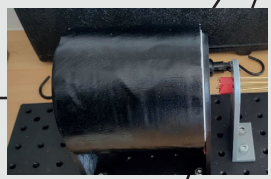
To keep the needles together Jette helped me to glue a shrinking tube (krimpkous) to one of the 6 needle rods.



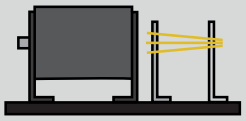
Protective sleeve addition



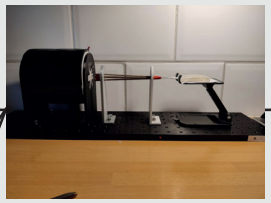
I added a vegan leather cover to the device. This was done to improve its dust resistance, but also to make the device more aesthetically pleasing.



Final design



This is the final assembled prototype and final design.



APPENDIX C
NEEDLE GUIDE TRADE-OF

To decide on the final needle guide, multiple experiments and design iterations were performed. This Appendix explains the design considerations and experiments resulting in the final needle guide design. To prevent the needle rods from buckling, needle guides were created. To create these needle guides a constant balancing act had to be performed. Having a wider cut lowered friction between the needle rod and the needle rod guide, but increased buckling chance. Similarly, using higher-amplitude waves increased friction between both parts, but lowered the chance of buckling. Seven different waves were created to decide on the optimal needle guide. These were cut to thicknesses of $0.5\,\mathrm{mm}$, $0.6\,\mathrm{mm}$, and $0.7\,\mathrm{mm}$, resulting in a total of 21 different needle guides. After post-processing, the needle guides were tested in a rudimentary setup (Figure 27). In this experiment, the needle rods were manually pushed and rotated to try and buckle the needle rods. The results from this experiment showed that a four-node wave with an amplitude of $0.3\,\mathrm{mm}$ was the most suitable wave. It has low friction between the needle rods and needle guide and a low chance of needle rod buckling. After evaluating the friction per cut width it was found that the $0.5\,\mathrm{mm}$ cut led to too much friction, while the 0.6 and $0.7\mathrm{mm}$ cut did not lead to noticeable friction. The smallest width had the lowest chance of buckling, thus a cut width of $0.6\,\mathrm{mm}$ was chosen. The final design can be seen in Figure 27.



Fig. 27: *The needle guide test setup with a buckling needle rod*

APPENDIX D
MATHEMATICS

This Appendix provides an overview of the calculations used to determine the inner-cam path, the diameter of the inner-cam, and the bending stress and deflection of the needle rods.

A. Inner-cam path

A path is engraved into the inner-cam to move the needle rods in a self-propelling sequence. This path is adapted from Fung-A-Jou *et al.* [25]. To create the desired sequence one needle rod has to advance, while simultaneously five needle rods retract. To achieve this the path is divided into six equal parts, where each part covers $\frac{\Pi}{3}$ radians. As five needle rods have to retract during rotation five path parts ($5\frac{\Pi}{3}$) need to have a downward path (negative direction coefficient). The remaining part has to advance the needle and will need an upward path (positive direction coefficient). This results in a check-mark-shaped path, similar to Figure 28. The problem, however, is that during directional change of the needle rod (i.e., transitioning from the upward to the downward slope) the needle rods will experience a shock. This shock is generated because the needle rod transitions from a constant (forward) speed to a constant speed in the opposite direction (backward). This leads to (theoretical) infinite acceleration during the directional change. Smoothening the parts where the rods change direction will help eliminate the shock, by allowing for finite deceleration and acceleration of the needle rod. This is done by changing the linear functions to parabolic functions at the points of directional change. The final path and mathematics are shown below in the Maple file and are adapted from Fung-A-Jou *et al.* [25].

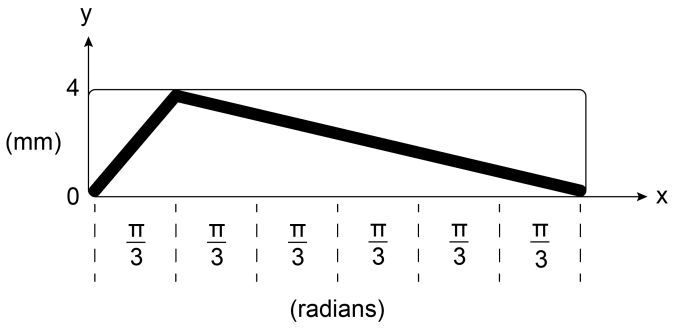
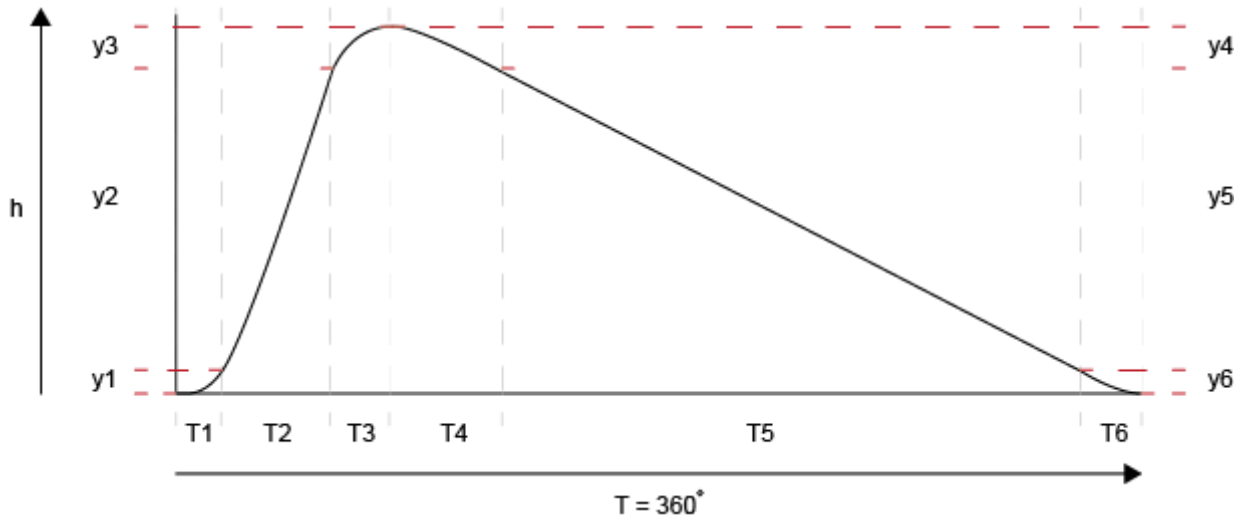


Fig. 28: *Visualisation of the check-mark-shaped inner-cam path without acceleration optimisation.*

```
> restart;
```

Profile

```
> with(plots):
> with(plottools):
> with(Units):
Automatically loading the Units[Simple] subpackage
>
```



Height, velocity and acceleration

Initialisation

```
> #rc1 = radius inner-cam [mm], rf = bearing radius [mm], H  = stroke length [mm], Ta
    =forwards stroke [degree], Tb = backwards strok [degree],
> #1 forward stroke and 5 backward strokes. So total T1 −T3 = 60 degrees and total T4 −T6 = 300
    degrees.
```

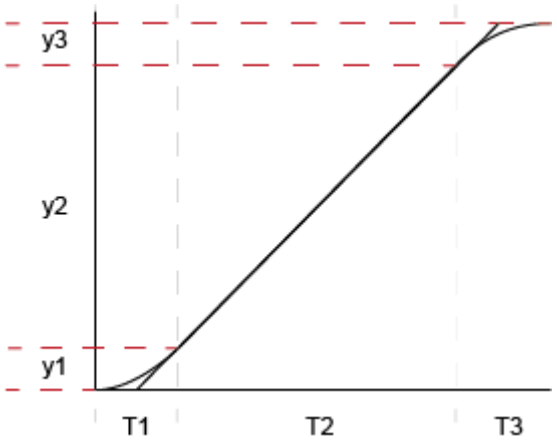
$$> rc1 := 30 : rf := 5 : Circumference := 2 \cdot \pi \cdot rc1 : H := 4 : T := \frac{360}{6} : Ta := 60 : Tb := 300 :$$

$$k := \frac{Circumference}{360} : T1 := \frac{T}{4} \cdot k : T2 := Ta \cdot k - T1 - T3 : T3 := \frac{T}{4} \cdot k : T4 := \frac{T}{4} \cdot k :$$

$$T5 := Tb \cdot k - T4 - T6 : T6 := \frac{T}{4} \cdot k :$$

Height (substitution)

```
> #This graphs shows the lines used to calculate the total height and y1-y3
>
```




```
> #With the use of substitutions, the differents y's can be calculated.
> Eq1 := 0.5·T1/T2 - Y1/Y2 = 0 :
      #Using trigonometry (similar right triangles, due to the same angle) y1 can be substituted.
> Y1 := solve(Eq1, Y1) :
> Eq2 := T2/(0.5· T3) - Y2/Y3 = 0 : #Using trigonometry (similar right triangles, due
      to the same angle) y2 can be substituted.
> Y2 := solve(Eq2, Y2) :
> Eq3 := H = Y1 + Y2 + Y3 : #Because the height is known, the individual y's can be calculated.
> Y3 := solve(Eq3, Y3) : Y1 : Y2 :
> Eq4 := 0.5·T4/T5 - Y4/Y5 = 0 : #Similar to the previous substitutions)
> Y4 := solve(Eq4, Y4) :
> Eq5 := T5/(0.5· T6) - Y5/Y6 = 0 :
> Y5 := solve(Eq5, Y5) :
> Eq6 := H = Y4 + Y5 + Y6 :
> Y6 := solve(Eq6, Y6) : Y4 : Y5 :
>
>
```

Profile based on x

```
> #Parabolefunction:=Y·(x/T)^2;
      #To avoid a shock, acceleration needs to be minimised during directional changes.
      Therefore,  parabolic funnctions are used. (T1, T3, T4, T6 are the places where parabolic
      functions are used)
> #Linearfunction:=Y·(x/T); #In T2 and T4 linear functions are used
> D1 := T1 : D2 := T1 + T2 : D3 := T1 + T2 + T3 : D4 := T1 + T2 + T3 + T4 : D5 := T1 + T2
      + T3 + T4 + T5 : D6 := T1 + T2 + T3 + T4 + T5 + T6 : #total distance
>
```

> $YD1 := Y1 \cdot \left(\frac{x}{T1} \right)^2$: #Parabole with min at zero, and plus to ensure u or valley shape.

> $YD2 := Y2 \cdot \left(\frac{x - D1}{T2} \right) + Y1$: #Determine the height during T2 traversal.

> $YD3 := -Y3 \cdot \left(\frac{(x - D3)}{T3} \right)^2 + Y1 + Y2 + Y3$:
#Determine the height during T3 traversal. Parabole with max at D3, and times minus to ensure n or mountain shape.

> $YD4 := -Y4 \cdot \left(\frac{(x - D3)}{T4} \right)^2 + Y1 + Y2 + Y3$:
#Parabole with max at D3, and minus to ensure n or mountain shape.

> $YD5 := -Y5 \cdot \left(\frac{x - D4}{T5} \right) + Y1 + Y2 + Y3 - Y4$: #downward thus minus

> $YD6 := Y6 \cdot \left(\frac{x - D6}{T6} \right)^2 + Y1 + Y2 + Y3 - Y4 - Y5 - Y6$:
#Parabole with min at D6, and plus to ensure u or valley shape.

Differentiation

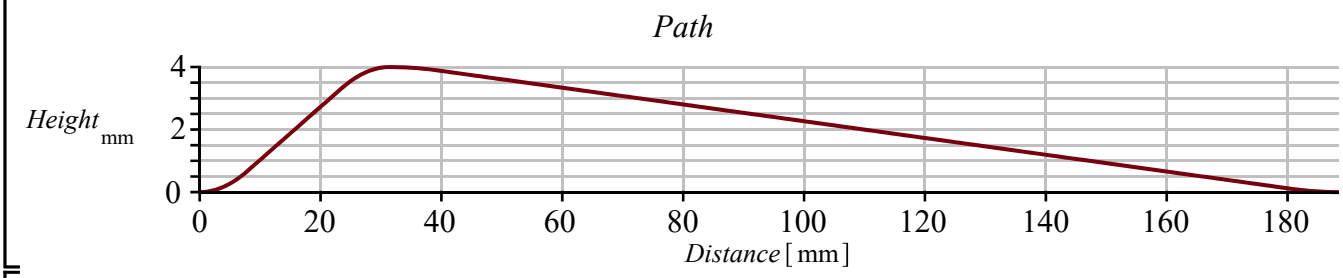
> $V1 := diff(YD1, x) : V2 := diff(YD2, x) : V3 := diff(YD3, x) : V4 := diff(YD4, x) : V5 := diff(YD5, x) : V6 := diff(YD6, x)$: #create velocity fucntions

> $A1 := diff(V1, x) : A2 := diff(V2, x) : A3 := diff(V3, x) : A4 := diff(V4, x) : A5 := diff(V5, x) : A6 := diff(V6, x)$: #create acceleration fucntions

Plots

> $S := piecewise(0 \le x \le D1, YD1, D1 \le x \le D2, YD2, D2 \le x \le D3, YD3, D3 \le x \le D4, YD4, D4 \le x \le D5, YD5, D5 \le x \le D6, YD6)$:

> $AAA := plot(S(x), x = 0 .. D6, axis = [gridlines = [10, color = grey]], labels = [Distance\ [\text{mm}], Height[\text{mm}]], title = Path)$;



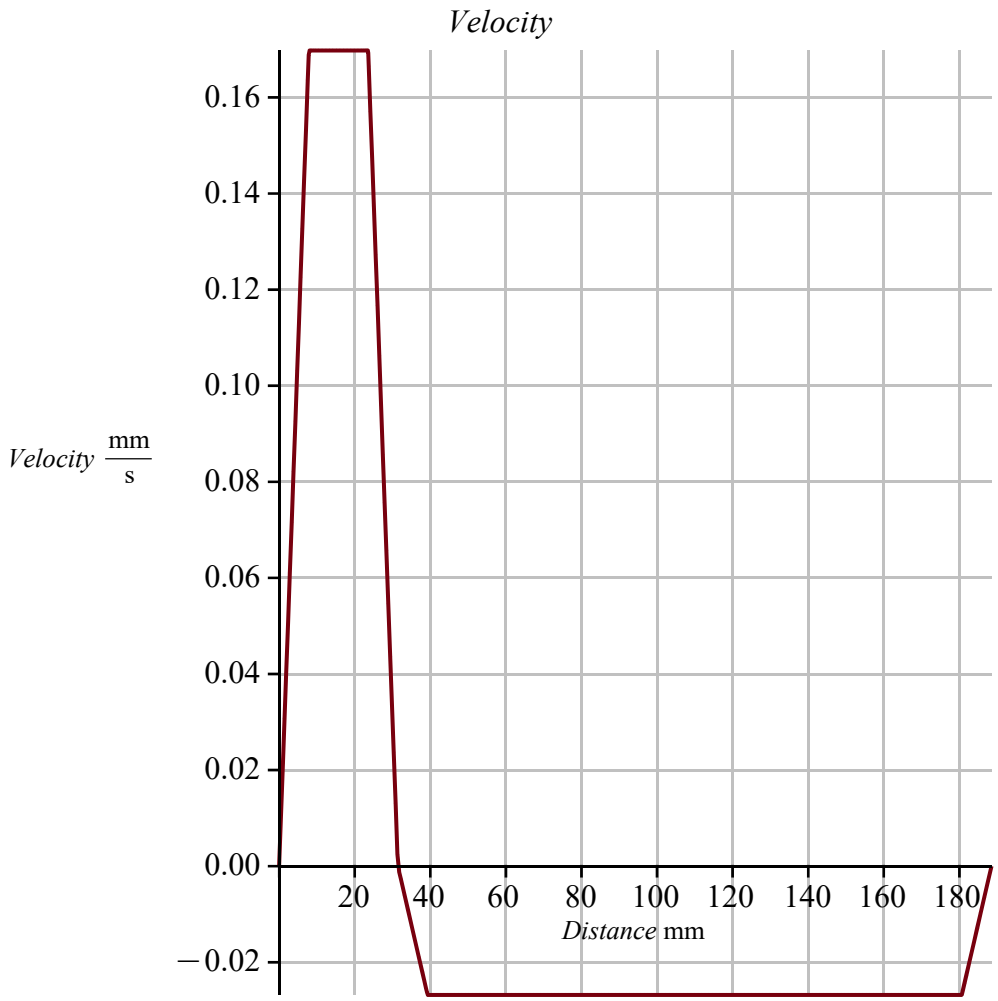
>

> $Y1 : Y2 : Y3 : Y4 : Y5 : Y6$:

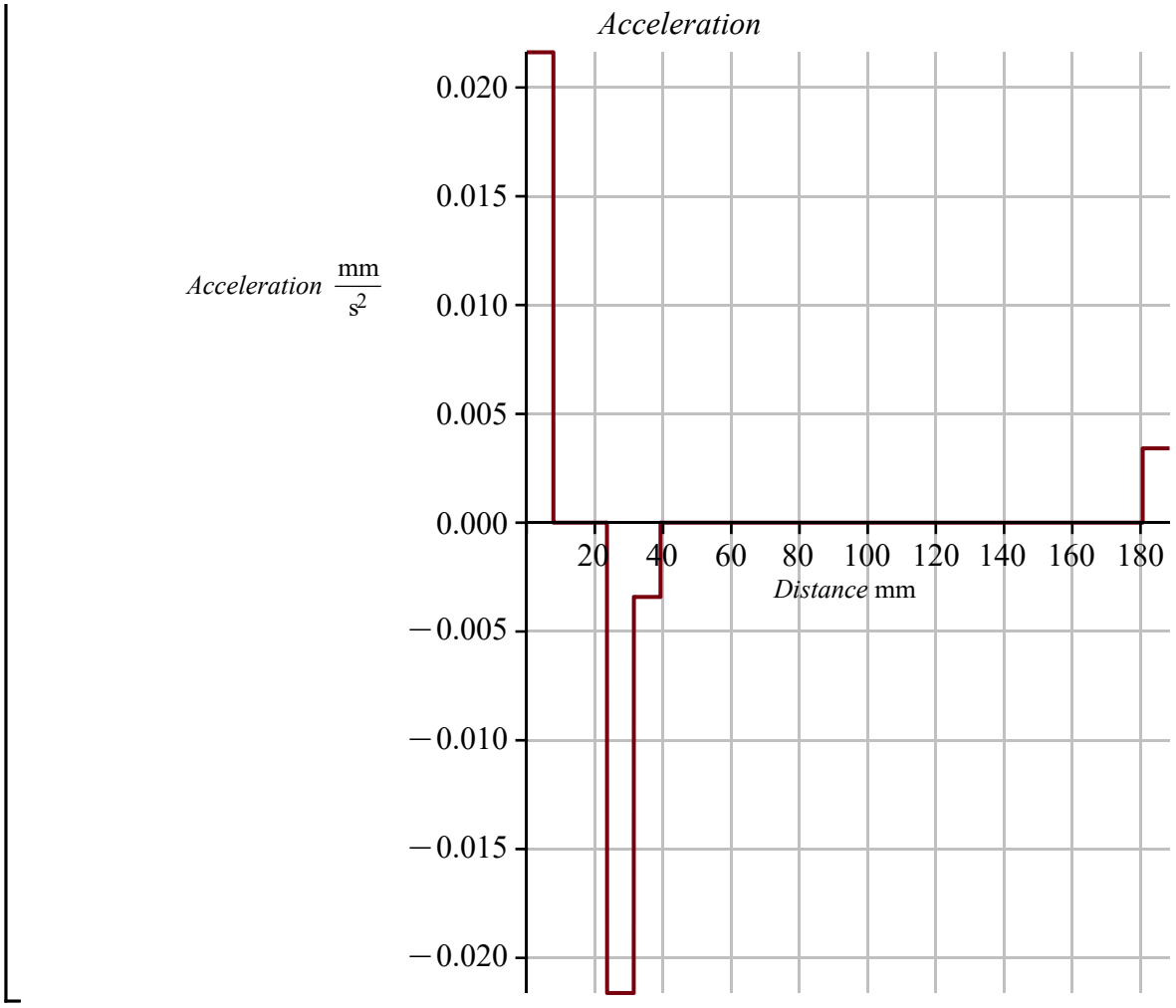
>

> $V := piecewise(0 \le x \le D1, V1, D1 \le x \le D2, V2, D2 \le x \le D3, V3, D3 \le x \le D4, V4, D4 \le x \le D5, V5, D5 \le x \le D6, V6)$:

> $plot(V(x), x = 0 .. D6, axis = [gridlines = [10, color = grey]], labels = [Distance\ \text{mm}, Velocity\ \text{mm}\ (/(s))], title = Velocity)$;




```
>
> A := piecewise(0 ≤ x ≤ D1, A1, D1 ≤ x ≤ D2, A2, D2 ≤ x ≤ D3, A3, D3 ≤ x ≤ D4, A4, D4
      ≤ x ≤ D5, A5, D5 ≤ x ≤ D6, A6) :
> plot(A(x), x = 0 .. D6, axis = [gridlines = [10, color = grey]], labels = [Distance mm,
      Acceleration mm (/(s^2)) ], title = Acceleration);
```


Acceleration
Acceleration mm/s²
0.020
0.015
0.010
0.005
0.000
−0.005
−0.010
−0.015
−0.020
20
40
60
80
100
120
140
160
180
Distance mm

B. Undercutting

The ball bearings are the parts that transmit the inner-cam movement to the needle rod connectors and needle rods. The ball bearings sit within the check-mark-shaped path and move up and down (i.e., parallel to the cylindrical axis of the inner-cam) during actuation. This movement is generated by rotating the inner-cam and restricting the movement of the ball bearing parallel to the cylindrical axis. This leads to ball bearings rolling along the check-mark-shaped profile (Appendix D-A). The path along which the bearings roll is circular. This affects the rolling behaviour of the ball bearing. If the diameter is too small, it can lead to undercutting of the ball bearings. In this context, undercutting means that the curvature of the path is too large for the ball bearings to move smoothly. This might lead to inconsistent movement of the ball bearings and sliding instead of rolling. To prevent undercutting, the diameter of the inner-cam is based on the width (i.e., diameter) of the ball bearing. How the diameter value is determined can be seen below in the Maple file. The threshold value is set to 0.015 as this value is said to be sufficient to prevent undercutting [25].

```
> restart;
```

Ball bearing

```
>
```

xiros® radial deep groove ball bearing, xirodur B180, glass balls, cage made of xirodur B180, mm



- non-metallic
- lowest wear
- smooth running
- very little humidity absoption
- chemical resistant
- seawater resistant
- dirt resistant
- cost-effective

Item no. B623B3G

Ø d1 [in]: 0.12 (3 mm)

Ø d2 [in]: 0.39 (10 mm)

b1 [in]: 0.16 (4 mm)

Installation size: 623

1 Pc.

Price:

USD 3.05

USD 3.05 / Pc.

Quantity discount

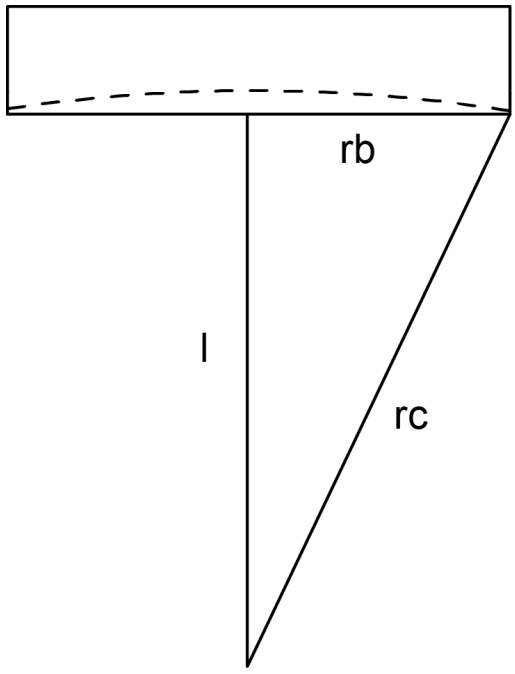
Ready to ship in 24 hours

Add to cart

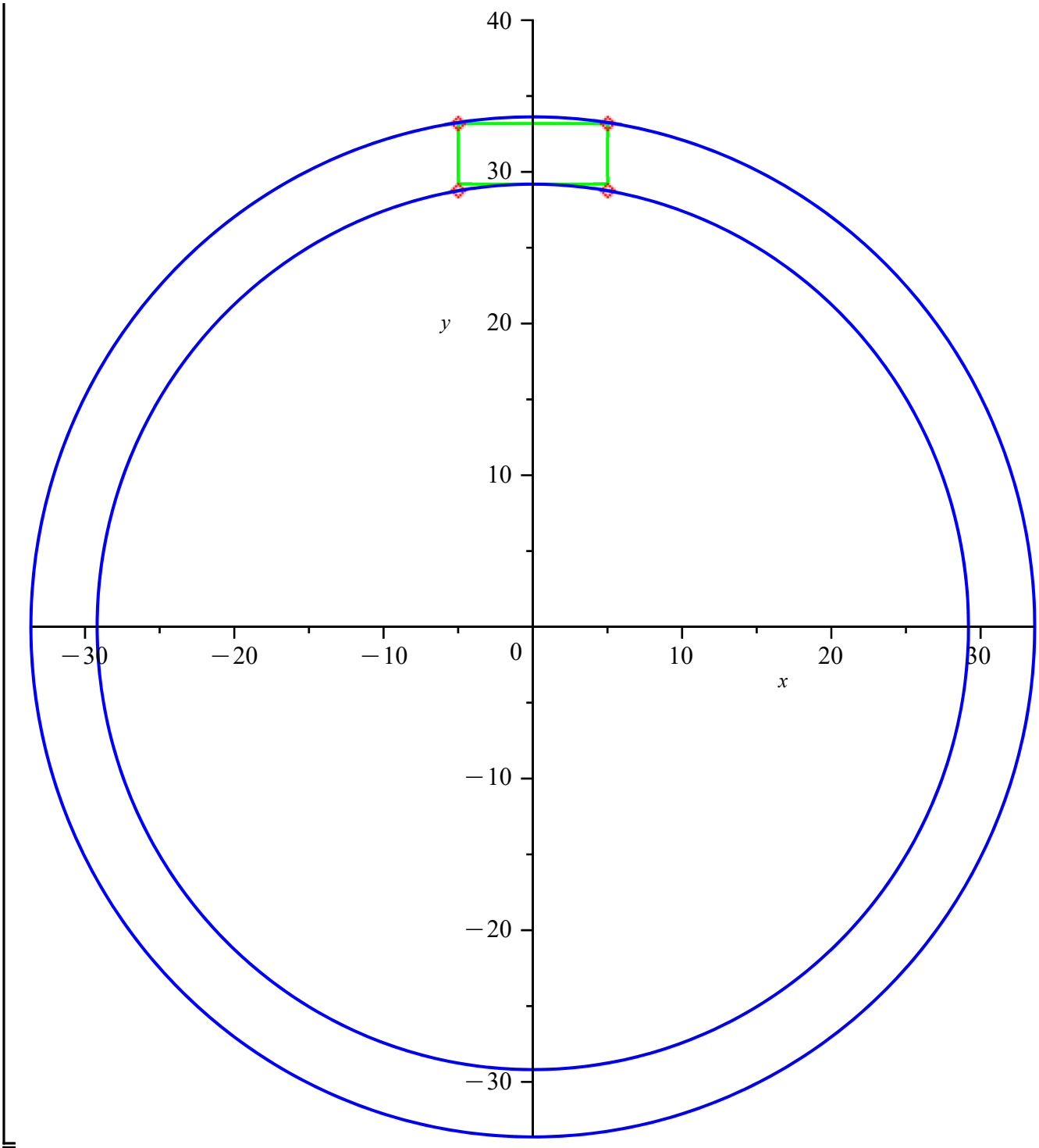
Add to wishlist

Undercutting visualisation

```
> restart;
> with(plots) :
> with(plottools) :
> #rb = radius  bearing [mm], hb = height bearing [mm], th = threshold [ − ],  rc = radius inner
      − cam [mm], l = vertical distance to bearing [mm]
> rb := 5 : hb := 4 : th := 0.015 :
>
```



```
> A := rc = sqrt(l^2 + rb^2) :
> B := rc/l = 1 + th : #l and rc should be approximately the same to prevent undercutting.
> S := (solve({A, B}, {rc, l})) :
> l := rhs((S[1])) :
> rc := rhs((S[2])) :
> Points := [[-rb, rc], [rb, rc], [rb, (hb + rc)], [-rb, hb + rc], [-rb, rc]] :
      #create ball bearing
> A := plot(Points, x = -10..10, y = 20..40, color = green) : #create ball bearing in green
> y1 := [l·(1 + th) + hb, l·(1 + th) + hb, l, l] :
> B := pointplot([[-rb, y1[1]], [rb, y1[2]], [-rb, y1[3]], [rb, y1[4]]], color = [red]) :
      #create the inner-cam points
> C := circle([0, 0], (rc + hb + rc·th), color = blue) : #create inner-cam path
> Dd := circle([0, 0], rc, color = blue) : #create inner-cam
> display(A, B, C, Dd);
```



>

> $Rout := rc + hb + rc \cdot th$; #Inner-cam path radius.

$$Rout := 33.62913236 \quad \textbf{(2.1)}$$

> $Rin := rc$; #inner-cam radius.

$$Rin := 29.19126341 \quad \textbf{(2.2)}$$

> $ThicknessWarp := Rout - Rin$; #minimal thickness solidworks warp

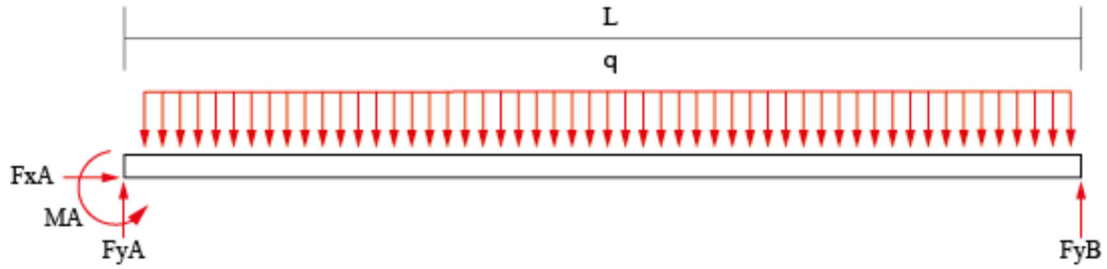
$$ThicknessWarp := 4.43786895 \quad \textbf{(2.3)}$$

>

C. Nitinol rod

The Nitinol needle rods bend as a result of their weight. If a Nitinol needle rod bends too much and the internal stresses are too high, it can lead to undesired plastic deformation. To determine if the Nitinol needle rods need to be supported to prevent plastic deformation before insertion, the maximum deflection and maximum forces were determined. Additionally, the critical load, that is the force at which the Nitinol needle rod buckles, is theoretically determined. Our design is optimised for Nitinol needle rods, not spring steel needle rods, as spring steel rods cannot be used in a clinical setting, whereas Nitinol likely can. For that reason, only the values for Nitinol needle rods are calculated.

Nitinol deflection



Equilibrium equation

```
> restart;
> Fy := FAy + FBy - q·L = 0 :
> Mr := -q/2·(L - x)·(L - x) + FBy·(L - x) :
> EIθ := int(Mr, x) + c1 :
> EIv := int(EIθ, x) + c2 :
> x := 0 :
> Eq1 := EIθ = 0 : Eq2 := EIv = 0 :
> c1 := rhs(Eq1); c2 := rhs(Eq2);
```

$$c1 := 0$$
$$c2 := 0 \qquad \textbf{(1.1.1)}$$

```
> x := L :
> FBy := solve(EIv, FBy);
```

$$FBy := \frac{3\,q\,L}{8} \qquad \textbf{(1.1.2)}$$

```
> FAy := solve(Fy, FAy);
```

$$FAy := \frac{5\,q\,L}{8} \qquad \textbf{(1.1.3)}$$

```
> x :='x':
> deflection := EIv/(E·Ixx);
```

$$deflection := \frac{-\frac{1}{24}\,q\,x^4 + \frac{5}{48}\,L\,q\,x^3 - \frac{1}{16}\,L^2\,q\,x^2}{E\,Ixx} \qquad \textbf{(1.1.4)}$$

Initialisation

```
> E := 28·10^9 :#Lowest youngs modulus of Nitinol in martensitic state (EDUPACK) [ Pa ]
> r := (0.25/2)·10^-3 :#radius Nitinol rod [ m ]
> p := 6.50·10^3 : #density Nitinol (EDUPACK) [ kg/m^3 ]
```

> $L := 300 \cdot 10^{-3}$: #length Nitinol rod [m]

> $g := 9.80665$: #universal gravity constant $\left[\frac{\mathrm{m}}{\mathrm{s}^2} \right]$

> $V := r^2 \cdot \mathrm{Pi} \cdot L$: $w := V \cdot p$: #weight Nitinol rod [kg]

> $q := \frac{(V \cdot p \cdot g)}{L}$:#distributed force on Nitinol due to its own weight $\left[\frac{\mathrm{N}}{\mathrm{m}} \right]$

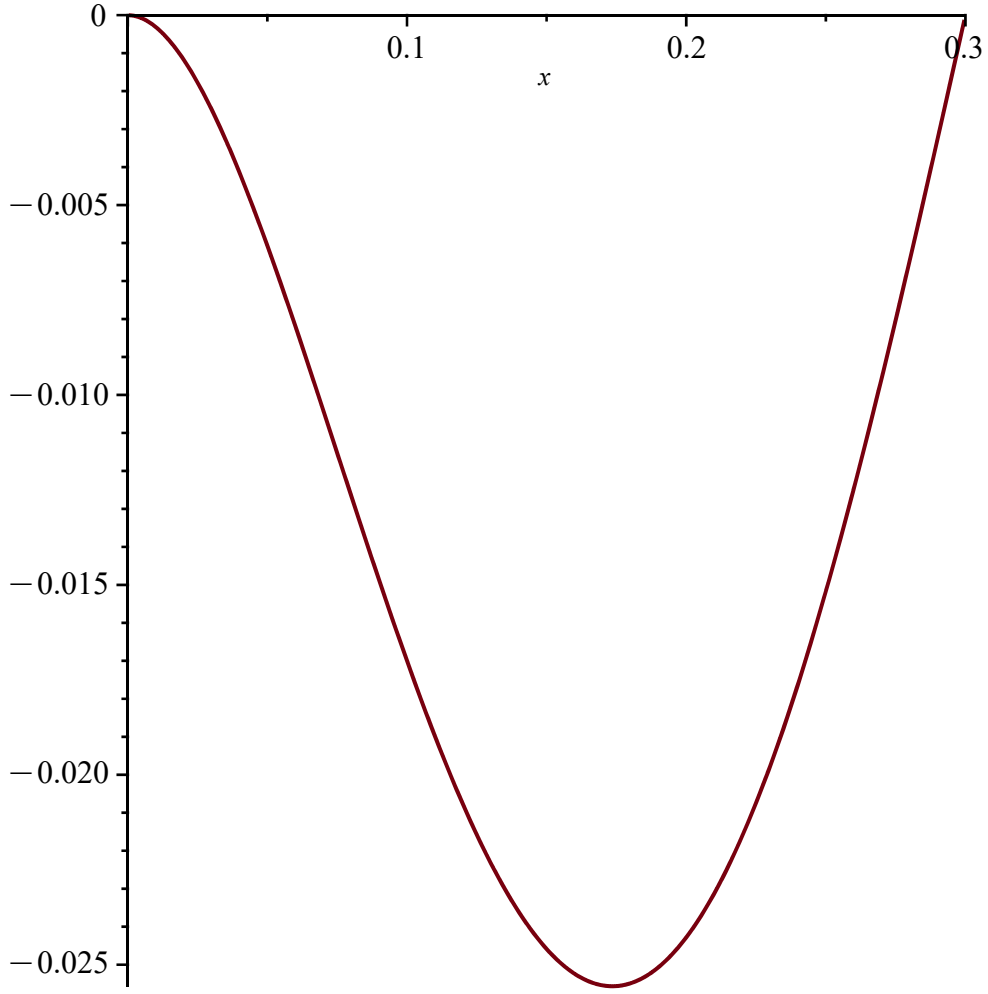
> $Ixx := \frac{\mathrm{Pi}}{4} \cdot r^4$: #Second moment of area Nitinol rod

> $Yield := 342 \cdot 10^6$: #Yield strength [Pa]

> $k := 0.780$: #adapted from Fung-A-Jou

Plots and maximum stresses

> $Deflection := plot(deflection(x), x = 0..L);$



> $MaximumDeflection := minimize(deflection, x = 0..L);$

$$MaximumDeflection := -0.02556756635 \quad \textbf{(1.3.1)}$$

>

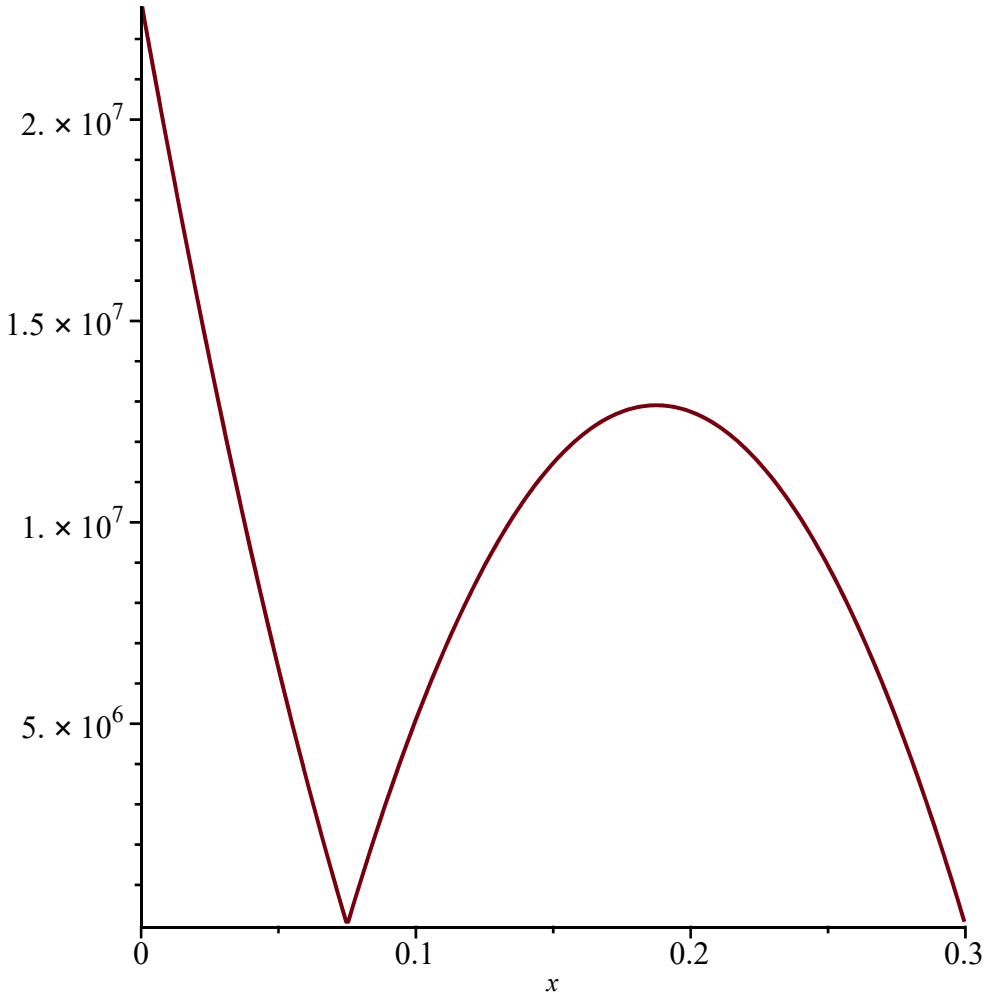
> $Placeofmaximumdeflection := solve(deflection = MaximumDeflection, x)[1];$

$$Placeofmaximumdeflection := 0.1735352905 \quad \textbf{(1.3.2)}$$

> $S := \frac{Ixx}{r}$:

> $\sigma y := \frac{\mathrm{abs}(Mr)}{S}$:

> $plot(\sigma y, x = 0..L)$;



> $\sigma ymax := maximize(\sigma y, x = 0..L)$; #maximum bending stress [Pa] :

$$\sigma ymax := 2.294756103 \times 10^7 \qquad \textbf{(1.3.3)}$$

> $\sigma xmax := 0$:

> $Q := \frac{\mathrm{Pi} \cdot r^2}{2} \cdot \frac{4 \cdot r}{3 \cdot \mathrm{Pi}}$: $V := FAy$: $\tau max := \frac{V \cdot Q}{Ixx \cdot (2 \cdot r)}$:

> $\sigma 1 := \frac{(\sigma ymax + \sigma xmax)}{2} + \mathrm{sqrt}\left(\left(\frac{(\sigma ymax - \sigma xmax)}{2} \right)^2 + \tau max^2 \right)$:

> $\sigma 2 := \frac{(\sigma ymax + \sigma xmax)}{2} - \mathrm{sqrt}\left(\left(\frac{(\sigma ymax - \sigma xmax)}{2} \right)^2 + \tau max^2 \right)$:

>

> $Vonmises := MaxStress = \sqrt{\sigma 1^2 - \sigma 1 \cdot \sigma 2 + \sigma 2^2}$; $MaxAllowed := MaxAllowablestress$

$= \frac{Yield}{2}$; #Max stress within limits [Pa]

$$MaxStress = 2.29 \times 10^{7}$$

$$MaxAllowablestress = 1.71 \times 10^{8} \quad \textbf{(1.3.4)}$$

> $Buckling := \frac{\pi^2 \cdot E \cdot Ixx}{(k \cdot L)^2}$; #Newton

$$Buckling := 0.0009677339907 \quad \textbf{(1.3.5)}$$

> $L := 'L'$: $Buckling := 'Buckling'$:

> $Buckling := \frac{\pi^2 \cdot E \cdot Ixx}{(k \cdot L)^2}$:

> $MaxUnsupportedLength := (solve(Buckling = 0.28, L)[2]) \cdot 10^3$;
#maximal unsupported needle rod length in mm based on the highest measured push force

$$MaxUnsupportedLength := 17.63681814 \quad \textbf{(1.3.6)}$$

>

>

APPENDIX E
MRI COMPATIBILITY DESIGN CONSIDERATIONS

This appendix describes the main design considerations to make the device MR-conditional. To make the device MR-conditional, MR-safe or MR-conditional materials must be used (Section II). However, MR-conditional materials can still create artefacts if their magnetic susceptibility is high. Hence, materials with lower magnetic susceptibility are preferred over materials with higher magnetic susceptibility, even if they are within the safe range ($< 10^{-2} A/m$) [54]. As a result, many materials are excluded or rejected. Leading to the exclusion of many off-the-shelf parts. This is especially noticeable with the number of compatible linear and ball bearings. To minimise friction between the linear bearing and inner-cam, a store-bought linear bearing would be ideal. Sadly, no off-the-shelf MR-safe or MR-conditional linear bearings were found. For this reason, the linear bearing had to be designed with the available manufacturing facilities in mind. We made nine custom-designed 3D printed parts, which together comprise the linear bearing. The linear bearing needs smooth surfaces for the balls (in the linear bearing) to roll with no or negligible friction. Sadly, 3D printing makes parts by layering, which negatively impacts surface roughness. For that reason, smooth surfaces and thus optimal conditions for minimising friction could not be created.

As described in Section IV, the design has an inner-cam with two paths in which ball bearings move (Figure 29). These ball bearings directly influence the size of the inner-cam. A large ball bearing radius requires a large inner-cam radius to ensure smooth movement along the inner-cam paths. This is further explained in Appendix D-B. The smallest MR-compatible ball bearing had a diameter of $10\,\mathrm{mm}$, leading to an inner-cam diameter of approximately $70\,\mathrm{mm}$. Utilising a follower instead of a ball bearing, could decrease the inner-cam radius, and thus the inner-cam weight and inner-cam linear bearing friction, but would increase the friction in the inner-cam path. As the needle rod connectors are made of aluminium, they easily bend. Increasing friction within the path could lead to warping of the aluminium tube, thereby leading to device malfunction. As a result, ball bearings were chosen instead of followers.

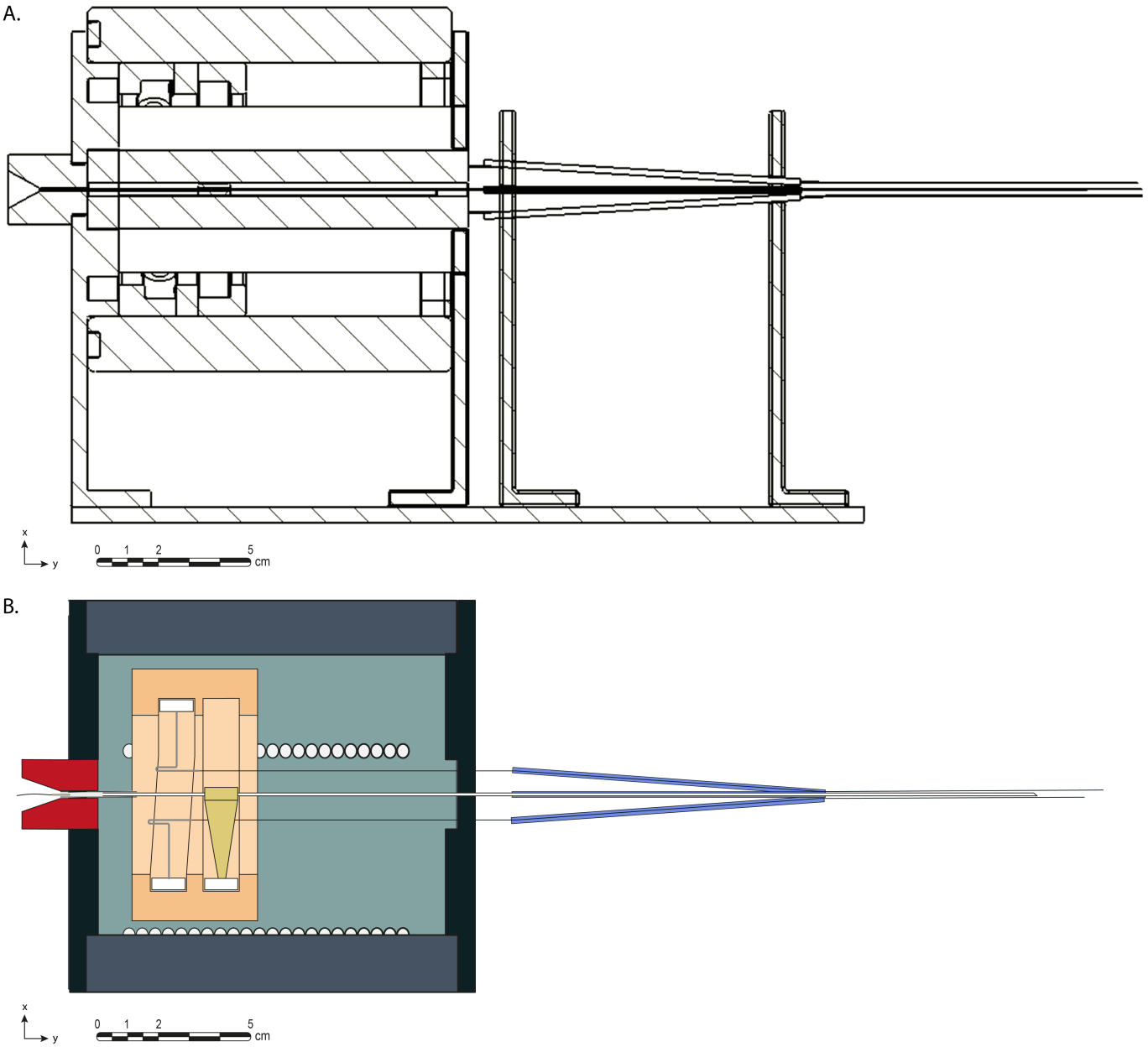


Fig. 29: *Cross-section of the actuation system, laser system, and needle system. A) Cross-section of the final device. B) Schematic cross-section of the final device, with the inner-axis, linear bearing basis and support basis removed for clarity. The inner-cam is portrayed in orange, the linear bearing (outer cylinder) in dark and light blue, the supports in blue, the linear bearing basis and the needle rods in black, the ball bearings and balls in white, and the funnel in red. Additionally, the intermediary tube, laser needle and needle rod connectors are portrayed in grey.*

APPENDIX F
MATERIAL CHANGE

This Appendix provides an overview of the parts used in the prototype that use a different material from their proposed material.

Part	**Prototype material**	**Proposed material**
Needle rod	Spring steel	Nitinol
Laser needle	Aluminium	Titanium
Ball	Steel	Glass
Needle guide	Acryl	PTFE

TABLE IV: *Overview of the parts in the prototype that use materials different from their proposed materials.*

APPENDIX G
NEEDLE SYSTEM DESIGN CONSIDERATIONS

This Appendix describes the main design considerations pertaining to the needle system. The needle rods ($0.3\,\mathrm{mm}$ diameter spring steel rods) must be enclosed every two centimetres to prevent buckling [25]. However, the needle rod also needs to be connected to the inner-cam at all times. On a larger scale, belts and rollers could be used to enclose needles at intervals, similar to, for example, a ski lift. However, on a small scale, this is not feasible due to manufacturing and availability constraints. Additionally, incorporating multiple movable parts makes the device more complex, and thus error-prone. Although other solutions are presented in scientific literature, such as origami-inspired supports [25], none were easily applicable to our design. For that reason, the design described in Section IV-A4 was used. Within this design, a needle rod connector can be seen. This connector is in the shape of an S. Early tests of the system showed that the inner-cam could only move backwards. No matter the turning direction of the linear bearing, the inner-cam always moved backwards. Finally, it was found that the reason for the backward movement was the shape of the needle rod connectors. During backward movement torque led to minimal or negligible deformation, as its design restricted movement in the clockwise direction, see Figure 30 A. When the needle was pulled forward by friction between the needle segments and the surrounding gelatin, the torque in the aluminium holder deformed the needle rod connector, instead of moving the needle rod connector, see Figure 30 B. Creating the S-shaped needle rod connector decreased the amount of deformation, and increased the forward movement, see Figure 30 C.

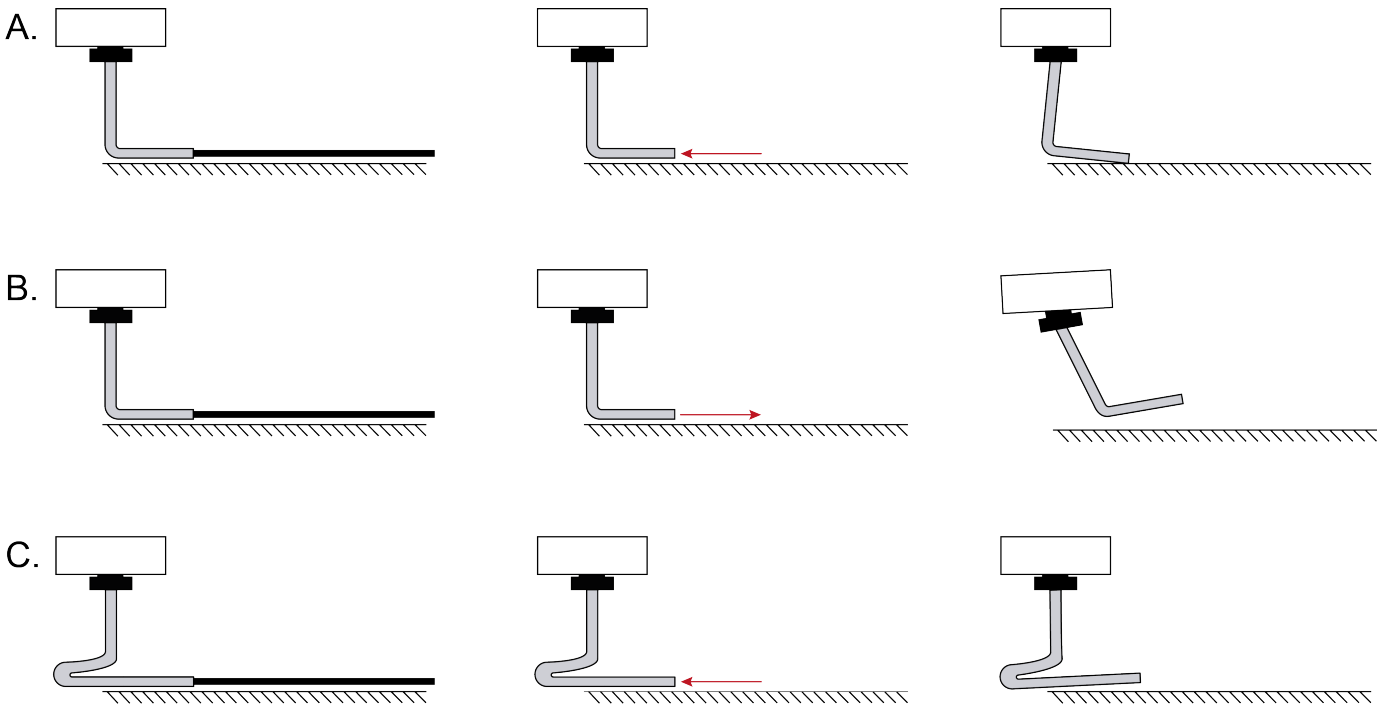


Fig. 30: *Visualisation of the needle rod-inner-cam connection problem. The needle rod as well as the connective parts are shown in black, the needle rod connectors in grey, and the ball bearings in white. The first column represents the neutral needle rod connector position. The second column represents the force acting upon the needle rod during movement. The third column represents how the needle rod connector deforms following the applied force. A) Backward movement of the first needle rod connector design. B) Forward movement of the first needle rod connector design. C) Forward movement of the needle rod connector redesign.*

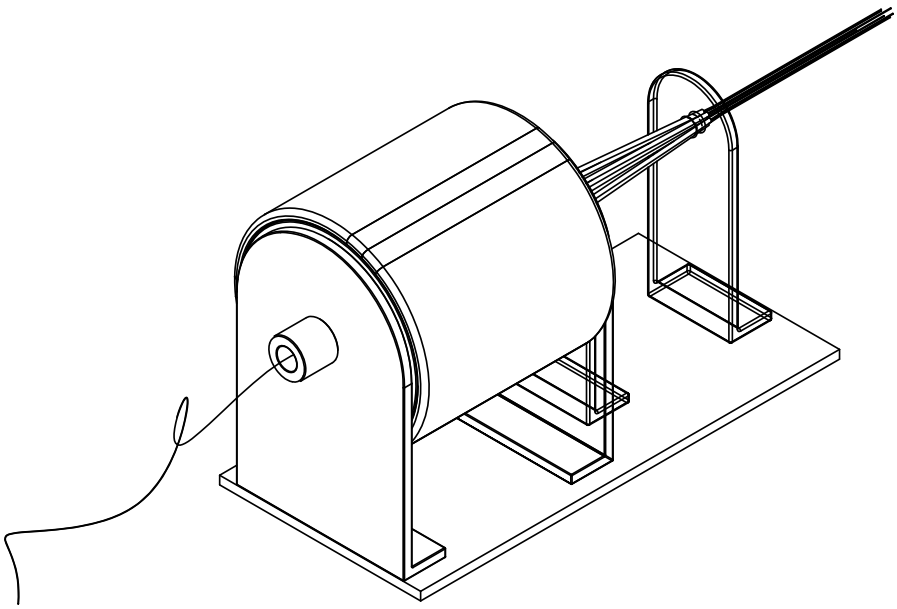
APPENDIX H
ASSEMBLY

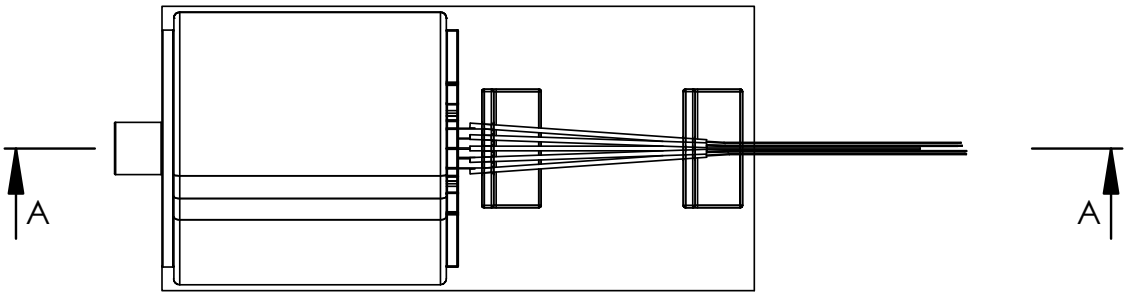
This Appendix describes the necessary steps to assemble the prototype. The steps are in chronological order.

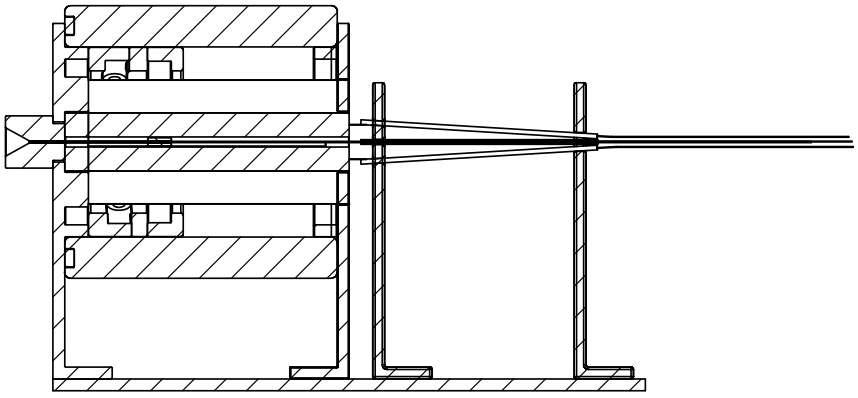
1) The needle rod guides are inserted into the inner-axis.
2) The Nitinol needle rods are placed in the aluminium needle rod connectors.
3) The needle rod connectors are glued into the needle rod holders.
4) The needle rod holders are inserted into the ball bearings.
5) The needle rod connectors are deformed to the desired S shape.
6) The six needle rod assemblies are placed in the inner-axis while ensuring the needle connectors are pushed through the needle rod guides.
7) The laser needle is glued to the laser needle holder.
8) The laser needle assembly is placed into the inner-axis.
9) If not done yet, the inner-cam is assembled using glue and sanded to remove excess glue. Now, the inner-cam is placed around the inner-axis.
10) The ball bearings are placed in the inner-cam paths.
11) The SLA-printed linear bearing parts are connected.
12) The connected SLA-printed linear bearing parts are placed between the three FDM-printed linear bearing parts.
13) The linear bearing ring is placed in the linear bearing groove.
14) The linear bearing assembly is wrapped in vegan leather to restrict movement.
15) The balls are placed in the linear bearing. Noteworthy: slightly fewer balls are placed than the possible maximum to minimise the initial friction between the inner-cam and linear bearing.
16) A protective cover is placed around the linear bearing.
17) The inner-axis top is placed on the inner-axis base.
18) The whole assembly is rotated vertically and placed onto the linear bearing base L (Section IV).
19) The linear bearing base R is placed on top of the linear bearing.
20) The whole assembly is rotated horizontally.
21) The supports are placed into the support base L.
22) The supports are inserted into the support base R.
23) The supports are taped together to limit unwanted movement.
24) The laser needle is inserted through the centrally located support.
25) The needle rods are inserted into their peripheral supports.
26) A one-centimetre long, $2\,\mathrm{mm}$ diameter PTFE tube is placed (distally) around the needle rods and laser needle.
27) The intermediary tube is glued to the funnel.
28) The intermediary tube is placed around the laser needle rod.
29) The funnel is glued to the linear bearing base L.
30) If desired the assembly can now be screwed to a base plate.

APPENDIX I
TECHNICAL DRAWINGS

This Appendix shows the technical drawings for the parts used in the final prototype. All parts were designed with a 3D modelling software called Solidworks.



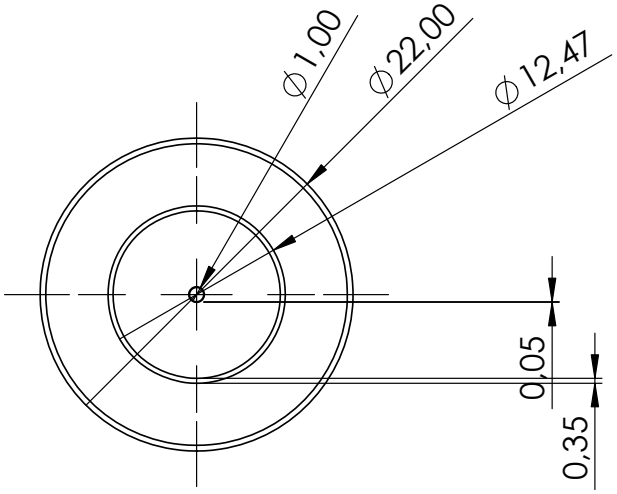


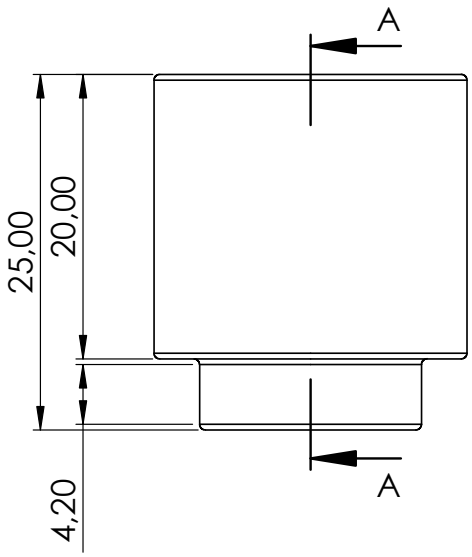


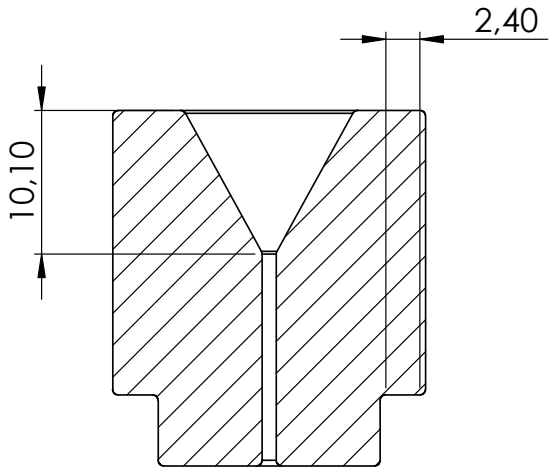
SECTION A-A

	units mm	scale 1:3	quantity 1	date 7-10-2024	remark
material				mass gr	
author David Vainer				group BME	TU Delft Delft University of Technology
name Final design assembly				format A4	drawing no.

C:\Users\david\Uni\Uni_Master\Uni_23-24\Thesis\Ideation\Fase6\Drawings\



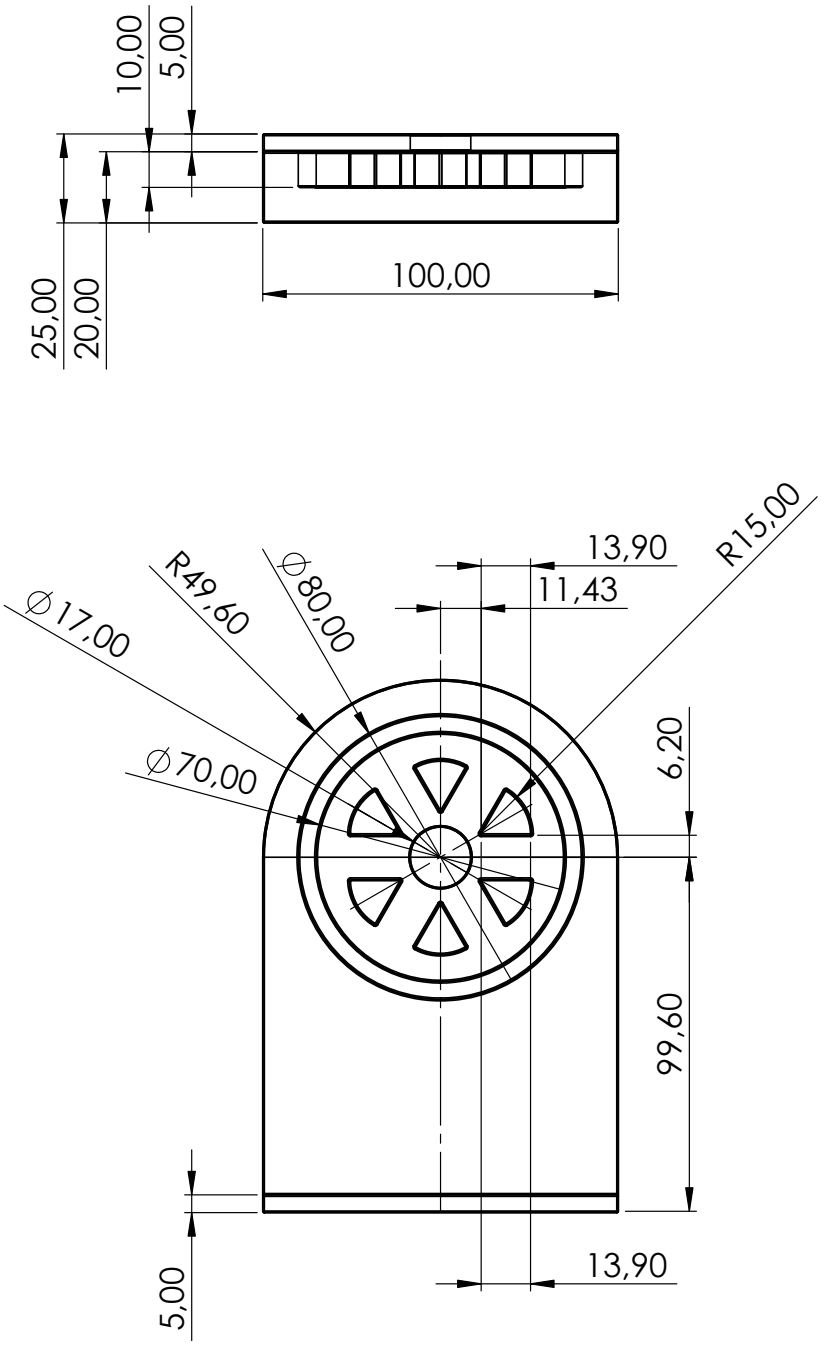




SECTION A-A

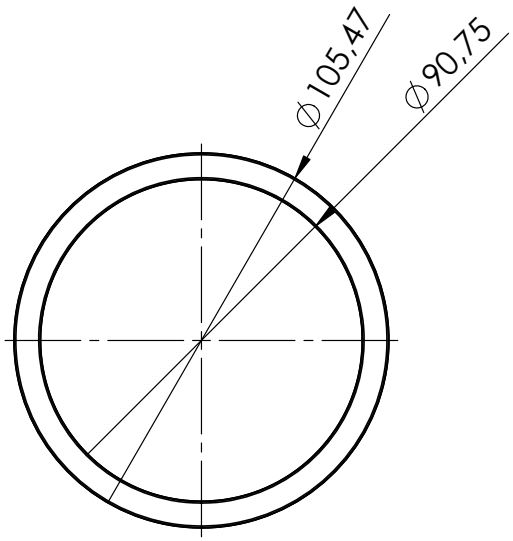
	units mm	scale 2:1	quantity 1	date 3-10-2024	remark All fillets are 0.4 mm unless stated otherwise
material Form grey				mass gr	
author David Vainer				group BME	TU Delft Delft University of Technology

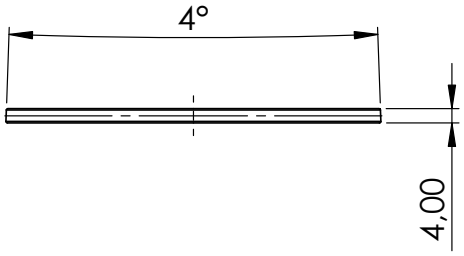
name **Funnel**	format A4	drawing no. 1
C:\Users\david\Uni\Uni_Master\Uni_23-24\Thesis\Ideation\Fase6\Drawings\		



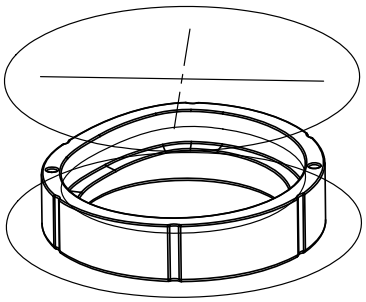
	units mm	scale 1:2	quantity 1	date 6-9-2024	remark All fillets are .4 mm unless stated otherwise
material PLA				mass gr	
author David Vainer				group BME	TU Delft Delft University of Technology
name Linear bearing base L				format A4	drawing no. 2

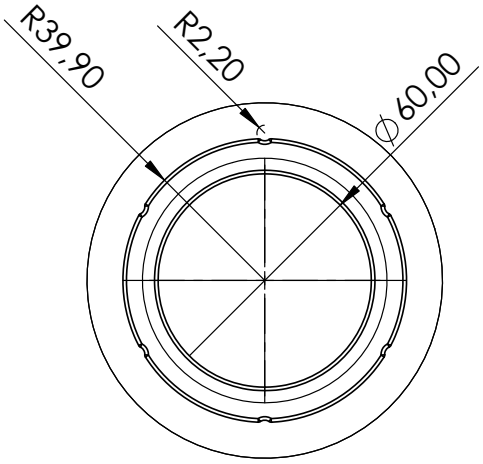
C:\Users\david\Uni\Uni_Master\Uni_23-24\Thesis\Ideation\Fase6\Drawings\

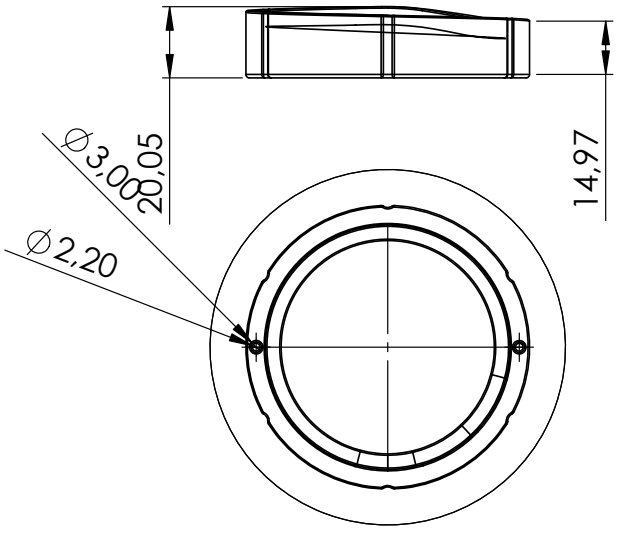




	units mm	scale 1:2	quantity 1	date 6-9-2024	remark All fillets are 0.4 mm
material PLA				mass gr	
author David Vainer				group BME	TU Delft Delft University of Technology
name Linear bearing ring				format A4	drawing no. 3



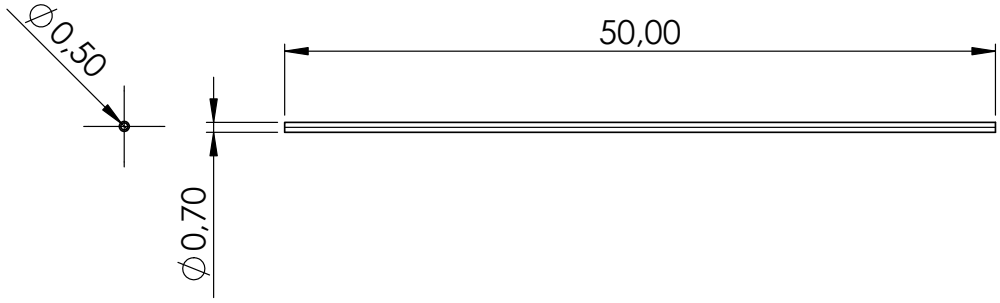




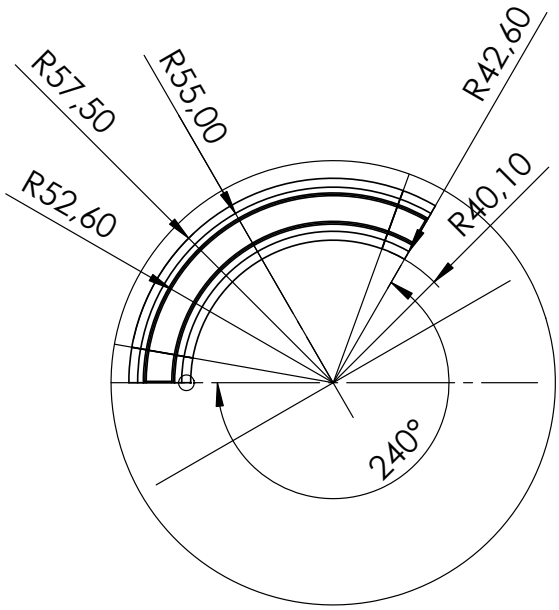
	units mm	scale 1:2	quantity 1	date 6-9-2024	remark All fillets are 1.0 mm, unless stated otherwise
material Form grey				mass gr	
author David Vainer				group BME	TU Delft Delft University of Technology

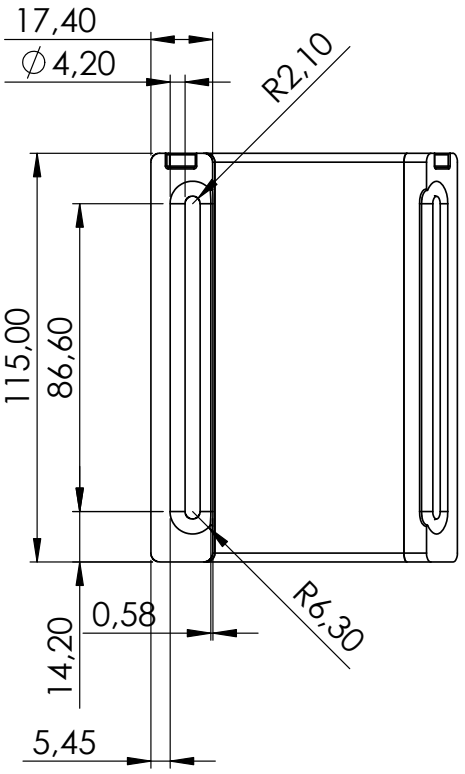
name **Inner-cam L**	format A4	drawing no. 4

C:\Users\david\Uni\Uni_Master\Uni_23-24\Thesis\Ideation\Fase6\Drawings\

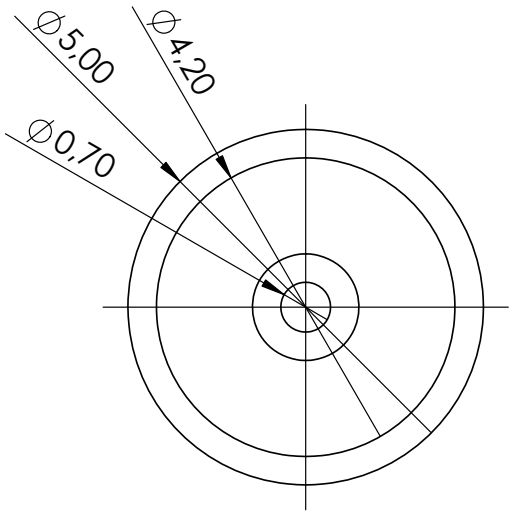


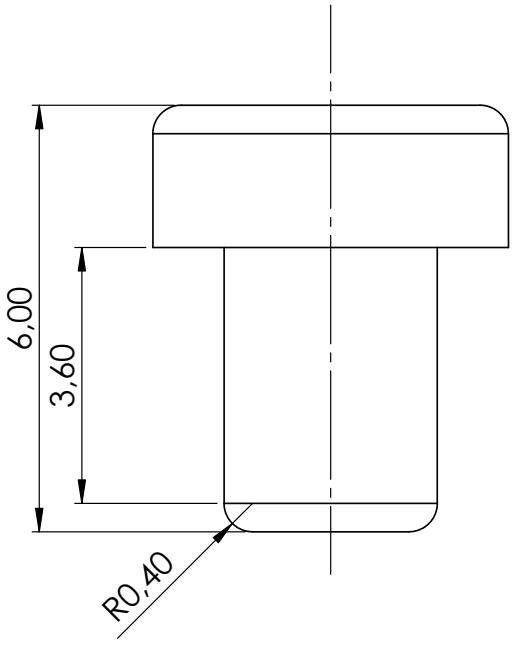
	units mm	scale 2:1	quantity 1	date 6-9-2024	remark Store bought
material Aluminium				mass gr	
author David Vainer				group BME	TU Delft Delft University of Technology
name **Intermediary tube** C:\Users\david\Uni\Uni_Master\Uni_23-24\Thesis\Ideation\Fase6\Drawings\				format A4	drawing no. 5



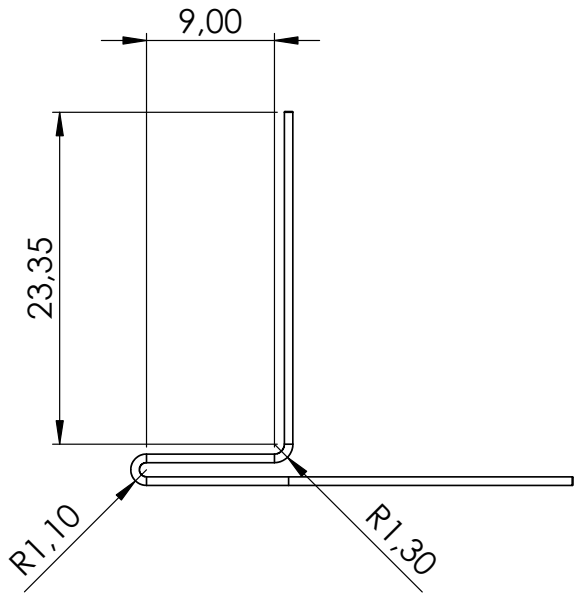


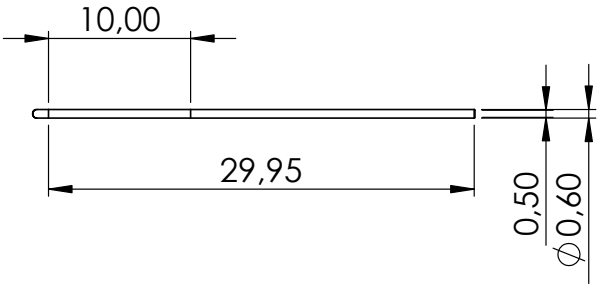
	units mm	scale 1:2	quantity 3	date 6-9-2024	remark
material PLA and Form grey				mass gr	
author David Vainer				group BME	TU Delft Delft University of Technology
name Linear bearing part				format A4	drawing no. 6



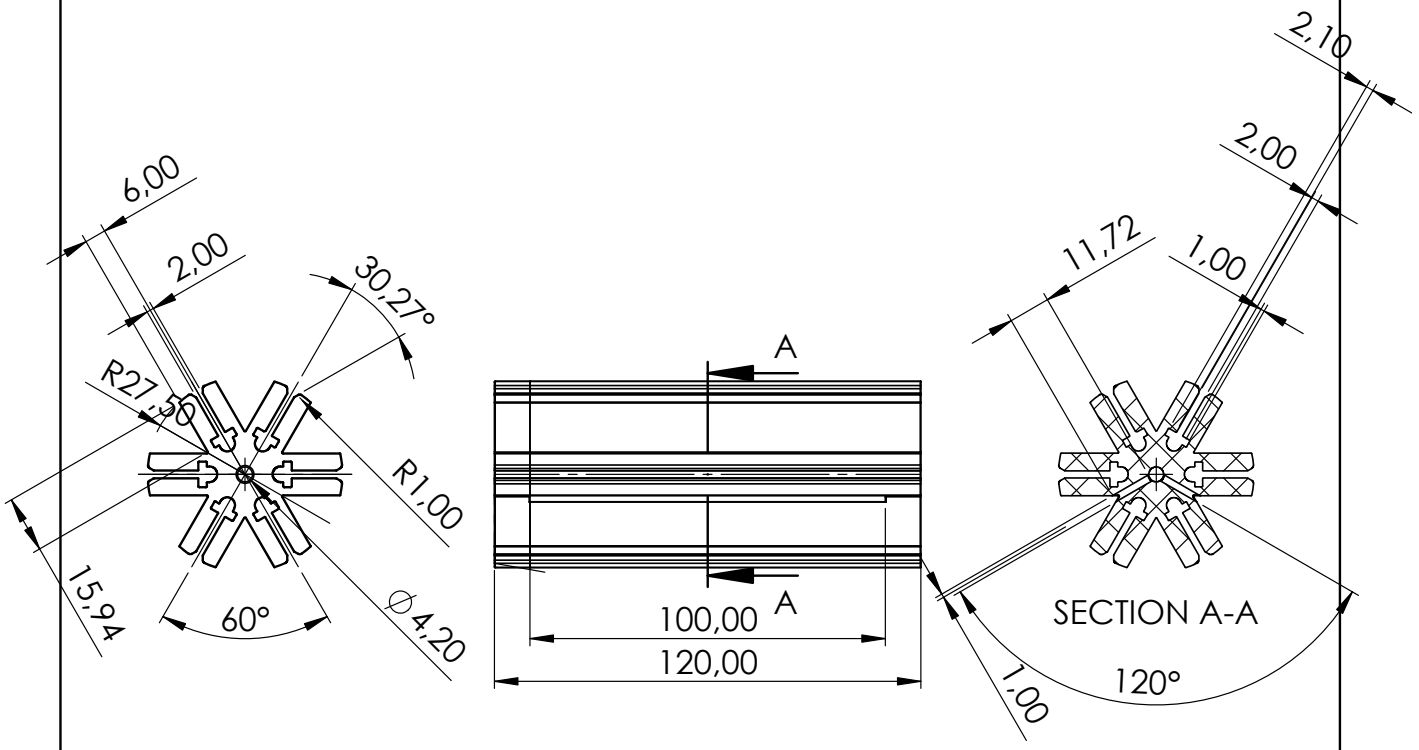


	units mm	scale 10:1	quantity 6	date 6-9-2024	remark
material Form grey				mass gr	
author David Vainer				group BME	TU Delft Delft University of Technology
name Needle rod holder				format A4	drawing no. 7

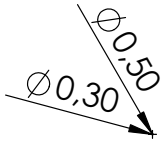


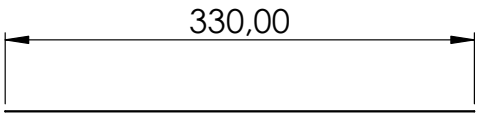


	units mm	scale 2:1	quantity 6	date 6-9-2024	remark Bought
material Aluminium				mass gr	
author David Vainer				group BME	TU Delft Delft University of Technology
name **Needle rod connector**				format A4	drawing no. 8

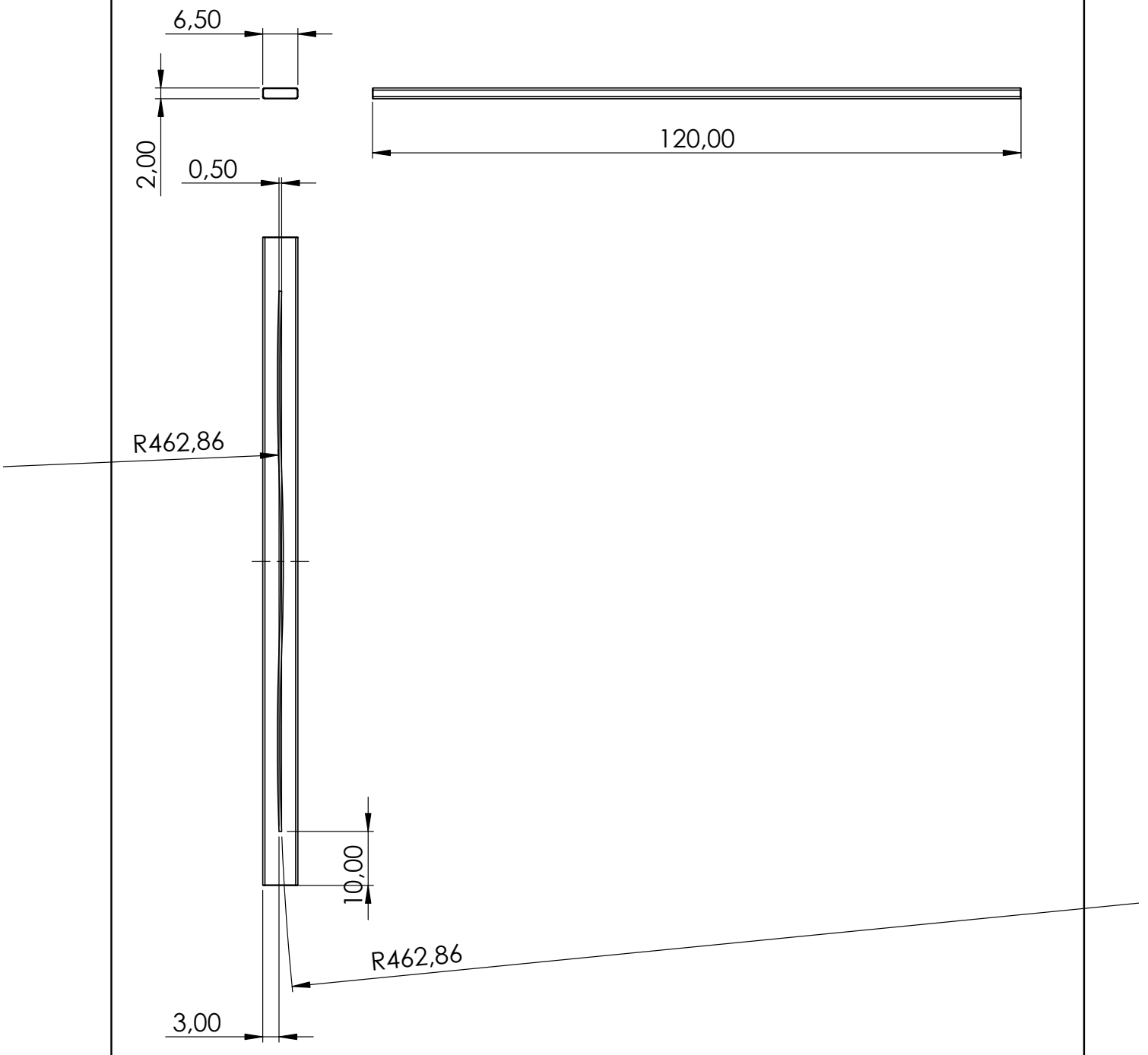


	units mm	scale 1:2	quantity 1	date 6-9-2024	remark To manufacter the part a split is used at the dotted line
material PLA				mass gr	
author David Vainer				group BME	TU Delft Delft University of Technology
name Inner-axis				format A4	drawing no. 9

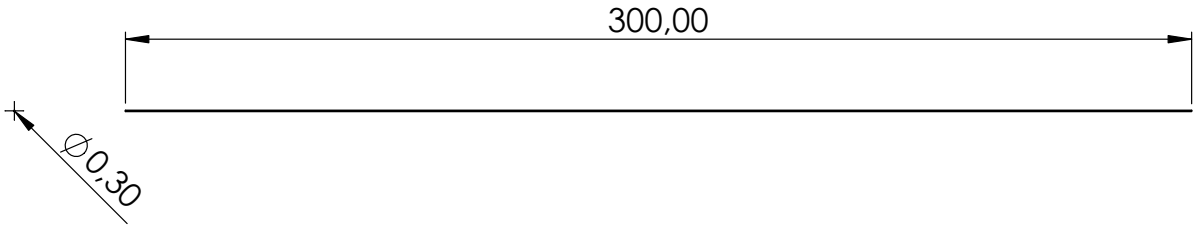




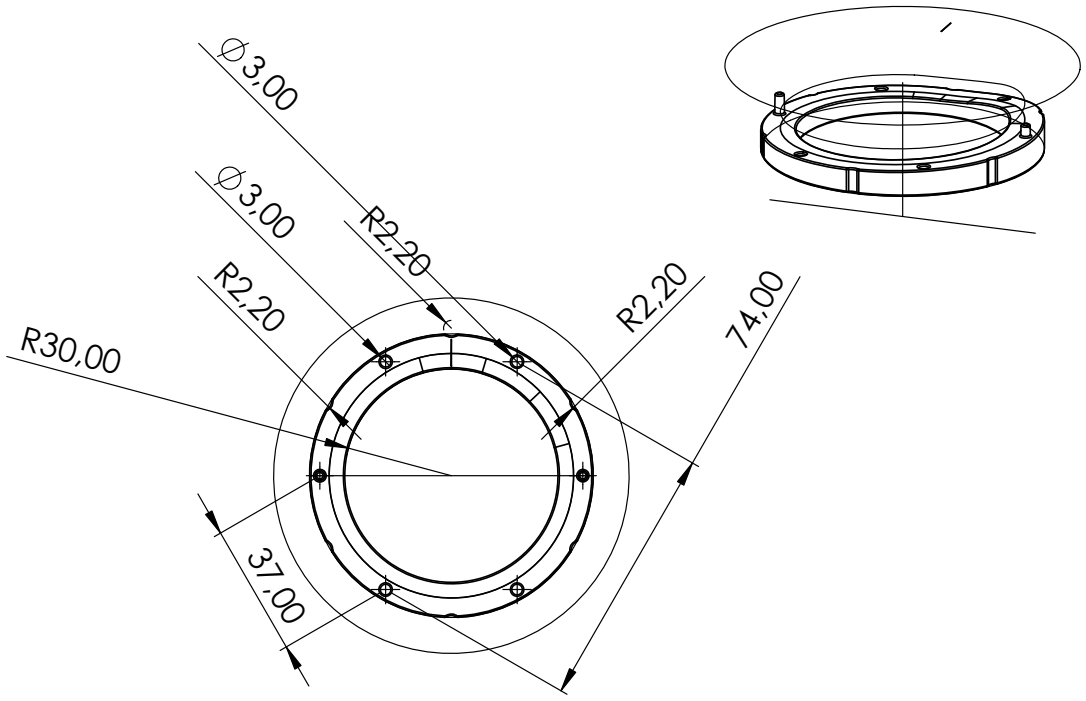
	units mm	scale 1:5	quantity 1	date 6-9-2024	remark <<Bought>>
material Aluminium				mass gr	
author David Vainer				group BME	TU Delft Delft University of Technology
name Laser needle				format A4	drawing no. 10

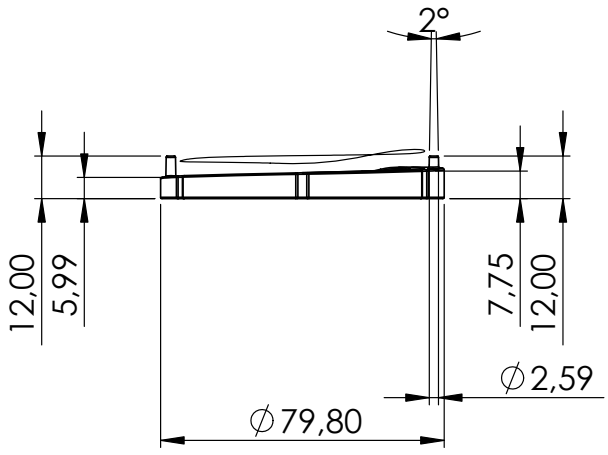


	units mm	scale 1:1	quantity 6	date 6-9-2024	remark
material Acryl				mass gr	
author David Vainer				group BME	TU Delft Delft University of Technology
name **Needle rod guide**				format A4	drawing no. 11

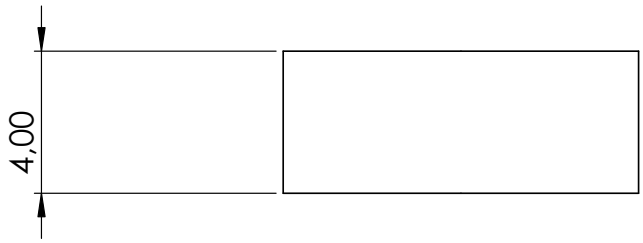


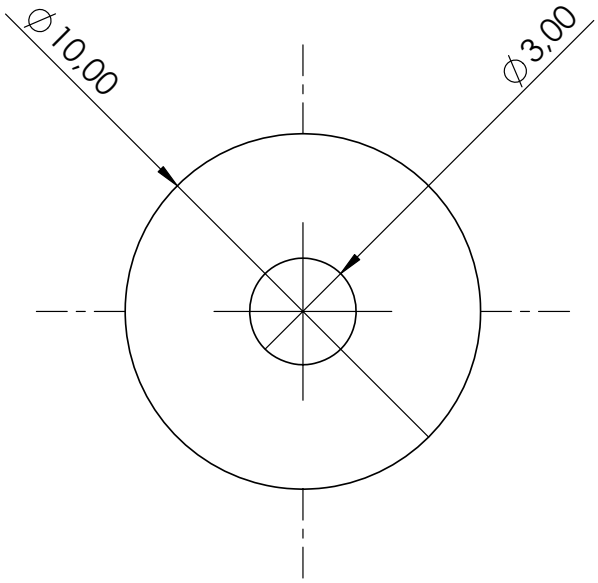
	units mm	scale 1:2	quantity 6	date 6-9-2024	remark Bought
material Spring steel				mass gr	
author David Vainer				group BME	TU Delft Delft University of Technology
name Needle rod				format A4	drawing no. 12



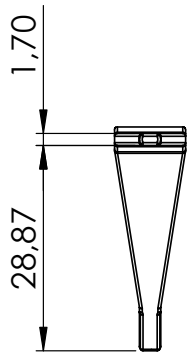


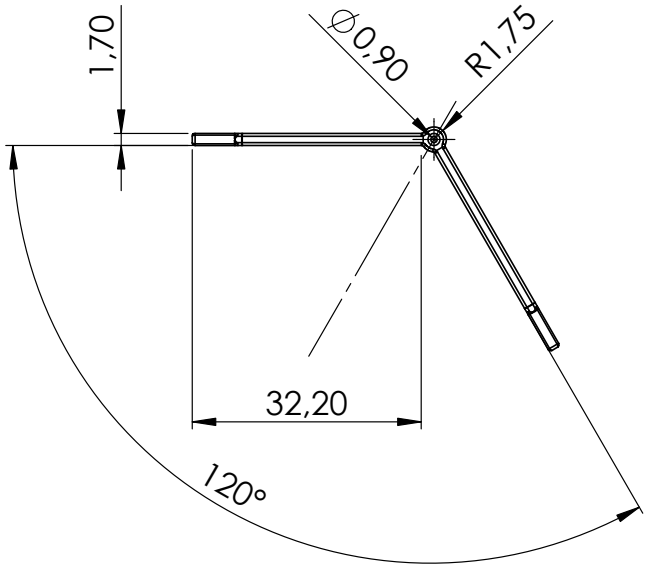
	units mm	scale 1:2	quantity 1	date 6-9-2024	remark All fillets are 0.4 mm, unless stated otherwise
material Form grey				mass gr	
author David Vainer				group BME	TU Delft Delft University of Technology
name Inner-cam M				format A4	drawing no. 13

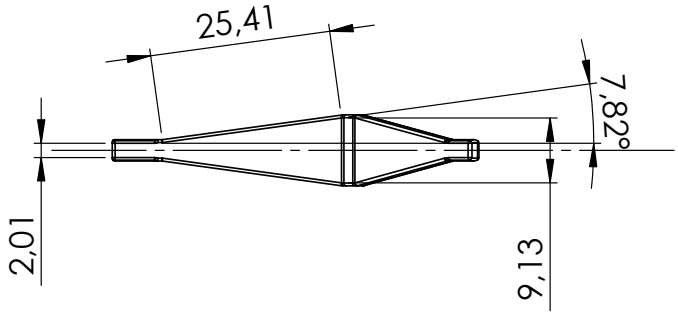




	units mm	scale 5:1	quantity 8	date 6-9-2024	remark Only for dimensional purposes. Does not represent the actual ball bearer.
material Xirodur B180 and glass				mass gr	
author David Vainer				group BME	TU Delft Delft University of Technology
name **Ball bearing** C:\Users\david\Uni\Uni_Master\Uni_23-24\Thesis\Ideation\Fase6\Drawings\				format A4	drawing no. 14

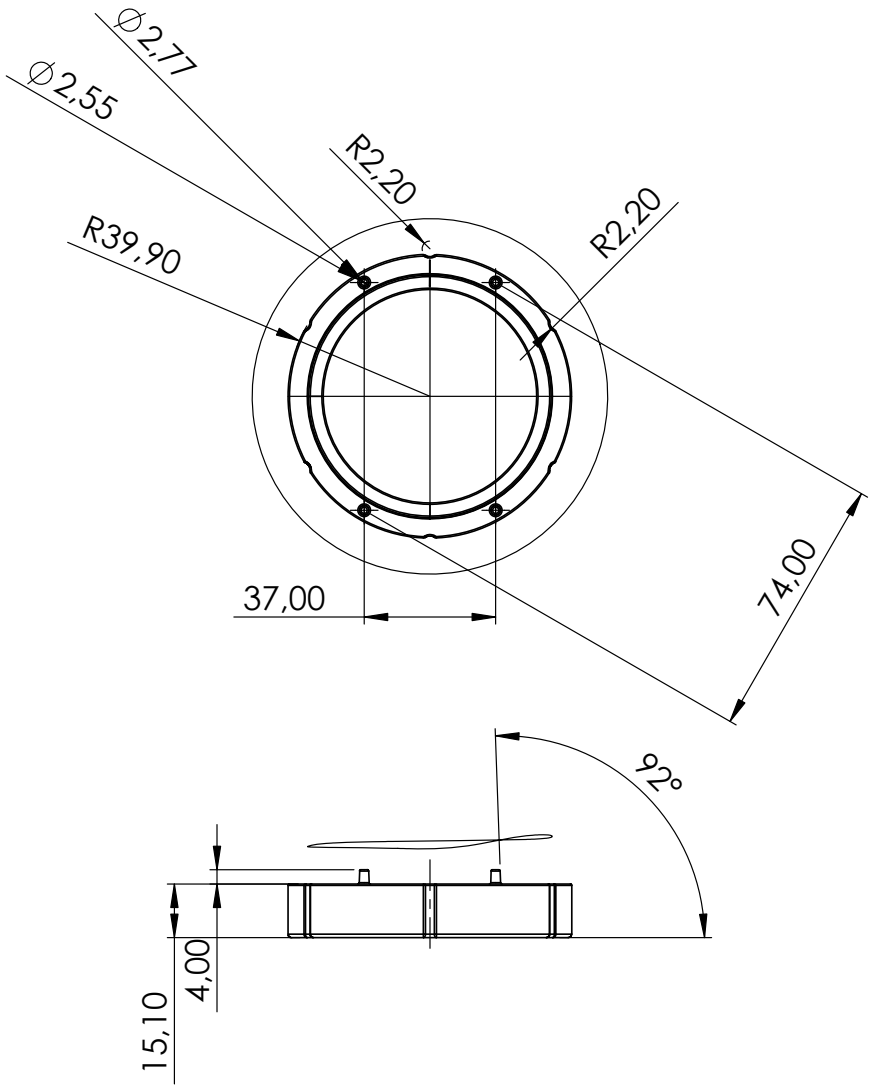




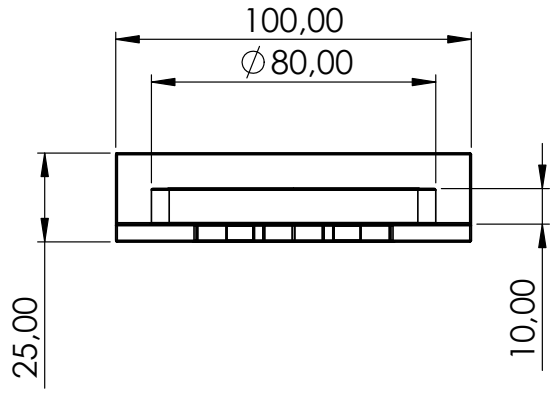


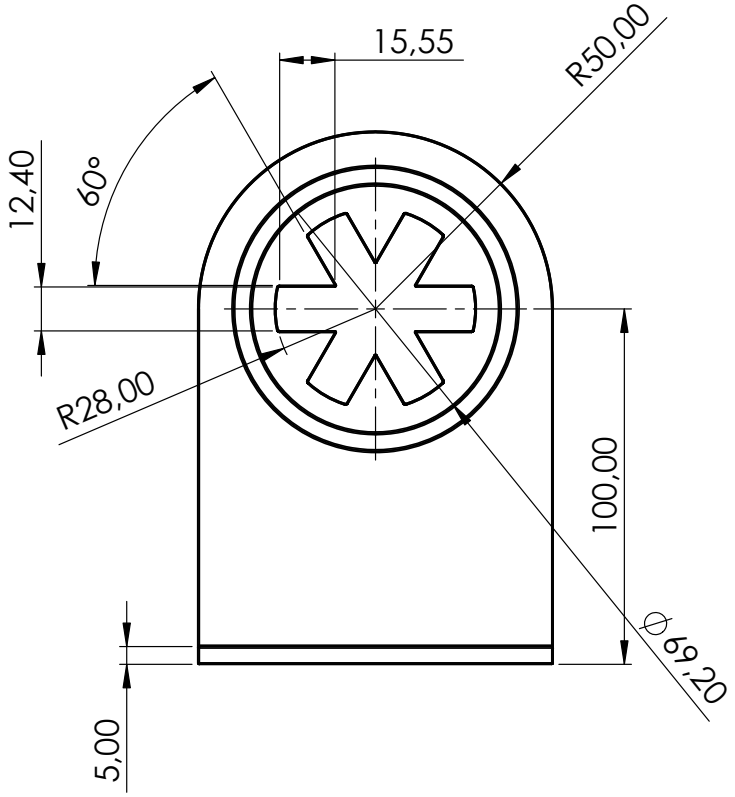
	units mm	scale 1:1	quantity 1	date 6-9-2024	remark
material `Form grey				mass gr	
author David Vainer				group BME	TU Delft Delft University of Technology
name Laser needle holder				format A4	drawing no. 15

C:\Users\david\Uni\Uni_Master\Uni_23-24\Thesis\Ideation\Fase6\Drawings\

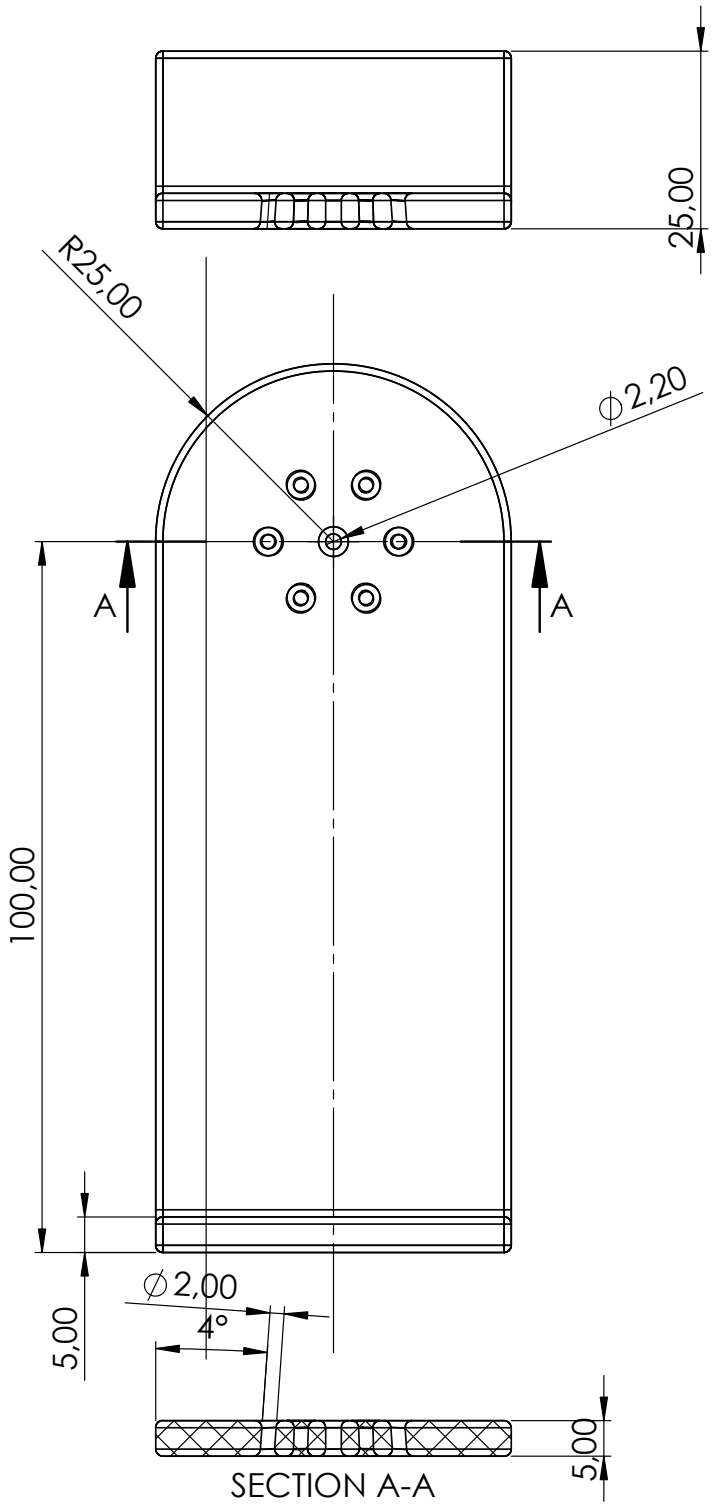


	units mm	scale 1:2	quantity 1	date 6-9-2024	remark All fillets are 0.4 mm
material Form grey				mass gr	
author David Vainer				group BME	TU Delft Delft University of Technology
name Inner-cam R				format A4	drawing no. 16

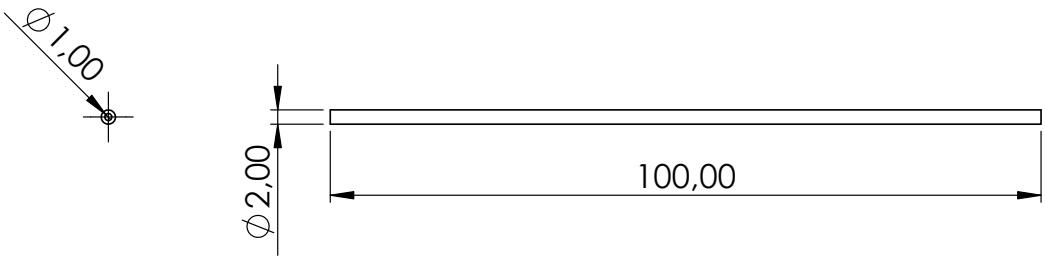




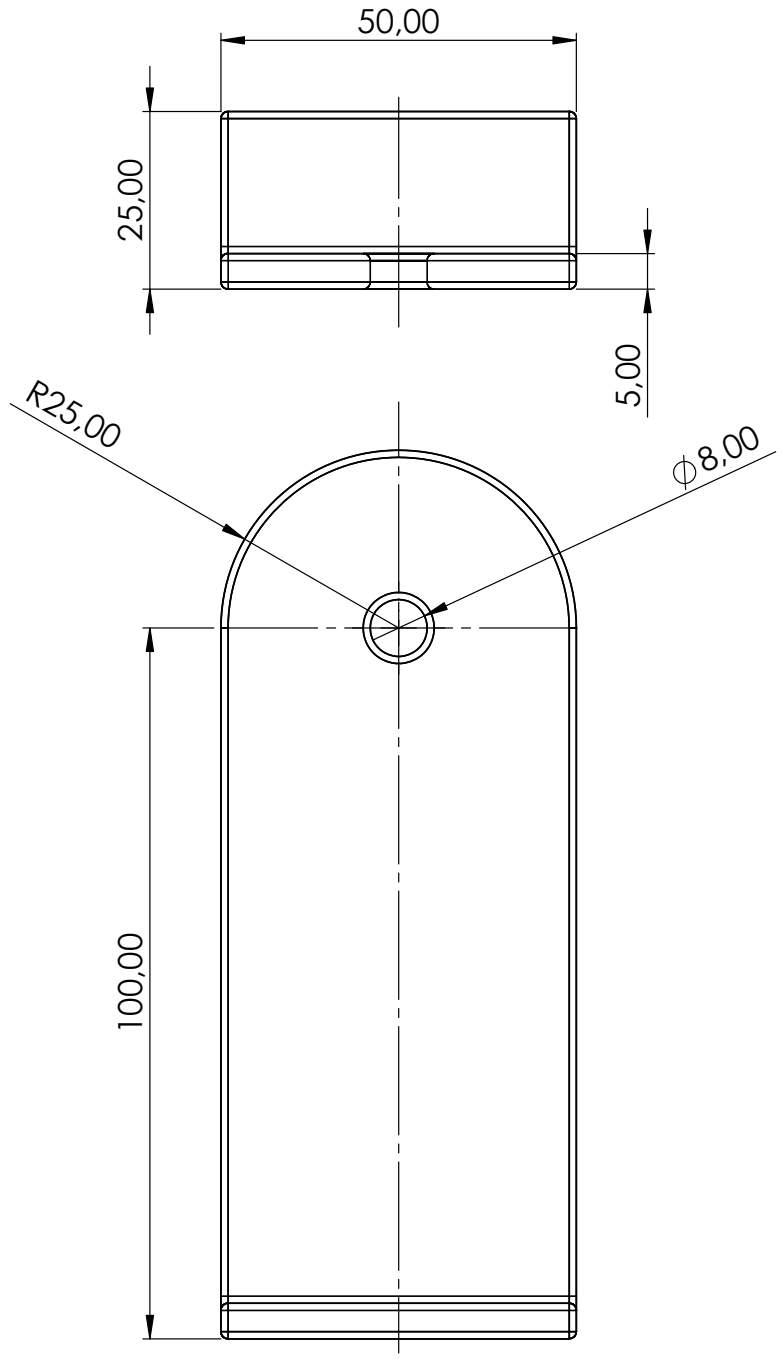
	units mm	scale 1:2	quantity 1	date 6-9-2024	remark All fillets are 0.4 mm
material PLA				mass gr	
author David Vainer				group BME	TU Delft Delft University of Technology
name Linear bearing base R				format A4	drawing no. 17



	units mm	scale 1:1	quantity 1	date 6-9-2024	remark All fillets are 1.0 mm
material PLA				mass gr	
author David Vainer				group BME	TU Delft Delft University of Technology
name Support base L				format A4	drawing no. 18



	units mm	scale 1:1	quantity 6	date 6-9-2024	remark
material Brass				mass gr	
author David Vainer				group BME	TU Delft Delft University of Technology
name Support				format A4	drawing no. 19



	units mm	scale 1:1	quantity 1	date 6-9-2024	remark All fillets are 1.0 mm
material PLA				mass gr	
author David Vainer				group BME	TU Delft Delft University of Technology
name Support base R				format A4	drawing no. 20